On Topological Phases in Disordered P-wave Superconducting Wires

Im Fachbereich Physik
der Freien Universität Berlin
eingereichte

Dissertation

von

Maria-Theresa Rieder

Berlin, im Juni 2015

1. Gutachter: Prof. Dr. Piet W. Brouwer
2. Gutachter: Dr. Emil J. Bergholtz

Tag der Einreichung: 5. Juni 2015
Tag der Disputation: 10. Juli 2015

Selbstständigkeitserklärung

Hiermit versichere ich, dass ich in meiner Dissertation alle Hilfsmittel und Hilfen angegeben habe, und auf dieser Grundlage die Arbeit selbstständig verfasst habe. Diese Arbeit habe ich nicht schon einmal in einem früheren Promotionsverfahren eingereicht.

Kurzfassung

Topologische Phasen der kondensierten Materie sind Gegenstand intensiver theoretischer und experimenteller Forschung. Die wohl bekanntesten Beispiele für solche Phasen sind: der Quanten-Hall Effekt, Topologische Isolatoren und Topologische Supraleiter. Letztere weisen sich durch spezielle Anregungen, die Majoranazustände, aus, welche man sich als die Hälften eines Elektrons vorstellen kann und die der Oberfläche eines solchen topologischen Supraleiters getrennt voneinander existieren können. Die Majoranazustände haben aufgrund ihren besonderen Eigenschaften ein großes wissenschaftliches Interesse geweckt. Sie besitzen eine nicht-Abelsche Flechtstatistik, welche sie zu nützlichen Bauteilen für einen möglichen fehlertoleranten Quantencomputer macht. In diesem Zusammenhang sind vor allem topologisch supraleitende Drähte wichtig, da in diesen die Positionen der Majoranazustände als die Drahtenden, den Oberflächen eines eindimensionalen Systems,eindeutig bestimmt sind.

Topologisch supraleitende Drähten treten zwar nicht in der Natur auf können aber von verfügbaren Materialien, Halbleiter- oder ferromagnetische Nanodrähten und konventionellen Supraleitern, konstruiert werden. Die Nanodrähte können aufgrund des Proximity-Effekts supraleitende Eigenschaften übernehmen und eine topologisch nichttrivial Phase aufweisen. Inzwischen wurden mehrere Experimente an solchen Hybridstrukturen durchgeführt und von Messergebnissen berichtet, welche mit den theoretischen Vorhersagen konsistent sind.

Die meisten theoretischen Arbeiten an solchen Drähten sind auf ein eindimensionales effektives Model beschränkt, den p-Wellen Supraleiter. Ein Nanodraht ist aber normalerweise ein quasi-eindimensionales System, mit einem kontinuierlichen, longitudinalen und einem quantisierten, transversalen Freiheitsgrad.

In dieser Doktorarbeit untersuchten wir die Verallgemeinerung eines topologisch supraleitenden Drahtes zu einem Mehrkanalsystem, indem wir einen zweidimensionalen $p + ip$-Supraleiter auf die Geometrie eines schmalen Streifens beschränkten. Solche Systeme können eine topologisch nichttriviale Phase aufweisen, welche durch die Existenz einer Nullenergieanregung, ein Majoranazustand, gekennzeichnet ist. Wir haben den Effekt verschiedener geometrischer Drahtendungen auf das Niedrigenergiespektrum eines solchen Drahtes untersucht und beobachtet, dass sich innerhalb der Energielücke des Supraleiters Zustände ansammeln, welche sich um die Nullenergie scharen. In der Zustandsdichte könnten diese den Majoranazustand verdecken und daher die Identifizierung der topologischen Phase wesentlich erschweren. Des weiteren haben wir die topologische Phase eines Mehrkanalsystems unter dem Einfluss eines Unordnungspotentials erforscht und eine Serie topologischer Phasenübergänge bei ansteigender Unordnungsstärke gefunden. Im Niedrigenergiespektrum des Drahtes werden die Phasenübergänge von der charakteristischen Dyson-Singularität begleitet.

Abstract

Topological phases of matter have been the subject of intense experimental and theoretical research during the last years. Prominent examples are the Quantum Hall Effect, Topological Insulators or Topological Superconductors. The latter host special excitations, the Majorana states, at their boundaries, which can be thought of as the halves of an electron that can exist separately in this special case. These Majorana states have attracted great interest as they exhibit so-called non-Abelian braiding statistics, which could make them useful tools in the search for fault-tolerant quantum computation. In this context topologically superconducting wires are particularly useful as the Majorana states are located unambiguously at the wire's end, where they form localized end states.

Topologically superconducting wires are not known to exist in nature but they can be engineered from commonly available ingredients: semiconductor or ferromagnet nanowires and conventional superconductors. The nano-wires can inherit superconductivity by the proximity effect and can then exhibit a topologically nontrivial phase. By now, several experiments have been performed on such hybrid structures, reporting measurements that are consistent with the existence of a topologically superconducting phase in the nanowire.

Most theoretical investigations on these systems, so far, have been restricted to a one-dimensional effective model: The one-dimensional p-wave superconductor, which is the prototype of a topologically superconducting wire. A nanowire, however, is in general in a quasi-one dimensional regime, with a continuous longitudinal but a quantized transverse degree of freedom.

In this Thesis we study the multichannel generalization of a topologically superconducting wire by means of a two-dimensional $p + ip$-superconductor that is restricted to a narrow-strip geometry. Such systems can be in a topological phase, characterized by the existence of a zero-energy excitation at the wires end—the Majorana bound state. We study the effect of various geometrical terminations on the low-energy spectrum of such a wire and find that subgap states tend to accumulate around zero energy. In a density-of-states measurement, these states potentially obscure the Majorana state thereby hindering the detection of the topological phase. We further investigate the effect of disorder on a multichannel wire and find that it induces a series of phase transitions with a reentrant topological phase. Due to disorder-localized states accumulating in the superconducting gap, the low-energy spectrum for a disordered wire contains a signature of the topological phase transitions as well: a singularity in the density of states, which is the well-known Dyson-singularity.

Contents

1 Introduction

The discovery of topological phases of matter marks a milestone of modern physics, that changed our understanding of phases in condensed matter and transitions between them. The traditional classification of phases of matter, going back to Landau, distinguishes phases by symmetries that are spontaneously broken at a transition point; an approach that has been successfully employed to explain many phenomena. Examples are the liquid-to-solid transition, where atoms break the translational symmetry upon ordering into a crystal, and ferromagnetism, associated with a broken rotational invariance of the magnetic field. More exotic phenomena include superfluids, in which a global $U(1)$-symmetry associated with the conservation of the number of atoms is broken, or superconductors, which break a local gauge symmetry coupling to photons and leading to the expulsion of magnetic fields from the material, known as the Meissner effect [Altl 09].

With the discovery of the Quantum Hall Effect in 1980 by Klaus von Klitzing et al. [Klit 80], who was subsequently awarded with a Nobel prize, it was realized that this concept of symmetry breaking is not sufficient to explain all states of matter that are observed in experiments. In fact, two states sharing the same symmetries can still be profoundly different in being separated by a quantum phase transition and distinguished by a topological quantum number. This quantity, though being a property of the system's bulk, has important consequences on the physics at the boundaries as it is linked to the existence of robust edge states. A Topological Insulator, for example, is a material that is insulating in its bulk, with an excitation gap just like an ordinary band insulator, but has metallic edge states at its boundaries. These boundary modes are insensitive to imperfections, like impurities, or smooth variations of system parameters [Hasa 10, Qi 11]. Similarly, there exist Topological Superconductors, whose edge state are even more peculiar as they host special excitations: the Majorana states. Intuitively, these can be viewed as the halves of an electron, which, at the surface of a superconductor, are physically separable but together still form one fermionic state. These Majorana states exhibit remarkable properties which make them of great interest in the search for fault-tolerant, the topological, quantum computation. Topological superconductivity is not known to appear naturally, however, it is possible to engineer systems resembling it and an immense experimental effort is happening currently to realize those [Mour 12, Das 12, Nadj 14, Wied 15].

In the following we will give a brief overview over the field of topological phases of matter and will then focus on the topic of this thesis, topologically superconducting wires.

1.1 Topological Phases of Matter

1.1.1 From The Quantum Hall Effect to Topological Insulators

The Quantum Hall effect is so important to modern physics not only because it is an example for a quantum effect on macroscopic scales but also– and arguably more importantly– is it the first example of a so-called topological phase of matter.

It had been known before that a quantum analog of the standard Hall effect exists in the sense that the Hall conductance develops steps at high magnetic fields [Ando 74, Engl 78, Kawa 78]. The revolutionary finding by von Klitzing et al. [Klit 80] was that these plateaus are actually quantized in integers of the so-called conductance quantum $G_0 = \frac{e^2}{h}$ to an unheard-of accuracy. As opposed to the naive expectation, imperfections of the system such as disorder cannot affect this measured value and, as long as the effect is present, even the underlying material has no influence on it.

Various successful approaches exist to describe the phenomenology of the Quantum Hall Effect [Laug 81, Pran 12], but ultimately this perfect quantization[1] is a consequence of the observed phase's topological nature: An (integer) topological quantum number n, the TKNN invariant named after its inventors Thouless, Kohmoto, Nightingale, and Nijs, can be defined for a periodic system, which determines the current in the presence of an edge [Thou 82]. Even though the current is mostly flowing at the system boundaries, its existence is a property of the bulk only, explaining its insensitivity to local perturbations.

An important feature in the discussion of the Quantum Hall conductance and topological protection of phases is the existence of a mobility gap. In fact, it is a necessary condition for the invariance of the conductance and the closing of the bulk gap is a hallmark for a phase transition between phases with different topological quantum numbers. As we will see later, this statement is generally true for topological phases of matter.

The transport in a Quantum Hall state is due to n-channel helical edge states at the boundaries of the system, which is made intuitive in a semi-classical picture: Electrons are forced on closed circular paths by a strong magnetic field in the bulk of the system. At the edges these circles are interrupted and the electrons move unidirectional on half-circles along the boundary line, see Fig. 1.1. The helicity of the electrons' motion forbids backscattering thereby causing the observed insensitivity to disorder; an impurity sitting at the edge just bends the boundary. This edge current is of great interest in two very different ways: On the one hand as the signature of a novel phase, on the other hand as a platform to study single (or few) channel transport and nano-scale electronics [Pran 12].

With the fundamentally new physics and the potential for applications found in the Quantum Hall Effect, it suggests itself to search for other topologically protected phases. A particularly interesting question is whether a similar phase could be realized without the presence of a strong magnetic field or whether one could even find a material that by itself is topologically non-trivial.

The first model to realize a Quantum Hall effect without a magnetic field was the Haldane model [Hald 88], which combines fermions on a honeycomb lattice with a complex arrangement of magnetic fluxes in each unit cell of the honeycomb model to obtain a zero

[1] In fact, this quantization is so accurate and universal, that it is used for calibration and even the definition of units.

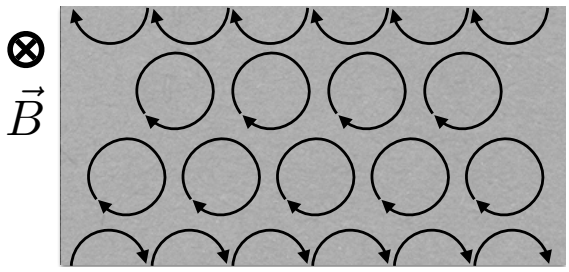

Figure 1.1: Schematic view of the semiclassical picture of edge states in the Quantum Hall Effect. The electrons paths, indicated by black arrows, are bended into circles in the bulk by a perpendicular magnetic field $\vec{B}$ while at the edges chiral propagating states are found.

net-magnetic field though time-reversal symmetry is broken. The actual breakthrough in the field, however, happened only in 2006, when Kane and Mele pointed out that Rashba spin-orbit coupling in graphene can give rise to what they called the *Quantum Spin Hall Effect* then and what is now known as the first *Topological Insulator* [Kane 05a]. Loosely speaking, this time-reversal invariant model combines two copies of the standard Quantum Hall Effect with opposite helicities for the two Kramers partners. From this picture it becomes intuitively evident that the TKNN invariant vanishes and a new topological invariant needs to be employed. In the present case the topological phase is characterized by a $\mathbb{Z}_2$-number [Kane 05b], distinguishing a topologically trivial and a nontrivial phase; the latter with dissipationless edge states, insensitive to weak disorder and interactions, protected by time-reversal symmetry. In the 3-dimensional analogs of the time-reversal-invariant Topological Insulators four independent $\mathbb{Z}_2$-numbers classify the topological phase [Roy 09, Moor 07, Fu 07b]. However only one of them indicates a phase with a metallic surface state that is protected against perturbations, the Strong Topological Insulator. The other quantum numbers are so-called weak topological invariants whose associated surface states are not stable against all perturbations breaking translational invariance.
The existence of topological insulator phases has been predicted for certain materials [Bern 06, Fu 07a] and signatures of them have been observed experimentally [Koni 07, Hsie 08, Xia 09, Zhan 09]. These achievements have stimulated great interest and by now a whole field of research is concerned with the study of topological phases of matter [Hasa 10, Hasa 11, Qi 11].
In the classification of topological phases of matter a crucial role in determining what kind of phases can occur is played by the symmetries respected by a system [Schn 08, Kita 09, Schn 09, Ryu 10]. The two basic symmetries are time-reversal and particle-hole symmetry, both of which are represented by anti-unitary operators which can square to either $+1$ or -1. A further symmetry, the chiral symmetry, arises from the combination of these two operators, yielding 10 different possible combinations to categorize a (gapped) noninteracting Hamiltonian, the so-called symmetry classes. The topological quantum number that characterizes a phase in a particular class depends on the dimension of the system and indicates whether a topologically non-trivial phase can exist at all and, if so,

		TRS	PHS	SLS	d=1	d=2	d=3
Standard	A (unitary)	0	0	0	-	$\mathbb{Z}$	-
(Wigner-Dyson)	AI (orthogonal)	+1	0	0	-	-	-
	AII (symplectic)	−1	0	0	-	$\mathbb{Z}_2$	$\mathbb{Z}_2$
Chiral	AIII (chiral unitary)	0	0	1	$\mathbb{Z}$	-	$\mathbb{Z}$
(sublattice)	BDI (chiral orthogonal)	+1	+1	1	$\mathbb{Z}$	-	-
	CII (chiral symplectic)	−1	−1	1	$\mathbb{Z}$	-	$\mathbb{Z}_2$
BdG	D	0	+1	0	$\mathbb{Z}_2$	$\mathbb{Z}$	-
	C	0	−1	0	-	$\mathbb{Z}$	-
	DIII	−1	+1	1	$\mathbb{Z}_2$	$\mathbb{Z}_2$	$\mathbb{Z}$
	CI	+1	−1	1	-	-	$\mathbb{Z}$

Figure 1.2: Figure from Ref. [Schn 08]: The table for topological classifications of quadratic, non-interacting Hamiltonians H with different symmetries. TRS refers to time-reversal symmetry and PHS refers to a particle-hole symmetry. SLS is the chiral (or sublattice) symmetry. The symmetry class of the Quantum Spin Hall effect (2D), AII, allows only for a $\mathbb{Z}_2$-type characterization of the topological phase. This means that next to the trivial phase there is only one non-trivial one. The same is true for 3D topological insulators. The conventional Quantum Hall effect, however, is in class A and has a $\mathbb{Z}$ classification: The integer plateaus. One concludes immediately that no Quantum-Hall effect can occur in three dimensions.

how many distinct phases could appear, see Fig. 1.2.

This classification scheme suggests that that also superconductors, which have a gapped excitation spectrum, can exhibit topologically non-trivial phases. It turns out that not only can these phases be found but also they host very special quasi-particle excitations, the Majorana states.

1.1.2 Topological Superconductors and Their Excitations

The topological classification discussed above applies to quadratic Hamiltonians, thus, in the discussion of topological superconductors a mean-field treatment is appropriate. Physically this is justified as the models we will be concerned with generally deal with proximity-induced superconductivity. The corresponding Hamiltonian can then be expressed in the framework of the Bogoliubov-de Gennes (BdG) equations

$$\hat{\mathbf{H}} = \frac{1}{2}\int dx\ \left(\hat{\psi}^\dagger(\mathbf{r}),\quad \hat{\psi}(\mathbf{r})\right)\begin{pmatrix}\hat{H}_0 & \hat{\Delta}\\ \hat{\Delta}^\dagger & \hat{H}_0^\dagger\end{pmatrix}\begin{pmatrix}\hat{\psi}(\mathbf{r})\\ \hat{\psi}^\dagger(\mathbf{r})\end{pmatrix}, \tag{1.1}$$

where $\psi(x)$ are fermionic annihilation (creation) operators in real space. $\hat{H}_0$ is the normal-state Hamiltonian, which can also contain a disorder potential, and $\hat{\Delta}$ is the pairing potential, which will be a function of the momentum operator $\hat{\mathbf{p}}$. In principle, the electrons'

spin can be included formally in this Hamiltonian by giving doubling the degrees of freedom of all entries in the above Hamiltonian: $\psi^{(\dagger)}(x)$ would become a spinor, and $\hat{H}_0$ and $\hat{\Delta}$ become 2×2-matrix operators. In the following we will restrict to spinless superconductors as these provide the simplest models of a topological superconductor. For equal-spin pairing to occur, the Pauli principle requires the pairing potential to be an odd function of momentum, which in its simplest– linear– form is the so-called p-wave superconductor.

The quasi-particle solutions to the above particle-hole symmetric Hamiltonian are superposition of electrons and holes

$$\gamma_\varepsilon = \int dx \left(u_\varepsilon(x)\psi(x) + v_\varepsilon(x)\psi^\dagger(x) \right) , \tag{1.2}$$

where $(u_\varepsilon(x), v_\varepsilon(x))^T$ is the eigenvector of the Bogoliubov-de Gennes Hamiltonian in Eq. 1.1 for the eigenenergy ε. The Hamiltonian is particle-hole symmetric in the sense that for every solution with positive energy ε, there exists a solution at $-\varepsilon$ with a corresponding eigenvector $(v^*_\varepsilon(x), u^*_\varepsilon(x))^T$. Thus, a redundancy is built into the framework as solutions at positive and negative energies correspond to a single fermionic state

$$\gamma_\varepsilon = \gamma^\dagger_{-\varepsilon} . \tag{1.3}$$

This equation implies that if an excitation at zero energy occurred, it would fulfill the so-called Majorana condition $\Gamma^\dagger = \Gamma$ and could be thought of as half a fermion. As the BdG equation has an even dimension by construction such Majorana excitations have to appear in pairs that could in principle gap out to finite energies but, as we will see below, in certain cases this can be avoided.

As already mentioned before, the simplest version of a topologically nontrivial superconductor is that of a p-wave superconductor, particularly one with pairing of the $p + ip$ type:

$$\hat{\mathbf{H}} = \frac{1}{2}\sum_{\mathbf{k}} \begin{pmatrix} \hat{c}^\dagger_{\mathbf{k}} & \hat{c}_{-\mathbf{k}} \end{pmatrix} \begin{pmatrix} \xi_{\mathbf{k}} & \hbar\Delta'(k_x + ik_y) \\ \hbar\Delta'(k_x - ik_y) & \xi^*_{-\mathbf{k}} \end{pmatrix} \begin{pmatrix} \hat{c}_{\mathbf{k}} \\ \hat{c}^\dagger_{-\mathbf{k}} \end{pmatrix} \tag{1.4}$$

where $\xi_{\mathbf{k}} = \hbar^2k^2/2m - \mu$ and $k = |\mathbf{k}|$. Such a system has been considered already in the study of the superfluid phases of Helium [Volo 76, Volo 99b, Volo 99a] but its importance in the context of their special zero-energy excitations has only been pointed out in 2000 by Read and Green, see Ref. [Read 00]. In a 2-dimensional system the p-wave superconductor hosts Majorana states as introduced above bound to the core of vortices in the superconducting parameter and, for an odd number of vortices, at the edge of the system. In a strictly 1-dimensional setting Majorana bound states appear as localized end states, where they can be viewed intuitively as the spatially separated halves of an electron [Kita 01]. The occupation of the latter does not enter the total energy of the system; it is decoupled. Consequently, there exists a two-fold degenerate ground state with the subspace spanned by two states distinguished by their occupancy of this fermion. As the superconductor can absorb only pairs of electrons, the Cooper pairs, transitions between these two ground states, which are accompanied by a unit change in the number of fermions, are protected by fermion parity.

The existence of Majorana states can be seen as a signature of topological superconductivity but the great interest and extensive research [Alic 12, Been 13a] on those excitations were sparked by a peculiar property: Their non-Abelian braiding statistics[Ivan 01]. In a 2-dimensional setup braiding paths are non-trivial in the sense that a particle can be taken around another one on a closed, non-contractable circle. Such an operation corresponds to a double exchange of two particles and will not change the two-particle wavefuncion when dealing with fermions or bosons. Particles do not necessarily have to follow bosonic or fermionic statistics but could, in principle, pick up any phase under exchange; then they are called *any*ons [Wilc 82]. As a phase factor, being a complex number, is commutative, the order in which several anyons are braided does not matter, they are 'Abelian' anyons. If the particles are associated with degenerate states that span a subspace in the Hilbert space, then a braiding process is associated with a unitary rotation in this degenerate subspace, which is generally non-commutative; such particles are called 'non-Abelian anyons'.

With the help of braiding operations on several particles it is in principle possible to define logical operations that can be used for topological quantum computation [Naya 08]. For these braiding protocols it is only important how often which particle has been taken around another one but not what the exact path was. In other words, only the topology of the braiding protocol matters, making them insensitive to local perturbations. Even though it has been shown that Majorana bound states do not allow for the implementation of all possible logical operations [Naya 08, Free 02], they are still useful tools in the search for universal topological quantum computation.

Even though there is speculation on whether the fractional Quantum-Hall state at filling 5/2, $SrRuO_4$-components or some oxide-interfaces might be p-wave superconductors, so far, no topological superconductors are known to occur in nature. However, it is possible to engineer those phases on the basis of systems which support proximity-induced superconductivity. The first proposal in this direction involved the surface of a strong topological insulator in contact to a superconductor, turning into an effective two-dimensional spinless $p+ip$-superconducting state [Fu 08]. Even though such a two-dimensional topological superconductor is of great interest, for general purposes of detecting and manipulating Majorana bound states they are not ideal. The vortices needed for those bound states might be poorly, or even not at all, accessible and their positions and number will generally not be known precisely. In contrast, in a topologically superconducting wire the Majoranas are unambiguously localized at the ends of the wire and easily accessible to, for instance, transport experiments. In the following section, such wires and their realizations will be discussed.

1.2 Topologically Superconducting Wires

It has been pointed out by Kitaev in 2001, see Ref. [Kita 01], that a 1-dimensional system with p-wave superconducting pairing exhibits a parameter range with a topologically nontrivial phase signalized by the existence of a zero-energy bound state at the wire's ends—a Majorana state. As mentioned above, these states can be viewed as the halves of an electron that decouple from the system, which can be seen easily in a tight-binding version

Figure 1.3: Schematic view of the topologically non-trivial phase of the Kitaev chain. The grey shaded regions mark the electronic sites ($j = 1 \cdots L$), each with two Majorana operators. At the special point $\Delta = t$, $\mu = 0$ discussed in the main text, the onsite terms (equal j) vanish and the Majoranas are coupled only to their nearest neighbours at the next site $j, j+1$ for $j = 1, L-1$, signified by thick grey lines. The Majorana operators at the two ends of the chain decouple from the rest of the system and form together a fermionic zero-energy excitation.

of a p-wave superconductor

$$H = -\sum_{j=1}^{N} \mu c_j^\dagger c_j + t\left(c_j^\dagger c_{j+1} + c_{j+1}^\dagger c_j\right) - \Delta\left(c_j c_{j+1} + c_{j+1}^\dagger c_j^\dagger\right) \tag{1.5}$$

where μ is the chemical potential, t is the normal hopping parameter and $\Delta \geq 0$ the superconducting parameter, which is assumed to be real for simplicity. One can formally split up the electron operators into their real and imaginary parts $c_j = a_{2j-1} + i a_{2j}$, which are hermitian operators describing Majorana fermions, yielding

$$H = -\frac{i}{2}\sum_{j=1}^{N} \mu a_{2j-1}a_{2j} + (t+\Delta)a_{2j}a_{2j+1} + (-t+\Delta)a_{2j-1}a_{2j+2}\,. \tag{1.6}$$

Consider the special point in the non-trivial phase $\Delta = t$ and $\mu = 0$, where the Majorana fermions connect only to neighboring electronic sites but not within one site, see Fig.1.3 and the operators at the ends, a_1 and a_{2L} remain uncoupled. These are the Majorana end states and the fermion $f = a_1 + i a_{2L}$ that they recombine to, defines the ground state degeneracy. The topological phase associated with this picture extends in parameter space and has a boundary to a trivial phase at $\pm 2t = \mu$. Away from the special point discussed here, the Majorana states will not sit only on a single site but it will have a wavefunction extending into the wire, however, exponentially decaying on a scale of the superconducting coherence length $\xi \propto 1/\Delta$. These zero-energy endstates are robust to moderate amounts of disorder.

1.2.1 Realizations of P-wave Superconducting Wires

The continuum generalization of the tight-binding model introduced above is a spinless p-wave superconducting wire, described in the Bogoliuobov-de Gennes picture by a one-dimensional version of Eq. 1.4. Such wires do not exist by themselves in nature but one can engineer one-dimensional or quasi-one dimensional systems that exhibit an effective p-wave pairing. Proposals include proximity-coupled topological insulator edges [Fu 08],

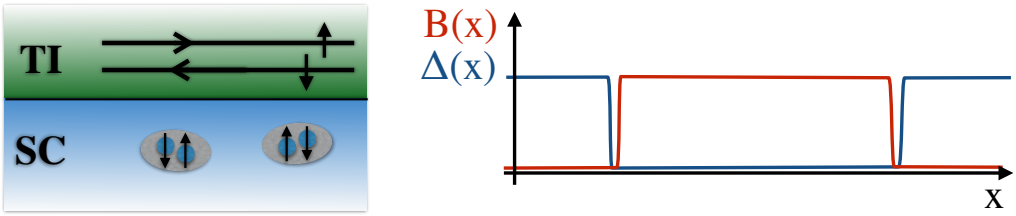

Figure 1.4: Left panel: Sketch of a topological insulator edge with helical edge state in proximity to a superconductor with spin-singlet Cooper pairs; Right Panel: Spatial profile of pairing potential and magnetic field as discussed in the main text. Majorana bound states will form at the boundaries.

semiconductor wires with strong spin-orbit coupling on a conventional superconductor [Oreg 10, Lutc 10], or ferromagnetic wires in proximity to superconductor with spin-orbit coupling [Duck 11, Chun 11, Pott 12].

Topological Superconductivity at the Surface of a Topological Insulator: The first attempts to construct a system that harbors Majorana states involved the surfaces of 3-dimensional or 2-dimensional topological insulators [Fu 08]; here, we focus on the second case. The edge of a quantum spin hall insulator as introduced in Ref. [Kane 05a] is a gapless, chiral system, which can be proximity coupled to an s-wave superconductor easily as counter-propagating modes carry opposite spins, see Fig. 1.4. For Majorana states to form a time-reversal symmetry breaking term is needed, such as an additional magnetic field . The Bogoliubov-de Gennes Hamiltonian of such a system reads

$$H_0 = v_F p \tau_z \sigma_x - B(x)\tau_z\sigma_z - \Delta(x)\tau_y\sigma_y \,, \tag{1.7}$$

where σ_i/τ_i are Pauli matrices in the spin/ electron-hole subspace, respectively, v_F is the Fermi velocity and x the longitudinal coordinate along the edge. For Majorana bound states to occur, the magnetic field B and the pairing potential Δ can in principle coexist and vary spatially in an appropriate fashion, but here we concentrate on the case were only on of the is non-zero at a time, see Fig. 1.4.

In a region where $B = 0$ but $\Delta \neq 0$, the system will show an effective p-wave pairing potential, however, still obeying time-reversal symmetry. For Majorana states to occur, a boundary has to be created. A region with $\Delta = 0$ and $B \neq 0$ will be gapped as well and simulate a vacuum to the this effecitve one-dimensional p-wave superconductor. At the boundary between these two, a zero-energy Majorana state appears.

Similarly, on the surface of a strong topological insulator a state resembling a 2-dimensional $p + ip$ superconductor is found, which has recently been investigated experimentally [Wied 15].

Spin-Orbit Coupled Semiconductor Wire on a Superconductor The previous setup in a way relied on a topologically superconducting state being formed when proximity-coupling an already topological state. However, it is also possible to construct an effective

p-wave superconductor from less exotic ingredient: a semiconductor wire with fairly strong spin-orbit coupling, subject to a magnetic field and a conventional s-wave superconductor [Oreg 10, Lutc 10], see Fig. 1.5. This is the system, which is experimentally best explored and most relevant to this Thesis. The general idea is that if one succeeds to induce superconductivity into a spin-polarized system, the pairing is necessarily of a spin-triplet and therefore odd in momentum. The underlying superconductor has s-wave pairing, which creates spin-singlet Cooper pairs, and without any further ingredients no superconductivity can be induced in the wire. This problem can be overcome with the help of spin-orbit interactions as can be seen below.

We choose again a description in the Bogoliubov-de Gennes picture

$$H(p) = (p^2/2m - \mu)\tau_z\sigma_0 + \alpha p\tau_0\sigma_x + B\tau_z\sigma_z + \Delta\tau_y\sigma_y\,, \tag{1.8}$$

where, again, σ_i/τ_i are Pauli matrices in the spin/ electron-hole subspace, respectively. Further, m is the effective mass and μ the chemical potential. The magnetic field B separates the two spin bands such that one obtains a spin-polarized system when the chemical potential μ is placed in between them. The spin-orbit coupling α allows proximity-induced superconductivity to be effective for the 'polarized' system as it breaks the spin-polarization axis in the wire and gives a finite singlet component to each pair of electronic excitations with momentum $p, -p$. Then, p-wave and s-wave type pairing terms coexist, with the first one dominating when $|B| > \sqrt{\Delta^2 + \mu^2}$. In this case, the wire is in a topologically non-trivial phase with Majorana bound states at its end. In the opposite case, $|B| < \sqrt{\Delta^2 + \mu^2}$, the magnetic field is not strong enough to polarize the wire, which is thus in its trivial, and no zero-energy states appear.

The low-energy part of the excitation spectrum exhibits two gaps: one at the Fermi points $p = \sqrt{2\mu m}$, controlled by Δ, and one at the center of the Brillouin zone $p = 0$, controlled by B and Δ. The latter is crucial to the existence of Majorana states and controls the entire physics in the limit of strong spin-orbit coupling $m\alpha^2 \gg B$. There, the Hamiltonian can be restricted to small momenta and one recovers the topological insulator edge in Eq. 1.7. The opposite limit $m\alpha^2 \ll B$ is adiabatically connected, but in this case the low energy subspace can be directly mapped onto a p-wave superconductor, a one-dimensional version of Eq. 1.4. This can be seen by writing the Hamiltonian in a basis of states that diagonalize the semiconductor wire in the absence of a superconductor and evaluating the effect of the pairing term perturbatively in this basis [Alic 11]. The difference of these two cases before the pairing term is taken into account are illustrated in Fig. 1.5.

As semiconductor wires, such as InAs or GaAs are readily available to experiments and well studied, a lot of experimental effort is going on to realized such systems [Mour 12, Das 12, Deng 12, Will 12, Rokh 12, Chur 13, Deng 14]. The individual observables that can be used to probe the topological phase will be discussed below. Here we only note that the wires used here are generally believed to be in a multichannel regime, which can also lead to a multichannel p-wave superconductor, which will be discussed in Chapter 2.

Ferromagnetic Wires Proximity Coupled to a Superconductor with Spin-Orbit Interactions Above, we discussed the possibility of creating an effective p-wave superconducting

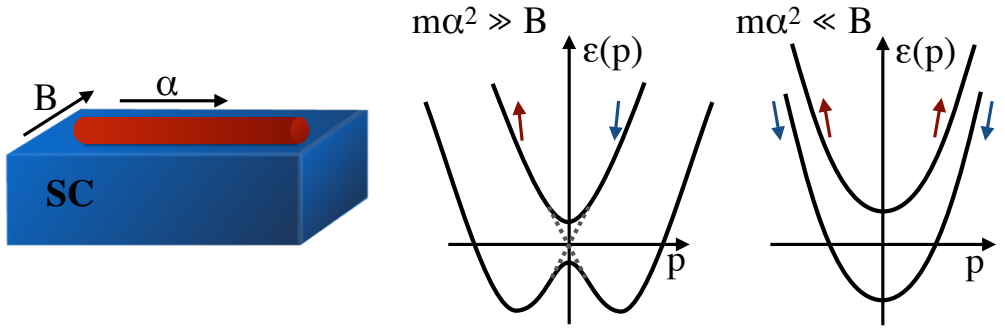

Figure 1.5: Left Panel: Illustration of semiconductor wire with spin-orbit coupling α and perpendicular magnetic field B on a superconductor; Right Panel: Normal state dispersion for the different limits of the topological non-trivial phase, $m\alpha^2 \gg B$ and $m\alpha^2 \ll B$, with spin direction for bands indicated.

state with the help of spin-orbit interactions in the wire where superconductivity should be induced. However, the spin-orbit coupling does not necessarily have to be in the wire but it could also be in the superconductor. This is the idea of another set of proposals to obtain Majorana states involving a ferromagnet (or half-metal) wire in proximity to a superconductor with strong spin-orbit coupling. In the latter, spin-polarization axis for the Cooper pairs is broken, which will allow a proximity effect to spin-polarized electrons in the wire to pair. The induced superconducting gap in the wire is then proportional to the spin-orbit coupling strength [Duck 11, Chun 11, Pott 12].

In principle, this scenario does not require an actual wire but it is enough to place a chain of magnetic atoms, forming a ferromagnet, on top of a superconductor. This approach has been realized recently in an experiment with Fe-atoms deposited on the surface of Pb, demonstrating the existence of zero-energy states strongly localized at the ends of the chain [Nadj 14].

1.2.2 Signatures of the Topological Phase in Transport Experiments on Wires

In the course of the last years many ways have been theoretically proposed to measure Majorana states and thereby prove the existence of the topologically superconducting phase. Some of those have been realized experimentally and the aim of this subsection is to give a brief overview over those efforts, focusing on the transport properties of the wires.

One of the simplest measurements that can be made to probe the topological superconductor is a measurement of the local density of states at one of the wire's ends. For this, a junction between a normal metal lead and the proximity coupled semiconductor wire is created with a tunneling barrier in the normal region. For weak tunneling, the conductance at a voltage bias V [Blon 82]

$$G_{\mathrm{NS}}(eV) = \frac{2e^2}{h}\mathrm{tr}\left(1 - r_{ee}(eV)r_{ee}^{\dagger}(eV) + r_{eh}(eV)r_{eh}^{\dagger}(eV)\right) \tag{1.9}$$

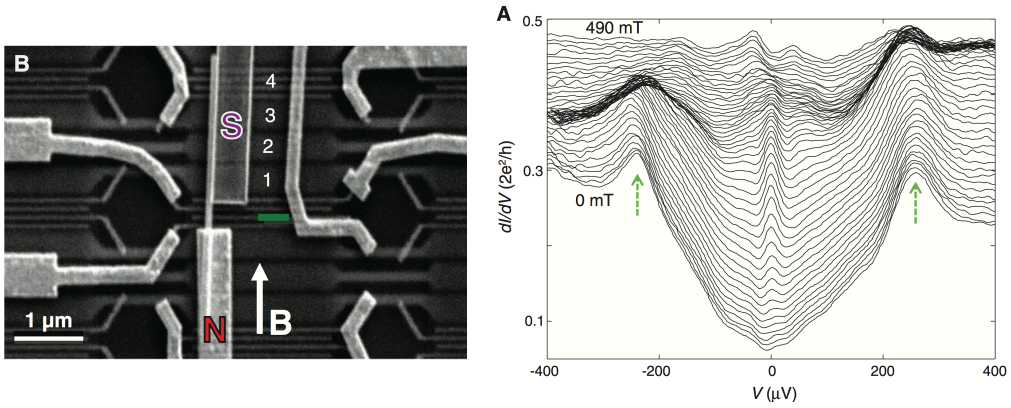

Figure 1.6: Left Panel: Picture of the experimental setup for a semiconductor wire (InSb) deposited on top of a superconducting electrode (NbTiN); Right Panel: Differential conductance dI/dV as function of bias voltage. Different curves correspond to different magnetic fields from $B = 0\,T$ to $B = 490\,mT$ and are offset for clarity. Figures taken from Ref. [Mour 12]

with the normal and Andreev reflection matrices for an electron impinging from the normal lead r_{ee} and r_{eh}, reflects the tunneling density of states at the wire's end at $\varepsilon = eV$. This can be understood in a picture of resonant tunneling: If the barrier is strong, an electron will be reflected there with a high probability. Andreev reflection can only occur if an electron passes to the superconductor, a process that is strongly suppressed unless promoted by a state that is formed between the superconductor and the barrier. In a p-wave superconductor, the Majorana state at zero energy will allow electrons to tunnel to the interface resonantly where they Andreev reflect. The corresponding conductance will exhibit a peak around zero energy, which should be quantized to $2e^2/h$ [Law 09, Wimm 11].

Several experiments aimed to measure this conductance peak in topologically superconducting wires fabricated from semiconductor wires [Mour 12, Das 12, Deng 12, Chur 13, Finc 13]. An example of the experimental setup and the corresponding data for the differential conductance dI/dV taken from Ref. [Mour 12] are shown in Fig. 1.6. In all experiments, the results are compatible with the theoretical expectations in that the zero-bias peak in the differential conductance shows up in a reasonable parameter range. Even though this can be caused by a Majorana bound state at the end of the wire, these measurements are not smoking-gun signatures of the topologically superconducting phase. In particular such a signature in the conductance does not necessarily have to originate from a Majorana bound state. Various mechanisms have been discussed to also cause a zero-bias peak, for example by disorder [Liu 12], a smooth confinement potential [Kell 12b] or the Kondo mechanism [Lee 12].

Another way of observing a zero-energy states that has been pursued in an experiment [Nadj 14] is to measure the local density of states with a STM-tip. With this it was also possible to also the localization of this bound state at the wire end.

Many more schemes to distinguish the topological non-trivial from the trivial phase have been suggested theoretically and are awaiting for experimental realization. For example,

the existence of a Majorana state has a unique signature in the ballistic limit of a normal metal-superconductor junction: Creating a quantum point contact in the normal metal and tuning the gate voltage to the single or few channel limit, one finds a first conductance step that is quantized to $2e^2/h$ is the superconductor is in a topologically non-trivial phase, as opposed to $4e^2/h$ for a conventional superconductor or e^2/h without any superconductor. In the presence of disorder, this signature is robust in the single-mode regime whereas the other two cases suffer from localization [Wimm 11]. Another possibility is to consider non-local transport for a topologically superconducting wire with normal metal leads attached to both ends[Nils 08, Fu 10]. A process called crossed Andreev reflection, which consists of a Cooper pair made up of electrons from the two different wires entering the wire, is enhanced by the presence of Majorana bound states and yields, for instance, a maximally correlated current noise.

Yet another promising route for the detection of Majorana states are topological Josephson junctions. These are built from two p-wave wires, with Majorana states at their ends, which are connected by a normal metal piece. The pairing potentials of the two superconductors have a relative phase difference ϕ. The Majoranas at the two connected ends hybridize and form a fermionic bound state with an energy that is 4π-periodic in the phase difference [Kita 01].

$$E = E_0 \cos \phi/2 \,. \tag{1.10}$$

In such setups, a dissipationless current—the Josephson current—may flow, which is just the derivative of the energy with respect to the phase and therefore also 4π-periodic, in contrast to the conventional 2π Josephson current. This is called the fractional Josephson effect. In a many-body state, this bound state can be either occupied or not and the two cases correspond to opposite Josephson currents. The energy spectrum of the two is related by shifting $\phi \to \phi + 2\pi$, causing an ambiguity in the ground state. In principle, a single electron can be added to the junction at low energy cost, which leads to a transition between those two ground states. However, as the superconducting wires, acting as leads to the junction, can only supply pairs of electrons, the Cooper pairs, such a transition is forbidden by the conservation of fermion parity. One says that the fractional Josephson effect is protected by fermion parity.

In a real system, this protection will always be broken by coupling to the environment, making it impossible to observe the fractional Josephson effect directly in the current-phase relation. Several theoretical proposals are dealing with the dynamics of the junction instead which can be used to reveal its topological nature. For example, it has been pointed out that the 4π-periodicity could be observed in the Shapiro steps, which are plateau-like features in the current-voltage characteristics of a *dc*-current biased Josephson junction exposed to an additional *ac*-voltage or current bias [Jian 11, Domi 12]. This has been probed experimentally for semiconductor wires, see Ref. [Rokh 12], finding results consistent with the theoretical predictions. Other works consider the dynamics [San 12, Piku 12] and current noise [Badi 11] of voltage-biased Josephson junctions.

Another possibility to examine the Majorana state is by probing directly its non-Abelian statistics [Alic 11]. Within the semiconductor model, a Majorana end state can be moved around by modulating the chemical potential spatially by means of many small gates below the wire that can be controlled individually. Then, one can build networks of

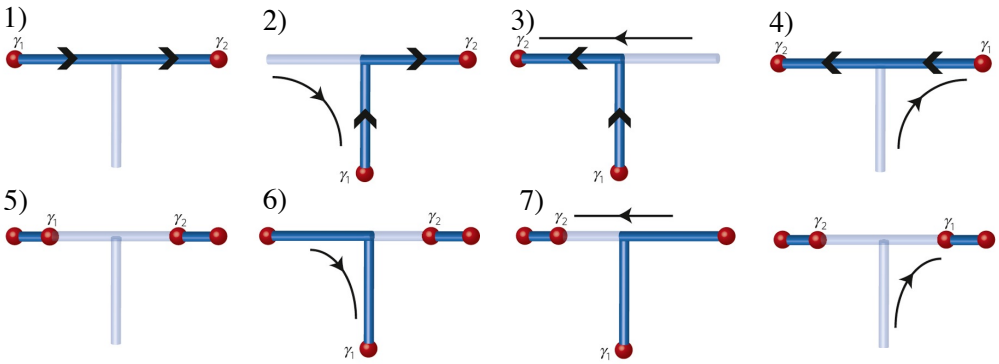

Figure 1.7: Visualization of a braiding protocol for two Majoranas at a T-junction of topologically superconducting wires. Blue regions indicate topologically non-trivial, grays regions trivial phases.

topologically superconducting wires and use those for braiding. For instance, at a T-junction, two Majoranas can be braided in a simple protocol as visualized in Fig. 1.7. Such a realization would certainly be a smoking-gun signature, however, is currently still out of experimental reach.

1.2.3 Disorder in P-wave Superconducting wires

A general feature of topological phases is their robustness to small, local perturbations that conserve the essential symmetries, such as disorder. Also p-wave superconductivity, and thereby the existence of the Majorana end state, is protected against moderate amounts of disorder. However, for spin-triplet pairing, Anderson's theorem [Ande 59] does not apply and one expects disorder to be effective once it becomes strong enough. Indeed, disorder causes states to localize in the superconducting gap which accumulate at zero-energy, eventually causing a topological phase transition [Motr 01]. Considering Gaussian white noise chemical potential disorder, $\mu \to \mu + V(x)$, with

$$\langle V(x) \rangle = 0 \qquad \text{and} \qquad \langle V(x)V(x') \rangle = \frac{v_F^2}{l} \delta(x - x') \,, \tag{1.11}$$

where v_F is the Fermi velocity and l is the normal-state mean free path used to parametrize the disorder strength, an analytical analysis of this phase transition can be performed [Brou 11a]. At a critical disorder strength $l = \xi/2$ a delocalization at zero energy due to the disorder-localized states occurs, causing the Majorana states at the ends to gap out. This transition is accompanied by a universal signature in the density of states: the Dyson singularity

$$\nu(\varepsilon) = \frac{1}{\varepsilon \left| \ln \varepsilon \right|^3} \,. \tag{1.12}$$

This result is valid for a p-wave superconducting wire with a certain disorder strength. It is important to note, however, that when considering this as the effective model of, say,

a semiconductor wire on a conventional superconductor the effective disorder strength can deviate from the one in the parent wire. In particular, it depends on the Zeeman field B, see Eq. 1.8, needed to drive the semiconductor wire into a topologically non-trivial phase, see Ref. [Brou 11b].

1.2.4 Quasi-One Dimensional P-wave Superconductors

The Kitaev-chain introduced above is the tight-binding model of the prototypical p-wave superconductor, the effective model of the proximity coupled semiconductor and ferromagnet wires. In this thesis we will be concerned with a multichannel generalization of this model which is introduced here. We consider spinless electrons with superconducting pairing in a strip geometry. The simplest multichannel generalization of the Kitaev chain is a square lattice with $N_x \times N_y$ lattice sites, where $Ny \ll N_x$ [Pott 10]. There is normal nearest neighbor hopping and a superconducting pairing term, which in real space involves also nearest neighbors

$$H = \sum_{i,j} \Big[-\mu c^\dagger_{i,j} c_{i,j} - t \left(c^\dagger_{i+1,j} c_{i,j} + c^\dagger_{i,j+1} c_{i,j} + \text{h.c.} \right) + \left(i\Delta_x c^\dagger_{i+1,j} c^\dagger_{i,j} - \Delta_y c^\dagger_{i,j+1} c^\dagger_{i,j} + \text{h.c.} \right) \Big] , \tag{1.13}$$

where the indices i, j label the x, y-coordinate as $x = ia$, $y = ja$, with the lattice constant a and run from 1 to N_x, N_y,respectively. μ is the chemical potential, t is the hopping strength, and Δ_x, Δ_y are the superconducting pairings strengths associated with a momentum in x, y. We will consider the continuum version of this model, which is obtained by considering the limit of $a \to 0$, while keeping the length $L = N_x a$ and width $W = N_y a$ constant [Kell 12a]. Upon identifying $\mu + 4t \to \mu$, $\hbar^2/ta^2 \to 2m$, and $\Delta_{x/y} a/2\hbar \to \Delta'_{x/y}$ we find a Hamiltonian

$$H = \int_0^L dx \int_0^W dy \left(\psi^\dagger(x,y), \quad \psi\ (x,y) \right) \left[\frac{1}{2} \left(\hat{\mathbf{p}}^2 - \mu \right) \sigma_z + \Delta'_x \hat{p}_x \sigma_x + i\Delta'_y \hat{p}_y \sigma_y \right] \begin{pmatrix} \psi\ (x,y) \\ \psi^\dagger(x,y) \end{pmatrix} \tag{1.14}$$

with the momentum operator $\hat{\mathbf{p}} = (\hat{p}_x, \hat{p}_y)$. In the following we will restrict to the limit of a narrow strip $W \lesssim \xi = \hbar/m\Delta'_x$, in which bound states appear only at the ends of the wire at $x \simeq 0, L$ and no lateral edge modes at $y \simeq 0, W$ appear [Pott 10]. Particularly in the limit of a very narrow wire $W \ll \xi$ the Hamiltonian can be simplified: the transverse momentum will be of the order of the inverse width $\langle \hat{p}_y \rangle \sim \frac{\hbar}{W}$. Thus, the pairing energy associated with the transverse direction is much smaller than the corresponding kinetic energy

$$\langle \Delta'_y \hat{p}_y \rangle \sim \frac{\hbar^2}{m\xi W} = \frac{\hbar^2}{mW^2} \frac{W}{\xi} \quad \ll \quad \langle \frac{\hat{p}_y^2}{2m} \rangle \sim \frac{\hbar^2}{mW^2} , \tag{1.15}$$

and can be treated in perturbation theory. The zeroth-order Hamiltonian can then be solved analytically with the wavefunctions quantized in the transverse direction with a

wavenumber $k_y = \hbar n\pi/W$, $n = 1, 2, ...$ The number of occupied transverse channels N is determined by the chemical potential

$$N = \text{int}\left(\frac{W}{\pi}\sqrt{k_F^2 - \xi^{-2}}\right), \tag{1.16}$$

with $k_F^{-1} \ll \xi$. Each transverse channel independently forms a one-dimensional p-wave superconductor with an energy spectrum

$$E_n(k_x) = \pm\frac{\hbar^2}{2m}\sqrt{\left(k_x^2 - k_n^2\right)^2 + 4\left(k_x\xi^{-1}\right)^2} \tag{1.17}$$

$$k_n^2 = k_F^2 - \frac{n^2\pi^2}{W^2} \tag{1.18}$$

and a Majorana bound state at each end. The wavefunction of the Majorana in the n-th channel at, for instance, the left end $x \simeq 0$ is

$$\phi_n(x, y) \propto \sin\left(\frac{n\pi y}{W}\right)\sin(k_n x)e^{-x/\xi} \tag{1.19}$$

up to a normalization factor. In total there will be N decoupled Majorana states at each end of the wire.

The effect of the perturbation on the low-energy spectrum is then two couple the zero-energy states which causes them to gap out in pairs [Kell 12a]. For an odd number of channels one therefore recovers a topologically non-trivial phase while an even number of channels will result in a trivial phase without Majorana bound states. In particular, upon changing the chemical potential one can change the parity of the number of channels, which causes an alternation between topologically trivial and non-trivial phases [Pott 10, Kell 12b], see Fig. 1.8 a). The gapped-out states will form subgap states that cluster around zero energy, see Fig. 1.8 b). The low-energy spectrum of such a multichannel p-wave superconductor will be discussed in the main text, see Chapter 2.

For wires that are broader, $W \simeq \xi$, the perturbative treatment employed before is analytically not justifiable. However, in a numerical analysis the same qualitative behavior is found [Kell 12a].

A different way to think about this perturbative approach is in term of the symmetry classification introduced before, see Fig. 1.2. The full Hamiltonian 1.14 has only particle-hole symmetry, placing the system in symmetry class D, which allows for a topological phase that is characterized by a $\mathbb{Z}_2$-number. This is just some binary value indicating whether a Majorana bound state is present or not. In zero-th order in the superconducting transverse coupling $\Delta' p_y$ an effective time-reversal symmetry (with the corresponding operator $\mathcal{T}^2 = 1$) is restored, which results in a chiral symmetry. In particular the reduced system is in symmetry class BDI and the topological invariant is a $\mathbb{Z}$-number, which corresponds here to the total number of Majorana bound states at each wire end.

The description with the strip geometry employed results in an effective Hamiltonian in the subspace of occupied channels, where to zeroth order each channel is an independent one-dimensional p-wave superconductor at a renormalized chemical potential $\mu_n = \hbar^2/2mk_n^2$. In principle one could also employ a picture of equivalent channels,

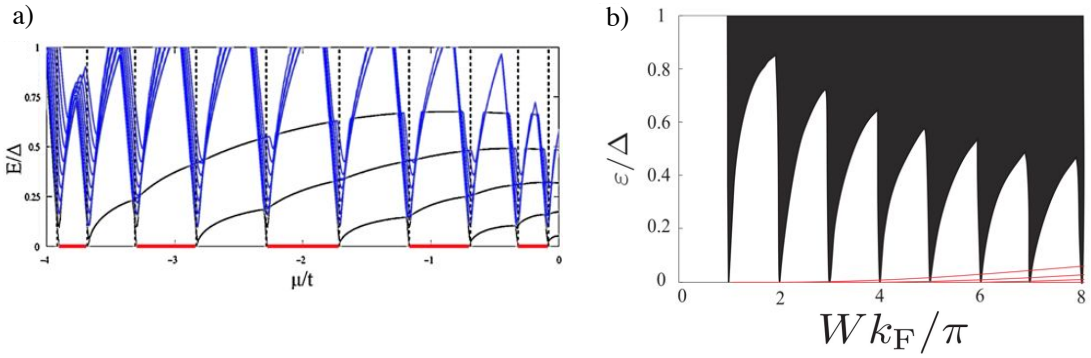

Figure 1.8: Spectrum of a multichannel p-wave superconducting wire as a function of the chemical potential. Panel a) Figure from [Pott 10]: Alternation of topologically trivial and non-trivial phases as the parity of the number of channels changes, $W \sim \xi$; Panel b) Figure from [Kell 12a]: The clustering of subgap states around zero-energy for narrow wires $W \ll \xi$.

where the number of channels is fixed and the chemical potential is the same for all of them. For the physics discussed in the main part of this thesis, these two approaches are qualitatively similar.

As discussed above, the model of a semiconductor wire in proximity to a s-wave superconductor yields an effective p-wave superconductor. In an experiment, those wires will generally be in a multichannel regime. This does not imply immediately an effective multichannel p-wave superconductor but there is a parameter range in which the model discussed in this section can be realized, which will be discussed in Chapter 2

1.3 Methods: Scattering Theory

The main method used in the projects comprising this thesis is the formalism of scattering theory, a description of quantum transport valid for low temperatures and voltages, and in the absence of interactions [Land 57, Land 87, Butt 86, Butt 88]. It provides a powerful framework to treat mesoscopic systems [Been 91, Been 97]. We here review briefly its main aspects.

1.3.1 General Introduction

A system, such as a wire can be described by its scattering properties by attaching a number of leads, in which electronic wave can propagate freely, to it. The system under study is then viewed as a scatterer and many physical observable can be deduced in this approach. Here, we will consider only the cases of one or two metallic leads, which could have several transverse modes.

Consider now the case of two leads attached to a scattering region, see Fig. 1.9, with N propagating modes arising from a transverse quantization. We restrict to one transverse, the y, direction and consider a hard-wall boundary confinement of width W. The basis

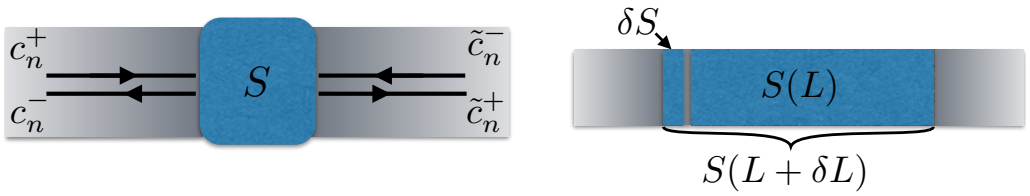

Figure 1.9: Left panel: Schematic view of a scatterer with a scattering matrix S connected to two leads with incoming modes c_n^+, $\tilde{c}_n^-$ and outgoing modes c_n^-, $\tilde{c}_n^+$. Right panel: The concatenation of a scattering matrix of a wire with length L and a short piece of length δL to a combined scattering matrix $S(L+\delta L)$.

states in the leads are then electronic wavefunctions at an excitation energy ε propagating to the left and right

$$\psi_{\pm,n}(x,y) = \sqrt{\frac{2m}{W\hbar k_n}} \sin\left(\frac{n\pi y}{W}\right) e^{\pm i k_n x}\,,$$
$$k_n = \sqrt{\left(k_F^2 - \frac{n^2\pi^2}{W^2}\right)} \tag{1.20}$$

with $n = 1, \cdots, N$ and the electron mass m. One could also consider a multichannel lead arising from a strip geometry such as in Sec. 1.2.4, which would add a transverse wave function $\propto \sin(n\pi y/W)$ to the basis states and modify the momentum and velocity $k(\varepsilon), v(\varepsilon) \to k_n(\varepsilon), v_n(\varepsilon)$ accordingly.

The scatterer connects the different basis states with coefficients $c_n^\pm$ in the left lead and $\tilde{c}_n^\pm$ in the right lead. For notational convenience we will suppress the dependence on the energy for the coefficients in the following. There is a set of coefficients propagating towards the scatterer, C^{in}, and one set C^{out} leaving it

$$C^{\text{in}} = \begin{pmatrix} \mathbf{c}^+ \\ \tilde{\mathbf{c}}^- \end{pmatrix}, \qquad C^{\text{out}} = \begin{pmatrix} \mathbf{c}^- \\ \tilde{\mathbf{c}}^+ \end{pmatrix}, \tag{1.21}$$

where $\mathbf{c}^+ = (c_1^+, c_2^+, ..., c_N^+)^T$. These coefficients are related to each other by the scatterer, which is captured in a scattering matrix

$$C^{\text{out}} = S(\varepsilon) C^{\text{in}}\,, \qquad S(\varepsilon) = \begin{pmatrix} r(\varepsilon) & t'(\varepsilon) \\ t(\varepsilon) & r'(\varepsilon) \end{pmatrix}, \tag{1.22}$$

which has to be unitary $S^\dagger S = 1$ and describes reflection in the left/right lead r, r' and transmission from the left to the right t and vice versa t'.

If the scatterer is a superconductor, electrons can be reflected or transmitted into as a hole; a process called Andreev reflection [Andr 64]. It is the scattering formulation of the proximity effect, where a electron is absorbed into a superconductor, where it has to form a Cooper pair, which happens by the emission of a hole. This process can be incorporated

into the scattering matrix with an electron-hole grading of the basis states

$$\psi^{(\mathrm{e})}_{\pm,n}(x) = \frac{1}{2\pi v_F}\begin{pmatrix}1\\0\end{pmatrix} e^{\pm i k_F x}\,, \tag{1.23}$$

$$\psi^{(\mathrm{h})}_{\pm,n}(x) = \frac{1}{2\pi v_F}\begin{pmatrix}0\\1\end{pmatrix} e^{\mp i k_F x}\,, \tag{1.24}$$

Note that for hole-like wave functions the group velocity is reversed, such that right-moving modes have negative momentum $-k_F$. With this, the coefficients for incoming and outgoing waves become vectors $c^{\pm}_n = \begin{pmatrix} c^{\pm(\mathrm{e})}_n \\ c^{\pm(\mathrm{h})}_n \end{pmatrix}$ and the reflection and transmission matrices double their dimensions accordingly

$$r^{(\prime)}(\varepsilon) = \begin{pmatrix} r^{(\prime)}_{\mathrm{ee}}(\varepsilon) & r^{(\prime)}_{\mathrm{eh}}(\varepsilon) \\ r^{(\prime)}_{\mathrm{he}}(\varepsilon) & r^{(\prime)}_{\mathrm{hh}}(\varepsilon) \end{pmatrix}\,, \qquad t^{(\prime)}(\varepsilon) = \begin{pmatrix} t^{(\prime)}_{\mathrm{ee}}(\varepsilon) & t^{(\prime)}_{\mathrm{eh}}(\varepsilon) \\ t^{(\prime)}_{\mathrm{he}}(\varepsilon) & t^{(\prime)}_{\mathrm{hh}}(\varepsilon) \end{pmatrix}\,. \tag{1.25}$$

In a similar fashion one could also take a spin-degree of freedom into account, which is, however, not relevant in the following.

The symmetries that are obeyed by the system acting as a scatterer restrict also the scattering matrix. Considering the system's Hamiltonian in a Bogoliubov-de Gennes formulation in momentum space, particle-hole symmetry can be expressed as $\sigma_x H^*_{-k}\sigma_x = -H_k$, and a form of time-reversal symmetry that will be considered later as $\sigma_z H^*_{-k}\sigma_z = H_k$, where σ_i are Pauli matrices acting in particle-hole space. The latter is obeyed for example in the $p + ip$-wave superconducting Hamiltonian introduced in Eq. 1.4, when $\Delta' k_y = 0$. These symmetries can be translated to the scattering properties and are expressed in terms of the scattering matrix as

$$S(\varepsilon) = \sigma_x S^*(-\varepsilon)\sigma_x \quad \text{and} \quad S(\varepsilon) = \sigma_z S^T(\varepsilon)\sigma_z\,, \tag{1.26}$$

respectively.

The scattering matrix can in principal be found by solving for the wave function in the scatterer, which from now on will be a wire, and matching it to the free modes in the leads with the initial condition that one coefficient of incident wave is 1 while all others are zero. However, an analytical solution can not always be found, as for example in the presence of disorder. In this case, one can construct the scattering matrix for a wire of length L by concatenating it from many small, identical pieces of length δL. If those pieces are short enough, their scattering matrices can be calculated analytically in Born approximation to linear order in δL. The coefficient of the scattering matrix connecting a particular incoming, initial state $\phi_i(x)$ at energy ε_i to a particular outgoing, final state $\phi_f(x)$ at energy ε_f is

$$\delta S_{i,f} = \delta_{i,f} - 2\pi i \delta(\varepsilon_f - \varepsilon_i) \int_0^{\delta L} dx\, dx'\, \phi^*_f(x)\phi_i(x')T(x,x')\,, \tag{1.27}$$

with the T-operator $T(x,x') = \langle x|\hat{T}|x'\rangle$. The latter contains the information on the scatterer and can be written in the Born series

$$\hat{T} = \hat{V} + \hat{V}\left(\varepsilon_i - \hat{H}_0 + i\eta\right)^{-1}\hat{V} + \hat{V}\left(\varepsilon_i - \hat{H}_0 + i\eta\right)^{-1}\hat{V}\left(\varepsilon_i - \hat{H}_0 + i\eta\right)^{-1}\hat{V} + \cdots , \tag{1.28}$$

where $\hat{V}$ is the part of the Hamiltonian that distinguishes the short piece of the wire from the leads, where $\hat{H} = \hat{H}_0$. With this, the scattering matrix δS can be obtained to linear order in δL, which for disorder requires the second order Born approximation in $\hat{T}$.

Two scattering matrices of adjacent scatterers can be combined to a single one with an infinite series expansion, taking into account all possible paths an electron could take. The scattering matrix of a wire with length $L+\delta L$, $S(L+\delta L)$, can thus be obtained from the concatenation of $S(L)$, with reflection and transmission matrices $r^{(\prime)}(L), t^{(\prime)}(L)$, and δS,with reflection and transmission matrices $\rho^{(\prime)}, \tau^{(\prime)}$, see Fig. 1.9. For instance,

$$\begin{aligned} r(L+\delta L) &= \rho + \tau' r(L)\tau + \tau' r(L)\rho' r(L)\tau + \cdots = \rho + \tau'\, r(L)\frac{1}{1-\rho' r(L)}\,\tau \\ t(L+\delta L) &= t(L)\tau + t(L)\rho' r(L)\tau + t(L)\rho' r(L)\rho' r(L)\tau + \cdots = t(L)\frac{1}{1-\rho' r(L)}\tau\,. \end{aligned} \tag{1.29}$$

In this way one can construct the scattering matrix at arbitrary lengths.

1.3.2 Probing Topological Phases with a Scattering Matrix

An, in the context of this thesis, important feature of scattering matrices is the information on the scatterer's topological phase encoded in them: the reflection amplitude of a wire at $\varepsilon = 0$ allows for a direct computation of the topological quantum number characterizing the topological phase [Fulg 11]. In particular, if the wire is in its topologically non-trivial phase the Majorana bound state at its end will give rise to resonant Andreev reflection [Wimm 11], which shows up explicitly in the scattering matrix. We here review the approach given in Ref. [Fulg 11] for the symmetry classes of interest to this thesis, class D and BDI, adapting the arguments to scattering matrices in the basis of electrons and holes.

The scattering matrix of a p-wave superconducting wire at $\varepsilon = 0$ can be parametrized as

$$r(\varepsilon = 0) = \begin{pmatrix} r_{\mathrm{ee}} & r_{\mathrm{eh}} \\ r^*_{\mathrm{eh}} & r^*_{\mathrm{ee}} \end{pmatrix} = \begin{pmatrix} U & 0 \\ 0 & U^* \end{pmatrix}\begin{pmatrix} \tau & i\kappa \\ -i\kappa & \tau \end{pmatrix}\begin{pmatrix} V & 0 \\ 0 & V^* \end{pmatrix}, \tag{1.30}$$

where U and V are unitary matrices, and τ, κ are real diagonal matrices. In the limit of a very long wire the reflection matrix becomes unitary, which implies that the elements of τ tend either to zero or to one and the elements of κ are restricted by $\tau^2 + \kappa^2 = 1$. For a scattering matrix describing a class-BDI wire an additional restriction $V = U^T$ reflects the chiral symmetry.

The topological quantum number Q equals the number of Majorana bound states at the wire's end. This quantity is found by connecting the wire to a metallic stub with hard wall boundary conditions at the other end and count the number of bound states that

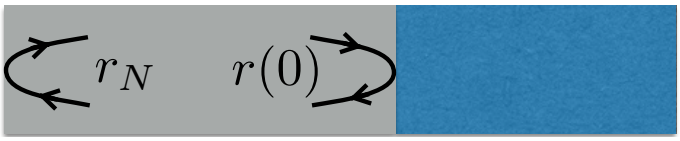

Figure 1.10: Sketch of the setup considered to determine the number of bound states at a wire's end (blue) with the help of a metal stub.

are formed in the metal, see Fig. 1.10. It equals the dimension of the zero-space to the equation

$$\mathbb{1}_{2N} = r_N r(\varepsilon = 0)\,, \tag{1.31}$$

where $\mathbb{1}_{2N}$ os the identity matrix of dimension $2N$ and $r_N = -\mathbb{1}_{2N}$ is the reflection matrix at the other end of the metal stub. In particular, we are looking for the solutions to the equation

$$\det(1 - r) = 0\,, \tag{1.32}$$

which is fulfilled whenever r has an eigenvalue -1. Further, we know that the classification of topological phase in class D is due to a $\mathbb{Z}_2$ number, such that there can be at most one such eigenvalue. All other eigenvalues of r are either one or phases that come in conjugate pairs. Thus, in class D the determinant of the reflection matrix suffices to characterize the topological phase

$$Q_D = \det r(\varepsilon = 0) \tag{1.33}$$

In class BDI several Majorana bound states can occur such that the determinant cannot serve as the quantum number and the dimension of the zero-space has to be found in a different way. Using the fact that for long wires $\tau^2 = \tau$ and $\kappa^2 = \kappa$ one finds

$$1 - r = \begin{pmatrix} U^\dagger & \tau \\ iU^T & -i\tau \end{pmatrix} \begin{pmatrix} U^* & -iU \\ \tau & +i\tau \end{pmatrix} \tag{1.34}$$

The dimension of the zero-space of this product is readily found as the number of zero-eigenvalues of τ. This number equals the non-zero eigenvalues of κ, which are also the eigenvalues of the submatrix of r describing Andreev reflection and one finds

$$Q_{BDI} = -i \operatorname{tr} r_{eh}\,, \tag{1.35}$$

1.3.3 Density of States

Another useful feature for scattering matrices lies in their relation to the density of states. Consider a setup in which a wire is connected to a metallic lead at, say, the left end and subject to hard wall boundary conditions at the right one. Then, only reflection is defined

and constitutes the scattering matrix $r(\varepsilon, L)$, with eigenvalues $e^{i\phi_n(\varepsilon,L)}$, the scattering phases.

The total scattering phase $\phi(\varepsilon, L) = \sum_n \phi_i(\varepsilon, L) = \det r(\varepsilon, L)$ is defined only modulo 2π but is sensitive to the number of states by transitions through its branch cuts. More specifically, as the wire length L is increased $e^{\phi(\varepsilon,L)}$ moves around the unit circle and the total number of states at energy ε increases by one each time the phase passes through 2π. This is captured in Friedel's sum rule, which explicitly relates the density of states to the scattering (reflection) matrix [Hews 93]

$$\nu(\varepsilon) = \frac{1}{2\pi i}\frac{\partial}{\partial\varepsilon}\lim_{L\to\infty}\left(\ln\det r(\varepsilon, L) - \ln\det r(\varepsilon, 0)\right) . \tag{1.36}$$

To study the density of states it is therefore necessary to follow the evolution of the reflection matrix under increments of the wire length. In some cases the analysis can be carried out analytically: by choosing a suitable parametrization for the scattering matrix it is possible to explicitly calculate the change of these parameters under changes of the wire length $L \to L + \delta L$ from Eq. 1.29. This way, a Langevin equation can be derived, whose solution can be used to obtain the density of states. Such an approach has been employed to study chiral wires [Brou 00] but also to analyze the disorder-induced topological phase transition in a 1-dimensional p-wave superconductor [Brou 11a]. Such a phase transition has an unambiguous signal in the density of state, the Dyson-singularity mentioned in Sec. 1.2.3, which allowed for an identification of the critical disorder strength.

1.4 Outline

In this Thesis we will consider various aspects of multichannel p-wave superconducting wires. In Chapter 2 we will investigate the low energy spectrum of subgap states in a $p + ip$-superconducting wire, which is formed by the gapped Majorana states from the different channels. We will consider various wire geometries and disorder potential. In Chapter 3 we will investigate the stability of the topological phase to a disorder potential and calculate the topological quantum number at arbitrary disorder strengths. By this we identify critical disorder strengths associated with topological phase transitions. Finally, in Chapter 4 we study the density of states in the gap as a wire is driven through the disorder-induced topological phase transitions and discuss their signatures in this observable.

2 Endstates in multichannel spinless p-wave superconducting wires

Multimode spinless p-wave superconducting wires with a width W much smaller than the superconducting coherence length ξ are known to have multiple low-energy subgap states localized near the wire's ends. Here we compare the typical energies of such endstates for various terminations of the wire: A superconducting wire coupled to a normal-metal stub and a weakly disordered superconductor wire. Depending on the termination, we find that the energies of the subgap states can be higher or lower than for the case of a rectangular wire with hard-wall boundaries. This chapter is based on Ref. [Ried 12].

2.1 Introduction

In the current search for Majorana fermions in nano-wire geometries [Been 13b, Alic 12] an important theoretical challenge is to understand the multiplicity of possible fermionic bound states that can form at the ends of the wire and how a possible Majorana bound state can be identified among them. This is particularly relevant for multichannel geometries, in which fermionic states localized near the ends of the wire are expected to occur at energies much smaller than the excitation gap for bulk excitations if the wire width is much smaller than the superconducting coherence length. In this chapter we explore the dependence of these sub-gap end-states on the details of the termination of the wire and on impurity scattering.

The interest in isolating Majorana fermions arises because their non-local properties and non-abelian braiding statistics render them potentially useful for fault tolerant quantum computation [Kita 03, Free 98, Read 00, Ivan 01, Kita 06, Naya 08, Wilc 09]. Majorana fermions occur — at least theoretically — at the ends of one-dimensional spinless p-wave superconductors [Kita 01]. Recent proposals suggest ways of engineering solid-state systems that effectively behave as spinless p-wave superconductors by combining an s-wave superconductor and a topological insulator [Fu 08, Cook 11], a semiconductor [Sau 10, Alic 10, Oreg 10, Lutc 10], or ferromagnet [Duck 11, Chun 11, Choy 11, Mart 12, Kjae 12]. Building on the proposals of Refs. [Oreg 10, Lutc 10], two experimental groups have reported an enhanced tunneling density of states at the ends of InAs and InSb wires in proximity to a superconductor, consistent with the existence of Majorana bound states at the ends of these wires [Mour 12, Das 12], whereas a number of other groups claim the observation of Majorana bound states using different methods [Will 12, Rokh 12, Deng 12].

Whereas the original proposals for Majorana fermions in wire geometries focused on one-dimensional systems, it is by now well established that the topological superconducting phase with Majorana end states may persist in a quasi-one-dimensional multichannel setting [Wimm 10, Pott 10, Lutc 11, Pott 11a, Pott 11b, Stan 11, Zhou 11, Kell 12a,

Pott 12, Lim 12, Gibe 12, Tewa 12b]. A difference between the quasi-one-dimensional and one-dimensional settings is, however, that a possible zero-energy Majorana state localized at the wire's end may co-exist with other fermionic sub-gap states, analogous to those found in vortex cores of bulk superconductors [Caro 64]. For the case of an N-channel spinless $p + ip$ superconductor with a rectangular geometry and with width W much smaller than the superconducting coherence length ξ, three of us recently showed that the number of such fermionic subgap states is $\sim N/2$, and that their typical energy is $\varepsilon_{\rm typ} \sim \Delta(W/\xi)^2$, Δ being the superconducting gap size [Kell 12a]. The lowest-lying and highest-lying fermionic subgap states have energies $\varepsilon_{\rm min} \sim \varepsilon_{\rm typ}/N \ln N$ and $\varepsilon_{\rm max} \sim N\varepsilon_{\rm typ}$, respectively. The fermionic subgap states also exist in a non-topological phase without zero-energy Majorana end-state, thus posing a potential obstacle for the identification of the topological phase through the observation of an enhanced density of states near zero energy.

Potter and Lee [Pott 12] observed that the dependence of the energy of the lowest-lying fermionic subgap state on system parameters changes qualitatively if the rectangular geometry of Ref. [Kell 12a] is replaced by a geometry with rounded ends. They point out that the calculation of the energy of the fermionic subgap state for the rectangular geometry is plagued by a subtle cancellation, which does not appear for a generic wire ending. In particular it was found in Ref. [Pott 12] that the lowest-lying fermionic subgap state has an energy significantly above the prediction of Ref. [Kell 12a] for a wire with width $W \sim \xi$ and rounded ends.

Motivated by these observations we present here a detailed investigation of the effect that the wire termination has on the energies of the fermionic subgap states for the multichannel spinless $p + ip$ superconductor. Remarkably, we find that, depending on the details of the wire ending, the energies of the fermionic subgap states can be significantly above, as well as below the rectangular-wire case of Ref. [Kell 12a]. We find an increase of the energies of the subgap states if an arbitrarily-shaped normal layer is attached to the wire's end, the magnitude of the increase being consistent with the estimate of Ref. [Pott 12] for a wire with rounded ends. On the other hand, the presence of impurities — weak enough to preserve the topological phase [Motr 01, Brou 11b] — on average *reduces* the energies of the fermionic end states below the estimate of Ref. [Kell 12a], while a smooth confinement (with a slowly increasing potential energy providing the confinement along the wire's axis) leads to even smaller energies of the fermionic subgap states.

Our results are derived for the two-dimensional spinless $p + ip$ superconducting strip of width W. The model of a spinless $p + ip$ superconductor is an effective low-energy description for the various proposals to realize one-dimensional or quasi-one-dimensional topological superconductors, provided the number N of propagating channels at the Fermi level is chosen equal to the number of spinless (i.e., helical or spin-polarized) channels in the case of the semiconductor or ferromagnet proposals. (The edges of a topological insulator always have $N = 1$, so that a multichannel $p + ip$ model is not relevant in that case.) A mapping between the spinless p-wave model and the semiconductor-wire proposals is given in Chapter 2.3.

The remainder of this chapter is organized as follows: In Sec. 2.2 we briefly review the symmetries of the model (2.2) and the reason for the appearance of multiple low-lying states if the wire width W is much smaller than the superconducting coherence length

ξ. In Sec. 2.4 we describe the scattering theory of fermionic subgap states with arbitrary wire endings and in Sec. 2.5 we discuss the $p + ip$ model with weak disorder. We conclude in Sec. 2.6.

2.2 $p + ip$-Model

Our calculations are performed for a two-dimensional spinless $p+ip$ superconductor, which is described by the two-component Bogoliubov-de Gennes Hamiltonian, which we write as

$$H = H_0 + H_y + H_V, \tag{2.1}$$

with

$$\begin{aligned} H_0 &= \left(\frac{p^2}{2m} - \mu\right)\tau_z + \Delta' p_x \tau_x, \\ H_y &= -\Delta' p_y \tau_y, \\ H_V &= V(\mathbf{r})\tau_z. \end{aligned} \tag{2.2}$$

Here τ_x, τ_y, and τ_z are Pauli matrices in particle-hole space, Δ' specifies the p-wave superconducting order parameter, $\mu = \hbar^2 k_\mathrm{F}^2/2m$ and m are the chemical potential and electron mass, and $V(\mathbf{r})$ a potential that describes the confinement at the ends of the wire as well as the scattering off impurities. The two-dimensional coordinate $\mathbf{r} = (x, y)$, where $0 < y < W$, with hard-wall boundary conditions at $y = 0$ and $y = W$. The superconducting order parameter derives from proximity coupling to a bulk superconductor, so that no self-consistency condition for Δ' needs to be employed.

Hypothetical end states are localized within a distance of the order of the superconducting coherence length $\xi = \hbar(\Delta' m)^{-1}$ from the wire's ends. For thin wires with $W \ll \xi$ it is a good starting point to analyze the Hamiltonian $H = H_0 + H_V$ without the term H_y. The Hamiltonian H_0 has a chiral symmetry [Tewa 12a], $\tau_y H_0 \tau_y = -H_0$, and there exist

$$N = \mathrm{int}\left[(W/\pi)\sqrt{k_\mathrm{F}^2 - \xi^{-2}}\right] \tag{2.3}$$

Majorana bound states at each end of the wire [Kell 12a, Pott 12, Gibe 12, Tewa 12b]. The stepwise increase of the number of Majorana end states for wire widths W such that $(W/\pi)\sqrt{k_\mathrm{F}^2 - \xi^{-2}}$ is an integer is accompanied by a closing of the bulk excitation gap of H_0. Inclusion of the potential term H_V does not lift the degeneracy of the Majorana end states, since H_V preserves the chiral symmetry, although it may change the boundaries of the phases with different N if H_V is nonzero in the bulk of the wire. In contrast, the term H_y breaks the chiral symmetry and couples the N Majorana bound states, giving rise to (generically) int $(N/2)$ fermionic states at each end and a single Majorana end state if N is odd. If $W \ll \xi$ the splitting of the end states is small in comparison to the bulk energy gap $\Delta = \Delta' \hbar k_F$, and the resulting fermionic states cluster near zero energy [Kell 12a, Pott 12].

A schematic picture of the end-state spectrum as a function of W is shown in Fig. 2.1. The end states are characterized by the energy ε_min of the lowest-lying fermionic end state, the typical end-state energy ε_typ, and the energy ε_max of the highest-lying end state.

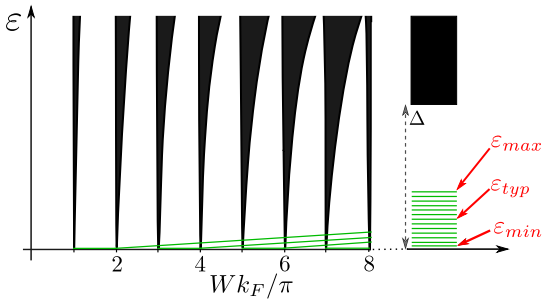

Figure 2.1: Schematic picture of the spectrum of low-energy excitations of the a $p + ip$ wire as a function of its width W. The gap for bulk excitations closes at those values of W for which $(W/\pi)\sqrt{k_{\mathrm{F}}^2 - \xi^{-2}}$ is an integer. When the bulk gap is finite, there are low-energy subgap states localized near the ends of the wire. In the text, we use $\varepsilon_{\mathrm{min}}$ to denote the energy of the lowest-lying fermionic subgap state, $\varepsilon_{\mathrm{typ}}$ for the typical energy of a subgap state, and $\varepsilon_{\mathrm{max}}$ for the energy of the highest-lying fermionic subgap state.

For small N these three energy scales are comparable, but for large N they may differ considerably. The energy $\varepsilon_{\mathrm{min}}$ serves as the "energy gap" protecting the topological state and sets the required energy resolution if the presence or absence of a Majorana end state is detected through a tunneling density of states measurement.

The specific case of a rectangular wire geometry, with hard-wall boundary conditions at each end of the wire and without disorder, was investigated in Ref. [Kell 12a]. We now investigate two other possible terminations, as well as the effect of disorder on the energies of subgap endstates in multichannel spinless p-wave superconducting wires.

2.3 Relationship between the $p + ip$ and the Proximity-Coupled Semiconductor Model

A practical realization of a the $p + ip$ model can be found in semiconducting nanowires with strong spin-orbit coupling, laterally coupled to a standard s-wave superconductor and subject to a Zeeman field. In the following we discuss the precise relationship between the models. A related discussion can also be found in Ref. [Alic 10].

In two dimensions, and without coupling to the superconductor, the Hamiltonian for this system reads

$$H_{\mathrm{N}} = \frac{p^2}{2m} - \mu + B\sigma_x + \alpha\sigma_y p_x - \alpha'\sigma_x p_y, \tag{2.4}$$

where α and α' set the strength of the spin-orbit coupling and $B > 0$ is the Zeeman energy of the applied magnetic field. In the limit of a narrow wire (width W much smaller than the coherence length ξ of the induced superconductivity), subgap states as well as the above-gap quasiparticle states have a vanishing expectation value of the transverse

momentum k_y, which allows us to treat the transverse spin obit term as a perturbation, initially setting $\alpha' = 0$. Without the term proportional to α' different transverse channels do not couple to each other and the eigenfunctions of the Hamiltonian H_{N} are of the form

$$\psi^{\pm}_{n,k}(\mathbf{r}) \propto \begin{pmatrix} e^{-i\theta_k} \\ \pm 1 \end{pmatrix} \frac{1}{\sqrt{W}} e^{ikx} \sin\frac{\pi n y}{W}, \tag{2.5}$$

where the angle θ_k is defined as

$$\sin\theta_k = \frac{\alpha k}{\sqrt{B^2+\alpha^2k^2}}, \quad \cos\theta_k = \frac{B}{\sqrt{B^2+\alpha^2k^2}}, \tag{2.6}$$

and the corresponding energies are

$$\varepsilon^{\pm}_{k,n} = \frac{\hbar^2k^2}{2m} + \frac{\hbar^2\pi^2n^2}{2mW^2} - \mu \pm \sqrt{B^2+\alpha^2k^2}. \tag{2.7}$$

Upon laterally coupling the semiconductor wire to an s-wave superconductor, the excitations are described by the Bogoliubov-de Gennes Hamiltonian

$$\begin{aligned} H_{\mathrm{BdG}} &= \begin{pmatrix} H_{\mathrm{N}} & \Delta\sigma_y \\ \Delta\sigma_y & -H^*_{\mathrm{N}} \end{pmatrix} \\ &= \left(\frac{p^2}{2m} - \mu + B\sigma_x + \alpha\sigma_y p_x\right)\tau_z \\ &\quad - \alpha'\sigma_x p_y + \Delta\sigma_y\tau_x, \end{aligned} \tag{2.8}$$

where τ_x, τ_y, and τ_z are Pauli matrices in electron-hole space. Without the transverse spin-orbit coupling α', the Bogoliubov-de Gennes Hamiltonian has a chiral symmetry, $\tau_y H \tau_y = -H$. In the basis of the normal-state eigenfunctions $\psi^{\pm}_{n,k}$, the Bogoliubov-de Gennes Hamiltonian (2.8) takes the form

$$\begin{aligned} H_{\mathrm{BdG}} = \left(\frac{\hbar^2k^2}{2m} + \frac{\hbar^2\pi^2n^2}{2mW^2} - \mu\right)\tau_z + \sigma_z\tau_z\sqrt{B^2+\alpha^2k^2} \\ + \Delta\sigma_y\tau_x\cos\theta_k + \Delta\sigma_z\tau_x\sin\theta_k \\ - \alpha' p_y(\sigma_z\cos\theta_k + \sigma_y\sin\theta_k). \end{aligned} \tag{2.9}$$

In the limit, when both Δ and the spin orbit energy are smaller than the Zeeman splitting, the s-wave pairing term proportional to σ_y is ineffective, and each transverse channel separately maps to two spinless p-wave superconductors, one for $\psi^{+}_{n,k}$ and one for $\psi^{-}_{n,k}$. Neglecting $|\alpha k|$ in comparison to B, the corresponding pairing term $\Delta\sin\theta_k\sigma_z\tau_x \approx -\Delta' k\sigma_z\tau_x$, with

$$\Delta' = -\frac{\alpha\Delta}{B}. \tag{2.10}$$

Without the term proportional to α', the transverse channels in Eq. (2.9) can be treated independently (at least in the bulk of the wire, see below). If $\mu < B$, only the "$-$" channels

(eigenspinors of σ_z with eigenvalue -1) in Eq. (2.9) are topologically nontrivial and can possibly have end states [Read 00]. Projecting the Bogoliubov-de Gennes Hamiltonian in the rotated basis (2.9) onto these channels, one finds an effective Hamiltonian of the form

$$H_{\mathrm{BdG}}^{\mathrm{eff}} = \left(\frac{\hbar k^2}{2m} + \frac{\hbar^2 \pi^2 n^2}{2mW^2} - \mu - B \right) \tau_z + \Delta' \hbar k \tau_x + \alpha' p_y \,, \tag{2.11}$$

Without the transverse spin-orbit coupling α', the effective Hamiltonian (2.11) has chiral symmetry and N Majorana end states at each end of the wire. The chiral symmetry is broken by the transverse spin-orbit coupling α'. Because of the particle-hole symmetry of the Majorana modes, the matrix elements of this perturbation between the N Majorana end-state of $H_{\mathrm{BdG}}^{\mathrm{eff}}$ with $\alpha' = 0$ are the same as the matrix elements of the p-wave superconducting pairing H_y of Eq. (2.2), if we identify $\Delta' = \alpha'$ in the expression for H_y.

If the condition $\mu < B$ is not met, the relation between the semiconductor and $p + ip$ models is more complicated. For transverse channels for which $\hbar^2\pi^2 n^2/2mW^2 < \mu - B$ the wire ends represent a chiral-symmetry-preserving perturbation that gaps out eventual Majorana end states, so that such channels may be disregarded when considering low-energy end states. For transverse channels for which

$$\mu - B < \frac{\hbar^2 \pi^2 n^2}{2mW^2} < \mu + B \tag{2.12}$$

the Majorana end state in the "$-$ band" (eigenspinors of σ_z at eigenvalue -1 in the rotated basis) is protected in the presence of the chiral symmetry, and only perturbations that lift the chiral symmetry can lead to a splitting of these end states. Projecting the Bogoliubov-de Gennes Hamiltonian in the rotated basis (2.9) onto these channels, one again an effective Hamiltonian of the form (2.11), but with the additional restriction that only those transverse channels that meet the condition (2.12) are considered. The number N of transverse channels that meet this condition may be smaller than the original number of propagating channels in the semiconductor.

2.4 Normal Metal Stub

In this section, we consider a quasi-one-dimensional spinless $p+ip$ superconductor without disorder and coupled to a normal-metal stub at its end. We choose coordinates, such that the spinless superconductor occupies the space $x > 0$, $0 < y < W$, see Fig. 2.2. Such a wire ending is relevant, *e.g.*, for the experimental geometry of Ref. [Mour 12], in which a topological phase is induced in a semiconductor nanowire by laterally coupling it to a superconductor, while a part of the wire sticks out from under the superconductor and is pinched off by a gate at a finite distance.

We take the Hamiltonian of the normal stub to be real and symmetric, in order to preserve the chiral symmetry of the Hamiltonian H_0. Following Ref. [Kell 12a] we first solve for the wavefunctions $\psi^{(j)}$ of the N Majorana modes for the Hamiltonian H_0 and then treat H_y in perturbation theory. The potential term H_V is set to zero throughout this calculation.

The Majorana states have support in the normal stub as well as in a segment of the superconducting wire of length $\sim \xi$. In the superconducting region $x > 0$ the wavefunctions ψ of the Majorana states can be written as

$$\psi(\mathbf{r}) = \sum_n a_{n-}\phi_{n-}(\mathbf{r}) + a_{n+}\phi_{n+}(\mathbf{r}), \tag{2.13}$$

where the basis states $\phi_{n\pm}$, $n = 1, 2, \ldots, N$, read

$$\phi_{n\pm}(\mathbf{r}) = \begin{pmatrix} e^{i\pi/4} \\ e^{-i\pi/4} \end{pmatrix} \sqrt{\frac{2m}{W\hbar k_n}} e^{\pm i k_n x - x/\xi} \sin\left(\frac{n\pi y}{W}\right), \tag{2.14}$$

with

$$k_n = \sqrt{k_\mathrm{F}^2 - (n\pi/W)^2}. \tag{2.15}$$

The basis states $\phi_{n\pm}$ have been normalized to unit flux. The above expressions for the basis states and their normalization are valid up to corrections of order $(W/\xi)^2$, which we neglect throughout this calculation.

The coupling to the normal-metal stub imposes boundary conditions on the coefficients $a_{n\pm}$, which we express in terms of the scattering matrix $S_{nn'}$ of the normal stub,

$$a_{n+} = \sum_{n'} S_{nn'} a_{n'-}, \quad a_{n-} = \sum_{n'} S^*_{nn'} a_{n'+}, \tag{2.16}$$

Because the Hamiltonian of the normal stub is real and symmetric, the scattering matrix $S_{nn'}$ is unitary and symmetric, $S_{nn'} = S_{n'n}$, which ensures that the $2N$ equations (2.16) have N independent solutions, corresponding to the N Majorana end states.

For finding an explicit representation of the N Majorana states $\psi^{(j)}$, $j = 1, 2, \ldots, N$ we use the fact that the scattering matrix S and the Wigner-Smith time-delay matrix[Wign 55, Smit 60] $Q = i\hbar S^\dagger \partial S/\partial\mu$ of the normal stub can be simultaneously decomposed as

$$S = U^\mathrm{T} U, \quad Q = U^\dagger \mathrm{diag}\,(\tau_1, \ldots, \tau_N) U, \tag{2.17}$$

where U is an $N \times N$ unitary matrix and the $\tau_i > 0$, $i = 1, 2, \ldots, N$, are the so-called "proper time delays". With this decomposition, a solution to the boundary conditions (2.16) is given by

$$a^{(j)}_{n+} = U_{nj}, \quad a^{(j)}_{n-} = U^*_{nj}, \quad j = 1, 2, \ldots, N. \tag{2.18}$$

The N states that are defined through these coefficients,

$$\tilde{\psi}^{(j)}(\mathbf{r}) = \sum_n a^{(j)}_{n-}\phi_{n-}(\mathbf{r}) + a^{(j)}_{n+}\phi_{n+}(\mathbf{r}), \tag{2.19}$$

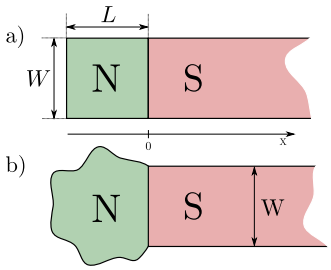

Figure 2.2: Schematic drawing of a spinless p-wave superconducting wire (S) coupled to a normal-metal (N) stub at one end. The top panel shows a rectangular stub, the bottom panel shows a chaotic cavity attached to the superconducting wire.

are Majorana modes (they satisfy $\tilde{\psi}^{(j)*} = \tau_x \tilde{\psi}^{(j)}$), but they are not necessarily orthonormal. In order to construct an orthonormal set, we first calculate the scalar product M_{jl} of the modes $\tilde{\psi}^{(j)}$,

$$\begin{aligned} M_{jl} &= \int_0^\infty dx \int_0^W dy\, \tilde{\psi}^{*(j)}(\mathbf{r})\tilde{\psi}^{(l)}(\mathbf{r}) \\ &+ \int_{\text{stub}} d\mathbf{r}\tilde{\psi}^{*(j)}(\mathbf{r})\tilde{\psi}^{(l)}(\mathbf{r}) \\ &= \sum_n \frac{2m\xi}{\hbar k_n} \text{Re}\left(U_{nj}U_{nl}^* + \frac{U_{nj}U_{nl}^*}{1 - ik_n\xi}\right) + 2\tau_j\delta_{jl}, \end{aligned} \tag{2.20}$$

Here we used the relation between the Wigner-Smith time delay matrix and the normalization of scattering states in order to perform the integration over the sub, see Ref. [Smit 60]. The overlap matrix M is real, positive definite, and symmetric. It is manifestly diagonal if the scattering matrix S and the time-delay matrix Q are diagonal or in the "large-stub limit", which is defined as the limit in which the mean inverse dwell time $\hbar/\bar{\tau}$ is much smaller than the superconducting gap. In both cases, one obtains an orthonormal basis for the N Majorana modes by setting $\psi^{(j)} = \tilde{\psi}^{(j)}/\sqrt{M_{jj}}$. In the general case, M is not diagonal, however, and one has to construct an orthonormal system with the help of the orthogonal transformation O that diagonalizes M, *i.e.*, $O^T M O = \lambda^2$, where $\lambda = \text{diag}\,(\lambda_1, \lambda_2, \ldots, \lambda_N)$ is a diagonal matrix with positive elements. The corresponding orthonormal basis set one thus obtains reads

$$\psi^{(j)}(\mathbf{r}) = \sum_{n=1}^{N} \tilde{\psi}^{(n)}(\mathbf{r}) O_{nj} \lambda_n^{-1}. \tag{2.21}$$

Inclusion of H_y, which breaks the chiral symmetry, gives rise to a splitting of the N degenerate Majorana end states constructed above. With respect to the unnormalized

states $\tilde{\psi}^{(j)}$, this splitting is described by the $N \times N$ matrix

$$\begin{aligned}\tilde{H}^{(1)}_{jl} &= \langle\tilde{\psi}^{(j)}|H_y|\tilde{\psi}^{(l)}\rangle \\ &= \frac{4i\Delta' m}{W}\sum_{nn'}\frac{nn'[1-(-1)^{n+n'}]}{(n'^2-n^2)\sqrt{k_n k_{n'}}} \\ &\times\sum_{\pm}\left[\mathrm{Im}\,\frac{U_{nj}U^*_{n'l}}{k_{n'}\pm k_n}+\frac{2}{\xi}\mathrm{Re}\,\frac{U_{nj}U^*_{n'l}}{(k_{n'}\pm k_n)^2}\right],\end{aligned} \tag{2.22}$$

where we neglected corrections smaller by a factor of order $(W/\xi)^2$. The matrix $\tilde{H}^{(1)}_{jl}$ is antisymmetric and purely imaginary, which ensures the existence of a single zero-energy bound state if N is odd. In order to find a true effective Hamiltonian $H^{(1)}$, the eigenvalues of which represent the energies of the fermionic end states, one should transform to the basis of orthogonal states $\psi^{(j)}$ introduced in Eq. (2.21),

$$H^{(1)} = \frac{1}{\lambda}O^T\tilde{H}^{(1)}O\frac{1}{\lambda}. \tag{2.23}$$

In the special case $N = 2$, this transformation can be carried out for an arbitrary scattering matrix S and the energy of the resulting single fermionic bound state is

$$\varepsilon = \frac{|\tilde{H}^{(1)}_{12}|}{\sqrt{M_{11}M_{22}-M^2_{12}}}. \tag{2.24}$$

We now discuss two particular realizations of a metal stub in detail.

2.4.1 Rectangular Stub

First, we consider a rectangular stub of length L attached to the spinless p-wave superconducting wire, see Fig. 2.2a. For this geometry, both the scattering matrix S and the Wigner-Smith time-delay matrix Q are diagonal,

$$S_{nn'} = -e^{2ik_nL}\delta_{nn'}, \quad Q_{nn'} = \frac{2mL}{\hbar k_n}\delta_{nn'}, \tag{2.25}$$

with k_n given by Eq. (2.15). Since there is no mixing between different channels, the zero energy modes $\tilde{\psi}^{(j)}$ already form an orthogonal basis. The effective Hamiltonian in the normalized basis $\psi^{(j)} = \tilde{\psi}^{(j)}/\sqrt{M_{jj}}$ has $H^{(1)}_{jl} = 0$ if $j + l$ is even and

$$\begin{aligned}H^{(1)}_{jl} = \frac{4i\Delta_y\hbar jl}{W(\xi+2L)(l^2-j^2)}\sum_{\pm}\Bigg\{&\frac{\sin[L(k_j\pm k_l)]}{k_l\pm k_j} \\ &+\frac{2W}{\pi\xi}\frac{\cos[L(k_j\pm k_l)]}{(k_l\pm k_j)^2}\Bigg\}\end{aligned} \tag{2.26}$$

if $j + l$ is odd, up to corrections smaller by a factor of order $(W/\xi)^2$.

The second term in the effective Hamiltonian (2.26) is smaller than the first one by a factor of order W/ξ. However, only this second term contributes in the limit $L = 0$ in

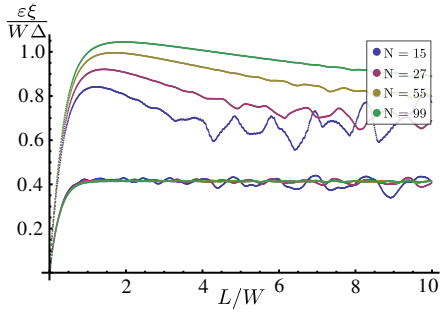

Figure 2.3: Typical and maximal energies of fermionic subgap states in a spinless p-wave superconductor with a rectangular normal-metal stub of length L as a function of L/W for different channels numbers ($N = 15, 27, 55, 99$). The maximal energies $\varepsilon_{\max}$ have a finite-N correction of order $\varepsilon_{\mathrm{m}}/\sqrt{N}$, which is why the curves for $\varepsilon_{\max}$ still show an N dependence for large N.

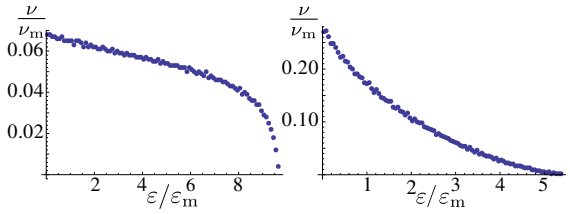

Figure 2.4: Level density of fermionic subgap states for a rectangular stub in the limit of large N, for $L/W = 0.1$ (left) and $L/W = 3$ (right). The level density is measured in units of $\nu_{\mathrm{m}} = N/\varepsilon_{\mathrm{m}}$.

which there is no normal metal stub [Kell 12a]. This is a variation of the cancellation effect pointed out by Potter and Lee [Pott 12]. We now analyze the eigenvalues of the effective Hamiltonian $H^{(1)}$ for finite L, when the first term between brackets dominates.

Since no closed-form expressions for the eigenvalues of $H^{(1)}$ could be obtained, we numerically diagonalized $H^{(1)}$ and investigated the dependence of the minimum, typical, and maximal positive eigenvalues on the ratio L/W as well as the channel number N. For $L \sim W$, this analysis gives

$$\varepsilon_{\mathrm{typ}} \sim \varepsilon_{\mathrm{m}} \equiv \frac{W\Delta}{\xi}, \tag{2.27}$$

see Fig. 2.3. The maximum and minimum energies of the subgap states scale as $\varepsilon_{\min} \sim \varepsilon_{\mathrm{typ}}/N$, $\varepsilon_{\max} \sim \varepsilon_{\mathrm{typ}}$. A similar analysis for $k_{\mathrm{F}}^{-1} \ll L \ll W$ gives estimates for $\varepsilon_{\min}$, $\varepsilon_{\mathrm{typ}}$, and $\varepsilon_{\max}$ which are smaller by a factor L/W, whereas for $L \ll k_{\mathrm{F}}^{-1}$, they are smaller by a factor $L^3 k_{\mathrm{F}}^2/W$. A crossover to the results of Ref. [Kell 12a] takes place for $L \lesssim (W^2/k_{\mathrm{F}}^2\xi)^{1/3}$. In the limit of large N the energies of the fermionic subgap states are best described through their level density, which is shown in Fig. 2.4.

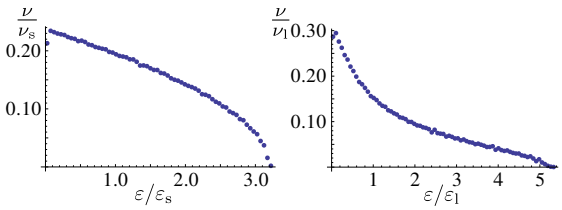

Figure 2.5: Level density of fermionic subgap states in the small-cavity limit (left) and large-cavity limit (right). The level density is measured in units of $\nu_\mathrm{s} = N/\varepsilon_\mathrm{s}$ and $\nu_\mathrm{l} = N/\varepsilon_\mathrm{l}$ for the left and right panels, respectively.

2.4.2 Chaotic Cavity

As a second example, we consider a chaotic cavity attached to the end of the superconducting wire, see Fig. 2.2b. In this case, the unitary matrix U is randomly distributed in the unitary group [Been 97], whereas the proper delay times have the probability distribution [Brou 97]

$$P(\tau_1, ..., \tau_N) \propto \prod_{j=1}^{N} \theta(\tau_j) \tau_j^{-3N/2-1} e^{-N\bar{\tau}/2\tau_j} \times \prod_{i<j} |\tau_i - \tau_j|, \tag{2.28}$$

with the average delay time $\bar{\tau}$. In this case, the matrix U is not diagonal, and the prescription of Eq. (2.23) needs to be used in order to construct the effective Hamiltonian $H^{(1)}$ for the low-energy subgap states. As in the previous case, we could not obtain closed-form expressions for the energies of the fermionic subgap states and had to resort to a numerical analysis, in which the unitary matrices U were generated according to the Haar measure on the unitary group and the time-delays τ_i according to the probability distribution given above, following the method described in Ref. [Crem 02]. This analysis gives different results for the limiting cases of a "small cavity" and a "large cavity", corresponding to the inverse mean dwell time $\hbar/\bar{\tau}$ large or small in comparison to the superconducting gap Δ.

Small-cavity limit. In the small-cavity limit, the normalization of the N Majorana states $\psi^{(j)}$ is dominated by the integration over the superconducting wire. Not counting the Majorana states, the excitation spectrum of the cavity has a gap comparable to the bulk excitation gap Δ. Upon including H_y one obtains N fermionic subgap states, which have a typical energy

$$\varepsilon_\mathrm{typ} \sim \varepsilon_\mathrm{s} \equiv \frac{W\Delta}{\xi}, \tag{2.29}$$

and $\varepsilon_\mathrm{max} \sim \varepsilon_\mathrm{typ}$, $\varepsilon_\mathrm{min} \sim \varepsilon_\mathrm{typ}/N$. The precise location of the subgap states depends on the precise scattering matrix of the cavity. The mean level density for an ensemble of cavities is shown in the left panel Fig. 2.5.

Large-cavity limit. In the large-cavity limit, the overlap matrix M_{jl} is dominated by the in-cavity parts of the wavefunctions, so that the Majorana modes $\tilde{\psi}^{(j)}$ are already

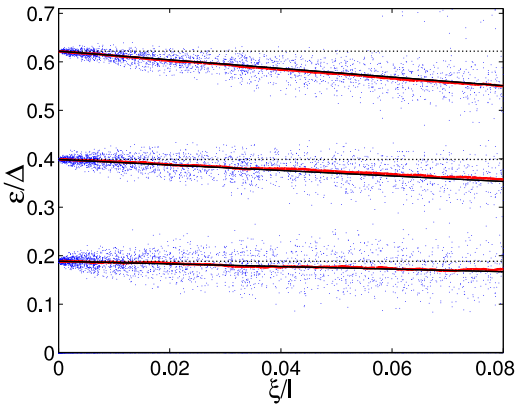

Figure 2.6: Top: Distribution of energies of fermionic subgap end states in a spinless p-wave superconductor with $N = 7$ channels , as a function of ξ/l. The red lines indicate the mean calculated from the local distribution of eigenvalues. The black lines, which are a linear fit to the mean values in red, share an approximate common intercept at the horizontal axis at $\xi/l = c^{-1} = 0.7$. Dotted grey lines indicate the unperturbed energies. Energies are measured in units of the bulk gap. The lattice parameters used in the numerical calculation correspond to $k_F W = f_F \xi \approx 23.5$.

orthogonal and the effective Hamiltonian $H^{(1)}_{jl} = \tilde{H}^{(1)}_{jl}/\sqrt{4\tau_j\tau_l}$, with $\tilde{H}^{(1)}_{jl}$ given in Eq. (2.22). Not counting the Majorana states, the cavity's excitation spectrum has a gap of order $E_{\rm T} = \hbar/\pi\bar{\tau}$ [Mels 96], where $\bar{\tau}$ is the mean dwell time in the cavity. In this case, the typical energy of the fermionic subgap states is

$$\epsilon_{\rm typ} \sim \varepsilon_1 \equiv \frac{E_{\rm T} W}{\xi}, \tag{2.30}$$

while $\varepsilon_{\rm max} \sim \varepsilon_{\rm typ}$ and $\varepsilon_{\rm min} \sim \varepsilon_{\rm typ}/N$. The mean level density of the subgap states for an ensemble of cavities is shown in the right panel of Fig. 2.5.

2.4.3 The case $W \sim \xi$

The results of the main text were derived for the case $W \ll \xi$, wire width much smaller than the superconducting coherence length. This is the appropriate limit if the induced superconductivity is weak. It applies, *e.g.,* in the semiconductor model if there is a barrier interface between the superconductor and the semiconductor nanowire, which suppresses the strength of the induced superconductivity and, hence, increases ξ. The limit $W \ll \xi$ ensures that all int $(N/2)$ fermionic subgap states have energy well below the bulk gap Δ. For wider wires, the condition $W \ll \xi$ may be violated (but this is not necessarily so; see Sec. 2.6), although the lowest-energy states remain localized near the wire's ends as long as $W \lesssim \xi$. (For $W \gg \xi$, the lowest-energy subgap states are extended along the wire's edges [Kell 12a, Zhou 11].)

Here, we discuss how our results are modified when W and ξ become comparable. Our discussion must be limited to $\varepsilon_{\rm min}$, because the energies of the fermionic states extend up

to and into the bulk spectrum if $W \gtrsim \xi$, so that the energy scales $\varepsilon_{\rm typ}$ and $\varepsilon_{\rm max}$ have lost their meaning. For the case of a $p + ip$ superconductor with a normal-metal stub, which was discussed in Sec. 2.4, we have verified that our estimates for $\varepsilon_{\rm min}$ remain qualitatively valid up to $W \sim \xi$. A numerical investigation similar to that of Fig. 2.7 of Sec. 2.5 shows that the lowest fermionic subgap levels in a $p + ip$ model with a rectangular ending are only weakly dependent on disorder, and on the average decrease with a common factor $(1 - c\xi/l)$, although the value numerical constant c differs from that obtained in the limit $W \ll \xi$ of the main text. An example is shown in the top panel of Fig. 2.6 below.

2.5 $p + ip$-Model with Disorder

Whereas strong disorder is known to destroy the topological superconducting phase in the $p + ip$ model in one dimension, weak disorder with mean free path $l > \xi/2$ preserves the topological phase [Motr 01, Brou 11b]. In this section we investigate the effect of weak disorder on the energies of the fermionic subgap states in a multichannel rectangular $p+ip$ model. Because the disorder is necessarily weak (strong disorder suppresses the topological phase), the effect of disorder can be treated in perturbation theory.

Starting point of our analysis is the chiral-symmetric Hamiltonian H_0, which has N normalized Majorana bound states $|\psi^{(j)}\rangle$, $j = 1, 2, \ldots, N$ at each end of the wire. We take a rectangular geometry, with a wire end and hard-wall boundary conditions at $x = 0$, and take the potential $V(\mathbf{r})$ to be a Gaussian white noise potential with mean $\langle V(\mathbf{r})\rangle = 0$ and variance

$$\langle V(\mathbf{r})V(\mathbf{r}')\rangle = \frac{v_{\rm F}^2}{k_{\rm F} l}\delta(\mathbf{r} - \mathbf{r}'), \tag{2.31}$$

where l is the mean free path and $v_{\rm F} = \hbar k_{\rm F}/m$ the Fermi velocity. In our perturbative analysis we treat both the impurity potential V and the transverse superconducting order as perturbations and write

$$H = H_0 + U, \tag{2.32}$$

where $U = H_y + H_V$ contains the superconducting correlations coupling to p_y as well as the impurity potential.

The effective Hamiltonian $H_{\rm eff}$ describing the splitting of the N Majorana states into fermionic subgap states can be found using the degenerate perturbation theory of Kato [Kato 49] and Bloch [Bloc 58]. (For additional details on this methodology see also Refs. [Mess 81] and [Jord 08].) Defining $P = \sum |\psi^{(j)}\rangle \langle\psi^{(j)}|$ as the projector onto the zero-energy subspace and $Q = 1 - P$, we can then write using Bloch's method

$$H_{\rm eff} = \quad PUP - PU\frac{Q}{H_0}UP + PU\frac{Q}{H_0}U\frac{Q}{H_0}UP - \frac{1}{2}\left(PU\frac{Q}{H_0^2}UPUP + PUPU\frac{Q}{H_0^2}UP\right). \tag{2.33}$$

It is essential to note that the disorder potential $V(\mathbf{r})$ alone cannot lift the degeneracy of the Majorana end states at any order of the perturbation theory. This can be understood directly from the observation that the disorder potential $V(\mathbf{r})$ does not break the chiral

symmetry of the unperturbed Hamiltonian H_0 that is responsible for the N-fold degeneracy. On the level of perturbation theory this can be understood immediately through the particle-hole symmetry present in the Majorana bound states and the knowledge that for each perturbative diagram that connects Majoranas through the positive energy bulk states there is a canceling path through the negative energy states.

Keeping terms to first order in H_y and up to second order in H_V only, we obtain

$$H_{\text{eff}} = H^{(1)} + H^{(2)} + H^{(3\text{a})} - H^{(3\text{b})}, \tag{2.34}$$

with

$$\begin{aligned}
H^{(1)}_{jl} &= \langle \psi^{(j)} | \, H_y \, | \psi^{(l)} \rangle \,, \\
H^{(2)}_{jl} &= - \langle \psi^{(j)} | \, H_y \frac{Q}{H_0} H_V + H_V \frac{Q}{H_0} H_y \, | \psi^{(l)} \rangle \,, \\
H^{(3\text{a})}_{jl} &= \langle \psi^{(j)} | \, H_y \frac{Q}{H_0} H_V \frac{Q}{H_0} H_V \, | \psi^{(l)} \rangle + \text{permutations}, \\
H^{(3\text{b})}_{jl} &= \frac{1}{2} \sum_k (V^{(2)}_{jk} H^{(1)}_{kl} + H^{(1)}_{jk} V^{(2)}_{kl}),
\end{aligned} \tag{2.35}$$

where

$$V^{(2)}_{jl} = \langle \psi^{(j)} | \, H_V \frac{Q}{H_0^2} H_V \, | \psi^{(l)} \rangle \,. \tag{2.36}$$

The effective Hamiltonian H_{eff} is antisymmetric, which implies that the diagonal elements of all the above terms are zero. The first-order term $H^{(1)}$ describes how the transverse superconducting correlations lift the degeneracy of the N Majorana modes in the absence of disorder. The second-order term $H^{(2)}$ is linear in the disorder potential. Its elements are random variables with zero mean and standard deviation that does not appreciably change with ξ. The third order term contains two terms, the first of which is also a random variable with zero mean and with a root-mean-square proportional ξ.

The term $H^{(3\text{b})}$ contains corrections to the effective Hamiltonian arising from the renormalization and re-orthogonalization of wavefunctions at the first order of the perturbation theory. Since this term is a weighted sum of first order elements $H^{(1)}_{jl}$, it is the only one of the higher-order perturbation corrections that gives a systematic dependence of energies on the disorder strengths. To see this in more detail, it is instructive to separate the diagonal and the off-diagonal elements of $V^{(2)}$ in the expression for $H^{(3\text{b})}$,

$$\begin{aligned}
H^{(3\text{b})}_{jl} = &\frac{1}{2} (V^{(2)}_{jj} H^{(1)}_{jl} + H^{(1)}_{jl} V^{(2)}_{ll}) \\
&+ \frac{1}{2} \sum_{k \neq j} (V^{(2)}_{jk} H^{(1)}_{kl} + H^{(1)}_{jk} V^{(2)}_{kl}).
\end{aligned} \tag{2.37}$$

The first term here is the most important because the weights $V^{(2)}_{kk}$ are positive definite random variables. A simple scaling analysis predicts that these variables have both mean and standard deviation proportional to the ratio ξ/l of coherence length and mean free

path. This term effectively renormalizes the entire first order contribution, on average driving the energies of the fermionic subgap states towards zero. The second term, which contains the contribution from the off-diagonal elements of $V^{(2)}$, is less important because the disorder potential here connects different Majorana modes. These matrix elements are therefore randomly distributed with zero mean and a root mean square proportional to the coherence length.

Motivated by these observations, we write the effective Hamiltonian in the form

$$H \approx \Delta_y' \left[\left(1 - c\frac{\xi}{l} \right) H^{(1)} + H' \right], \tag{2.38}$$

where $c = (l/N\xi) \sum_k V^{(2)}_{kk}$ is a number of order unity, and

$$H' = H^{(2)} + (H^{(3a)} - \frac{1}{2}\{V^{(2)} - \frac{c\xi}{l}, H^{(1)}\}). \tag{2.39}$$

The correction H' has zero mean.

We have numerically diagonalized a lattice version of the Hamiltonian (2.2) in order to provide numerical evidence for the applicability of the above arguments. Details of the relationship between the continuum and lattice models can be found in Ref. [Kell 12a]. Results of the numerical simulations are shown in Fig. 2.7. For weak disorder, the perturbation $H^{(2)}$ dominates the response of the fermionic subgap states, and the energies of the fermionic subgap states may both increase or decrease, depending on the specific realization of the disorder potential. While large fluctuations persist, for stronger disorder the quadratic-in-disorder perturbation $H^{(3b)}$ leads to a systematic decrease of the energies of the fermionic subgap states, which is well described by a linear dependence on ξ/l, consistent with the first term in Eq. (2.38).

2.6 Conclusions

In this chapter, we have investigated fermionic subgap states localized near the end of a spinless p-wave superconducting wires for two terminations of the wire — a normal-metal stub and a smooth confining potential — and in the presence of weak disorder. The three scenarios give qualitatively different estimates for the energies of the subgap states. However, they share the common feature that a wire with N transverse channels with a width W that is much smaller than the superconducting coherence length ξ has int $(N/2)$ fermionic end states, all with energy much below the bulk excitation gap Δ. These states appear for the topological phase (which has a Majorana fermion at the wire's end), as well as for the non-topological phase (which does not).

The appearance of low-energy fermionic end states poses an obstacle to the identification of Majorana fermions through a measurement of the tunneling density of states at the wire's end, unless the energy resolution of the experiment is good enough to resolve the splitting between the fermionic end states. The corresponding energy scale $\varepsilon_{\min}$ scales proportional to $\Delta/k_F\xi \sim \Delta^2/\mu$ in the most favorable scenario we considered (wire's end coupled to a small normal metal stub), which is the same dependence as the subgap states in a vortex core [Caro 64]. The important difference with the subgap states in a

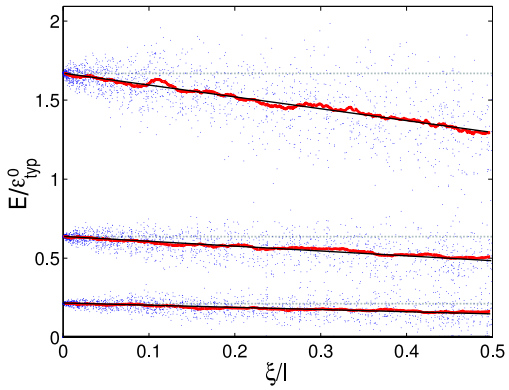

Figure 2.7: Distribution of energies of fermionic subgap end states in a spinless p-wave superconductor with $N = 7$ channels (dots), as a function of ξ/l. For small amounts of disorder the term $H^{(2)}$ dominates, pushing the subgap energies up or down with equal probability. At stronger disorder the term in $H^{(3b)} \propto \xi/l$ eventually dominates and pulls all energy levels towards zero. The red lines indicate the mean calculated from the local distribution of eigenvalues. The black lines, which are a linear fit to the mean values in red, share an approximate common intercept at the horizontal axis at $\xi/l = c^{-1} = 2.2$. Dotted grey lines indicate the unperturbed energies. Energies are measured in units of $\varepsilon^0_{\mathrm{typ}} = \Delta W^2/\xi^2$. The lattice parameters used in the numerical calculation correspond to $k_F W \approx 23$ and $k_F \xi \approx 320$.

vortex core is, however, that the number of fermionic end states is limited, so that there exists a maximum energy $\varepsilon_{\mathrm{max}}$, whereas no such maximum energy exists in a vortex. Other terminations, such as a rectangular end with or without disorder, or a smooth confinement potential, give significantly smaller values for $\varepsilon_{\mathrm{min}}$, and, hence, lead to stricter requirements for the energy resolution required to separate an eventual Majorana state from fermionic end states.

The recent experiments that reported the possible observation of a Majorana fermion involved semiconductor nanowires with proximity-induced superconductivity [Mour 12, Das 12]. Effectively, the induced superconductivity in these wires is of spinless p-wave type. However, it should be emphasized that this does not imply that the effective description of such a semiconductor wire with N transverse channels is a $p + ip$ model with the same number of transverse channels. Instead, only those channels in the semiconductor that are effectively spinless (*i.e.*, spin polarized or helical, depending on the relative strength of the applied magnetic field and the spin-orbit coupling) appear in the effective description in terms of a $p + ip$ model. (This latter distinction was overlooked in Ref. [Tewa 12b].) Typically, this number is smaller than the number of transverse channels in the semiconductor. In particular, the nanowires of the experiments of Refs. [Mour 12, Das 12] are believed to be thin enough that they map to a single-channel $p+ip$ model. Hence, we do not expect that the mechanism for the generation of fermionic end states we consider applies to those experiments. However, it will apply to nanowires with

a larger diameter, which we thus expect to exhibit a clustering of low-energy fermionic states in the topologically trivial as well as the topologically nontrivial phases. In this context, it is important to note that the condition that $W \ll \xi$ does not a priori prevent the applicability of our analysis to thicker wires, because the effective pairing potential Δ may decrease with W for proximity-induced superconductivity in the limit of thick wires (see Ref. [Duck 11] for an example in which $\Delta \propto W^{-1}$).

3 Reentrant topological phase transitions in a disordered spinless superconducting wire

In a one-dimensional spinless p-wave superconductor with coherence length ξ, disorder induces a phase transition between a topologically nontrivial phase and a trivial insulating phase at the critical mean free path $l = \xi/2$. Here, we show that a multichannel spinless p-wave superconductor goes through an alternation of topologically trivial and nontrivial phases upon increasing the disorder strength, the number of phase transitions being equal to the channel number N. The last phase transition, from a nontrivial phase into the trivial phase, takes place at a mean free path $l = \xi/(N+1)$, parametrically smaller than the critical mean free path in one dimension. Our result is valid in the limit that the wire width W is much smaller than the superconducting coherence length ξ. The content of this chapter has been published in Ref. [Ried 13].

3.1 Introduction

In one dimension, spinless superconductors appear in two topologically distinct phases. In one of these phases, usually referred to as the "trivial phase" the excitation spectrum is adiabatically connected to the ionic insulator. The other phase is "topologically nontrivial". Topologically protected zero-energy bound states appear at junctions between the trivial and nontrivial phases [Read 00, Kita 01]. These bound states are particle-hole symmetric and two of these combine to form a single fermionic excitation, which is why they are referred to as "Majorana bound states" [Wilc 09, Been 13b]. Interest in these systems has peaked after recent proposals to construct topological superconductors out of hybrid structures involving standard BCS superconductors and semiconductors [Oreg 10, Lutc 10] and reports of their subsequent experimental realization [Mour 12, Das 12].

The Pauli principle enforces that spinless superconducting correlations are odd in momentum. In a one-dimensional setting, this means that they must be of p-wave type. Unlike for s-wave superconductors, where the Anderson theorem protects the superconducting correlations against impurity scattering [Ande 59], backscattering by impurities suppresses p-wave superconducting order. In a one-dimensional wire any small amount of disorder already leads to subgap states at arbitrarily low energies, but it takes a finite amount of disorder to drive the system from the nontrivial superconducting phase into the trivial phase [Motr 01, Brou 11b]. For short-range disorder with normal-state mean free path l, the transition between these phases takes place if [Brou 11b]

$$l = \frac{\xi}{2}, \tag{3.1}$$

where ξ is the superconductor coherence length. Here and below we assume that the superconductivity is weak, ξ much larger than Fermi wavelength λ_{F}.

The one-dimensional description applies only if the system width W does not exceed the Fermi wavelength λ_F. If $W \geq \lambda_F$, the normal-state has $N = \text{int}\,(2W/\lambda_F) > 1$ propagating channels at the Fermi level, and without disorder the topologically nontrivial phase exists if N is odd, but not if N is even [Wimm 10, Pott 10, Lutc 11, Stan 11, Zhou 11, Kell 12a]. Numerical simulations and weakly-disordered perturbation theory indicate that the topological phases are stable against weak disorder in the multichannel case, too [Ried 12, Pott 11a, Pott 11b].

It is the purpose of this chapter to provide an analytical theory of the effect of disorder on the topological phase in the N-channel p-wave superconductor. Our main result is that increasing the disorder strength drives the system through a sequence of N topological phase transitions, taking place at

$$l = \frac{n\xi}{N+1}, \quad n = 1, 2, \ldots, N. \tag{3.2}$$

In particular, a topologically nontrivial phase persists for disorder strengths up to $l = \xi/(N+1)$, significantly larger than the critical disorder strength (3.1) at which the topological phase transition takes place in one dimension. Our analytical theory, as well as the precise location of the phase transitions given in Eq. (3.2), is valid in the limit of thin wires, width $W \ll \xi$. We have verified numerically that the alternation of topological phases persists for wire widths up to $W \sim \xi$. Note that the existence of N phase transitions is consistent with the known results for the weak disorder limit $l \to \infty$ (nontrivial phase if N is odd, and trivial phase if N is even), as well as the strong disorder limit $l \downarrow 0$ (system is in the trivial phase).

3.2 Multichannel $p + ip$ Superconductor

For the derivation of Eq. (3.2) we consider a spinless p-wave superconducting wire of length L, width W, and chemical potential $\mu > 0$ coupled to ideal normal-metal leads at its two ends. The Bogoliubov-de Gennes Hamiltonian of the system reads

$$H = \left(\frac{p^2}{2m} + V(x,y) - \mu \right) \sigma_z + \frac{1}{2} \left\{ \Delta'_x, p_x \right\} \sigma_x + \Delta'_y p_y \sigma_y, \tag{3.3}$$

where σ_x, σ_y, and σ_z are Pauli matrices in particle-hole space. The Hamiltonian (3.3) has particle-hole symmetry, $\sigma_x H \sigma_x = -H^*$, which places it in the (Altland-Zirnbauer) symmetry class D [Altl 97]. The superconductor occupies the volume $0 < x < L$, and the two leads are at $x < 0$ and $x > L$ respectively, see Fig. 3.1 (inset). The superconducting order parameters Δ'_x and Δ'_y are nonzero for $0 < x < L$ only. The superconducting coherence length is

$$\xi = \hbar/m\Delta'_x. \tag{3.4}$$

Although $\Delta'_x = \Delta'_y$ for an isotropic superconductor, we have chosen to use different symbols in order to underline the very different roles of these two parameters in the calculation that follows. We assume that the superconductivity is proximity-induced, so that we can treat Δ'_x and Δ'_y as externally-imposed parameters without self-consistency requirements.

The impurity potential has zero average and short-range fluctuations described by the Gaussian white noise correlator

$$\langle V(x,y)V(x',y')\rangle = \gamma\delta(x-x')\delta(y-y') \tag{3.5}$$

and is zero in the leads.

We determine the topological phase from the zero-energy reflection matrix r of the superconducting wire [Fulg 11]. In the particle-hole notation, the reflection matrix r for quasiparticles incident from the left takes the form

$$r = \begin{pmatrix} r_{\mathrm{ee}} & r_{\mathrm{eh}} \\ r_{\mathrm{he}} & r_{\mathrm{hh}} \end{pmatrix}, \tag{3.6}$$

where particle-hole symmetry imposes that $r_{\mathrm{hh}} = r_{\mathrm{ee}}^*$ and $r_{\mathrm{he}} = r_{\mathrm{eh}}^*$ at zero energy. Following Fulga *et al.*, the topological phase can be calculated from the determinant $Q = \det r$ [Fulg 11]: The topologically nontrivial phase has $Q = -1$, whereas the topologically trivial phase has $Q = 1$. (Note that particle-hole symmetry requires $\det r$ to be real; As no extended quasiparticle states exist in the superconductor away from the critical points, r must be unitary and hence $|\det r| = 1$.)

In the thin-wire limit $W \ll \xi$ the transverse pairing Δ_y' may be treated perturbatively [Kell 12a]. Without the transverse pairing, the Bogoliubov-de Gennes Hamiltonian H has an additional chiral symmetry $\sigma_y H \sigma_y = -H$ [Tewa 12b], which places it in the symmetry class BD I. With the chiral symmetry, the topological superconducting phases are characterized by an integer number Q_{chiral}. The topological quantum number Q is related to Q_{chiral} as

$$Q = (-1)^{Q_{\mathrm{chiral}}}. \tag{3.7}$$

The absolute value $|Q_{\mathrm{chiral}}|$ can be interpreted as the number of Majorana bound states at the end of the wire, when the normal metal leads are replaced by insulating ends [Fulg 11]. The quantum number Q_{chiral} can be calculated from the zero-energy electron-holes reflection matrix r_{eh} as [Fulg 11]

$$Q_{\mathrm{chiral}} = -i \lim_{L\to\infty} \operatorname{tr} r_{\mathrm{eh}}. \tag{3.8}$$

The limit $L \to \infty$ is taken in order to ensure that the reflection matrix r is unitary.

3.3 Mapping to Disordered Metal at $\varepsilon = 0$

With the chiral symmetry present it is possible to express the zero-energy reflection matrix r in terms of the system's normal-state scattering matrix at a slightly renormalized chemical potential $\tilde{\mu}$ [Adag 14]. To this end, we first rotate the Hamiltonian (3.3) to the Majorana basis

$$\begin{aligned} \tilde{H} &= e^{-i\pi\sigma_x/4} H e^{i\pi\sigma_x/4} \\ &= -\left(\frac{p^2}{2m} - \mu + V\right)\sigma_y + \Delta_x' p_x \sigma_x. \end{aligned} \tag{3.9}$$

At zero energy, the eigenvalue equation for $\tilde{H}$ consists of two decoupled equations describing particles that are exposed to an imaginary "gauge field" of magnitude $\hbar/\xi$ and pointing in opposite directions for the two equations [Hata 96, Brou 97]. This "gauge field" may be transformed away by the (non-unitary) transformation

$$\psi(x,y) \to \tilde{\psi}_{\pm}(x,y) = \begin{cases} \psi(x,y) & \text{if } x < 0, \\ \psi(x,y) e^{\frac{\pm x}{\xi}} & \text{if } 0 < x < L, \\ \psi(x,y) e^{\pm L/\xi} & \text{if } x > L. \end{cases} \tag{3.10}$$

The wavefunctions $\tilde{\psi}_{\pm}(x,y)$ satisfy the standard Schrödinger equation for the zero-energy wavefunction of a disordered wire,

$$\left(\frac{p^2}{2m} - \tilde{\mu} + V \right) \tilde{\psi}_{\pm}(x,y) = 0\,, \tag{3.11}$$

where $\tilde{\mu} = \mu + \hbar\Delta'_x/2\xi$.

After the gauge transformation, the wire is described as a disordered normal metal wire, whose scattering matrix, $\widetilde{S}$, properties are well known, see Ref. [Been 97]. It can be written in a polar decomposition

$$\widetilde{S} = \begin{pmatrix} \tilde{r} & \tilde{t}' \\ \tilde{t} & \tilde{r}' \end{pmatrix} = \begin{pmatrix} U & 0 \\ 0 & V \end{pmatrix} \begin{pmatrix} -\sqrt{1-\tilde{\tau}} & \sqrt{\tilde{\tau}} \\ \sqrt{\tilde{\tau}} & \sqrt{1-\tilde{\tau}} \end{pmatrix} \begin{pmatrix} U^{\mathrm{T}} & 0 \\ 0 & V^{\mathrm{T}} \end{pmatrix}, \tag{3.12}$$

with the $N \times N$ unitary matrices U, V and $\tilde{\tau} = \mathrm{diag}\,(\tilde{\tau}_1, \tilde{\tau}_2, \ldots, \tilde{\tau}_n)$. The asymptotic probability distribution of the eigenvalues $\tilde{\tau}_n$ in the limit of large L is well studied in the literature [Been 97]. The result is best parameterized in terms of the "Lyapunov exponents" $\tilde{\tau}_n = \cosh^{-2}(x_n L)$, which are self-averaging for large L, with mean

$$\langle x_n \rangle = \frac{n}{(N+1)l}, \quad n = 1, 2, \ldots, N, \tag{3.13}$$

and small fluctuations of order $1/\sqrt{(N+1)lL}$.

3.4 Scattering Matrix in class BDI and Q_{chiral}

Transforming back to the basis of the original Hamiltonian (3.3) allows us to express the reflection matrix r in terms of the reflection matrix $\tilde{r}$ (for particles incident from the left) and the transmission matrix $\tilde{t}'$ (for particles incident from the right) of the normal-state scattering problem specified by Eq. (3.11), which can be used to calculate the topological quantum number Q_{chiral}, see Eq. 3.8. We first sketch the derivation of the full scattering matrix.

The general solution to the Hamiltonian in Equ. 3.9 is composed of plane waves in the leads that are connected with each other by the wavefunctions in the wire

$$\psi_n(x) = \frac{1}{\sqrt{2}} \begin{cases} \begin{pmatrix} a_e \\ b_h \end{pmatrix} e^{ik_n x} + \begin{pmatrix} b_e \\ a_h \end{pmatrix} e^{-ik_n x} & x \le 0 \\ \begin{pmatrix} b'_e \\ a'_h \end{pmatrix} e^{ik_n x} + \begin{pmatrix} a'_e \\ b'_h \end{pmatrix} e^{-ik_n x} & x \ge L \\ \psi_e(x) \begin{pmatrix} 1 \\ 0 \end{pmatrix} + \psi_h(x) \begin{pmatrix} 0 \\ 1 \end{pmatrix} & 0 \le x \le L \end{cases} . \tag{3.14}$$

The scattering matrix relates the coefficients of the incoming waves $a_{e/h}, a'_{e/h}$ to the ones of the outgoing waves $b_{e/h}, b'_{e/h}$.
The basis rotation $e^{-i\pi\sigma_x/4}$ that is applied to the p-wave Hamiltonian corresponds to a basis change from $(1,0),(0,1)$ to $(1,i),(i,1)$. At zero energy the new basis describes two different decoupled excitations, that are denoted as $c_\pm, c'_\pm$ and $d_{e/h}, d'_{e/h}$, where the subscript $\pm$ indicates plane waves traveling to the right/left. From the basis change the new coefficients c, d are uniquely related to the old ones a, b.

The gauge transformation defined in Eq. 3.10 amplifies/suppresses exponentially the excitations c/d when passing from the left to the right lead. They can be related to each other with components of the normal metal scattering matrix $\widetilde{S}$ in Eq. 3.12 accounting for the exponential factor

$$\begin{pmatrix} c_- \\ c'_+ \end{pmatrix} = \begin{pmatrix} \tilde{r} & \tilde{t}' e^{-L/\xi} \\ \tilde{t} e^{L/\xi} & \tilde{r}' \end{pmatrix} \begin{pmatrix} c_+ \\ c'_- \end{pmatrix}, \tag{3.15}$$

$$\begin{pmatrix} d_- \\ d'_+ \end{pmatrix} = \begin{pmatrix} \tilde{r} & \tilde{t}' e^{L/\xi} \\ \tilde{t} e^{-L/\xi} & \tilde{r}' \end{pmatrix} \begin{pmatrix} d_+ \\ d'_- \end{pmatrix}. \tag{3.16}$$

Using these results we can transform back to the original electron-holes basis and find for the scattering matrix S of the class BDI-superconductor

$$S = \begin{pmatrix} r & t' \\ t & r' \end{pmatrix} = \begin{pmatrix} U & 0 & 0 & 0 \\ 0 & U^* & 0 & 0 \\ 0 & 0 & V & 0 \\ 0 & 0 & 0 & V^* \end{pmatrix} \begin{pmatrix} -\rho & \bar{\rho} & \tau & \bar{\tau} \\ -\bar{\rho} & -\rho & -\bar{\tau} & \tau \\ \tau & \bar{\tau} & \rho & -\bar{\rho} \\ -\bar{\tau} & \tau & \bar{\rho} & \rho \end{pmatrix} \begin{pmatrix} U^{\mathrm{T}} & 0 & 0 & 0 \\ 0 & U^\dagger & 0 & 0 \\ 0 & 0 & V^{\mathrm{T}} & 0 \\ 0 & 0 & 0 & V^\dagger \end{pmatrix}, \tag{3.17}$$

where we abbreviated

$$\begin{aligned} \rho &= \left[1 + \tilde{\tau} z_-^2\right]^{-1} \sqrt{1 - \tilde{\tau}} \\ \bar{\rho} &= i \left[1 + \tilde{\tau} z_-^2\right]^{-1} \tilde{z}_+ z_- \tau \\ \tau &= \left[1 + \tilde{\tau} z_-^2\right]^{-1} z_+ \sqrt{\tilde{\tau}} \\ \bar{\tau} &= i \left[1 + \tilde{\tau} z_-^2\right]^{-1} z_- \sqrt{\tilde{\tau}(1 - \tilde{\tau})}, \end{aligned} \tag{3.18}$$

with $z_+ = \cosh(L/\xi)$ and $z_- = \sinh(L/\xi)$.

Writing out explicitly the normal reflection part r_{ee} and the electron-hole reflection part r_{eh}, we find

$$\begin{aligned} r_{\text{ee}} &= [1 + \tilde{t}'\tilde{t}'^\dagger \sinh^2(L/\xi)]^{-1} \tilde{r}, \\ r_{\text{eh}} &= i \sinh(L/\xi) \cosh(L/\xi) [1 + \tilde{t}'\tilde{t}'^\dagger \sinh^2(L/\xi)]^{-1} \tilde{t}'\tilde{t}'^\dagger. \end{aligned} \tag{3.19}$$

Returning to Eq. (3.8), we find that topological number Q_{chiral} can be expressed as a sum over the eigenvalues $\tilde{\tau}_n(L)$ of $\tilde{t}'\tilde{t}'^\dagger$,

$$Q_{\text{chiral}} = \lim_{L\to\infty} \sum_{n=1}^{N} \frac{\sinh(L/\xi)\cosh(L/\xi)\tilde{\tau}_n(L)}{1 + \tilde{\tau}_n(L)\sinh^2(L/\xi)}. \tag{3.20}$$

The mean free path in the normal state $l = \lambda_F \hbar^2 v_F^2 \alpha_N/(2\gamma)$ is calculated from the reflection matrix for a short segment of length dL as $\mathrm{tr}\left(r_{ee} r_{ee}^\dagger\right) = NdL/l$, which is obtained in the first order Born approximation. α_N is a numerical factor that depends on the width W and reads

$$\alpha_N = N\left[\frac{3}{2}\sum_{n=1}^{N}\left((Wk_F/\pi)^2 - n^2\right)^{-1} + 2\sum_{n<m=1}^{N}\sqrt{((Wk_F/\pi)^2 - n^2)^{-1}((Wk_F/\pi)^2 - n^2)^{-1}}\right]^{-1}. \tag{3.21}$$

Substituting this result into Eq. (3.20), we find that

$$Q_{\mathrm{chiral}} = \sum_{n=1}^{N}\Theta\left[1 - \frac{n\xi}{(N+1)l}\right], \tag{3.22}$$

where $\Theta(z) = 0$ if $z < 0$ and 1 otherwise. Hence, upon increasing the disorder strength, the topological quantum number Q_{chiral} stepwise decreases from $Q_{\mathrm{chiral}} = N$ in the limit of zero disorder to $Q_{\mathrm{chiral}} = 0$ in the strong disorder limit. The transitions take place at the critical disorder strengths of Eq. (3.2). The topological quantum number Q is given by Eq. (3.7).

3.5 Topological Phases for Disordered $p + ip$ Superconducting Wire

When the transverse coupling proportional to Δ_y' is taken into account, the chiral symmetry is broken, and the topological quantum number Q_{chiral} is no longer meaningful. The quantum number Q remains well defined, however. Since the effect of Δ_y' is small if $W \ll \xi$ [Kell 12a], the value of Q remains unchanged upon inclusion of the transverse coupling. Upon increasing the disorder strength, we therefore expect alternation between topological trivial ($Q = 1$) and nontrivial ($Q = -1$) phases until, in the limit of strong disorder, $l < \xi/(N+1)$, the system remains in the trivial state. As long as $W \ll \xi$, the transition points should exhibit only a weak dependence on the transverse coupling Δ_y'. In fact, not only the form of the phase diagram does not change upon breaking the chiral symmetry, also the properties of the phase transitions are expected to remain unaffected, a phenomenon known as "superuniversality" [Gruz 05].

Alternatively (and equivalently), for a superconductor wire with hard-wall ends, the transverse coupling pairwise gaps out the Q_{chiral} Majorana bound states at each end of the superconducting wire, leaving behind a single Majorana state if and only if Q_{chiral} is odd. Since Q_{chiral} decreases stepwise from N to zero upon increasing the disorder strength, the number of Majorana bound states at the end of the wire with Δ_y' taken into account alternates between 0 and 1, the transitions taking place precisely at the disorder strengths given in Eq. (3.2). Since the presence or absence of a single Majorana fermion is topologically protected, inclusion of the transverse coupling $\Delta_y' p_y$ for sufficiently small W/ξ does not affect these transitions or the transition points.

For broader wires, $W \sim \xi$, the transverse coupling can not be treated perturbatively, and the results for the chiral limit $\Delta_y' \to 0$ at best have qualitative validity if the transverse coupling is included. In this respect, we note that the topological phase transitions no longer take place at weak disorder $l \gg \lambda_F$ if $W \sim \xi$. This can be seen from Eq. (3.2) upon substituting $W \sim (N+1)\lambda_F$, which gives $l \sim n\lambda_F$. Equation (3.13), which was essential for establishing the transition points, is derived under the assumption of weak disorder, $l \gg \lambda_F$ [Been 97], and no longer has quantitative validity if this condition is violated.

3.6 Numerical analysis

In order to further support our conclusions and to investigate the regime $W \sim \xi$, we have performed numerical simulations of the Bogoliubov-de Gennes Hamiltonian (3.3). We calculate the reflection matrix r by concatenating short segments of length $\delta L \ll \lambda_F$. We refer to Ref. [Brou 11a] for a description of the numerical method. The scattering matrix of a short segment is calculated to lowest order Born approximation. For technical reasons the numerical data were obtained by varying the magnitude of the superconducting parameters Δ_x' and Δ_y' and keeping a fixed mean free path l.

First, we verify our analytical results in the chiral limit, $\Delta_y' = 0$. Figure 3.1 shows the topological number Q_{chiral} as a function of the ratio ξ/l for a wire with $N = 9$ channels. The figure clearly shows the stepwise decrease of Q_{chiral} upon increasing the disorder strength in comparison to the superconducting order. For coherence lengths of the order of the localization length $(N+1)l$ the transition points closely follow the theoretical prediction (3.2). We attribute the quantitative deviation of the transitions at large Q_{chiral}, when $\xi \sim l$, where the relevant Lyapunov exponent x_n is comparable to the inverse mean free path, to a failure of the estimate (3.13) in this regime [Been 97].

The effect of the transverse coupling on the phase transitions is shown in Fig. 3.2. Both panels of Fig. 3.2 show the value of $Q = \det r$ as a function of $(N+1)l/\xi$ and of Δ_y'/Δ_x' at a fixed realization of the random potential V (*i.e.*, at a fixed value of the mean free path l). The top panel of this figure shows representative numerial data for a weakly disordered wire ($\lambda_F/l = 0.011$), where all transitions take place within the limit $W \ll \xi$. As expected, the sequence of topologically trivial and nontrivial phases does not significantly depend on the transverse coupling Δ_y' in this case. The bottom panel shows data for strong disorder ($\lambda_F/l = 0.43$), where the condition $W \ll \xi$ is no longer satisfied for small values of ξ/l. The disorder strength is chosen such that the condition $W \simeq \xi$ is met roughly at the 6th transition. For the necessarily finite wire lengths L in the numerical simulations, finite-size effects lead to a blurring of the topological phase transitions. The occurrence of values of $\det r$ different from -1 or 1 signals a breakdown of the insulating behavior of the superconductor. This behavior is consistent with Ref. [Brou 03], where it was found that for large N a spinless superconducting wire enters a quasi-critical region with algebraic instead of exponentially decaying transmission [Brou 00], which persists up to wire lengths L much larger than the normal-state localization length and out of range of our numerical simulations. It is also consistent with the approach of the two-dimensional limit, in which the one-dimensional thermal insulator transitions into a two-dimensional thermal metal [Medv 10].

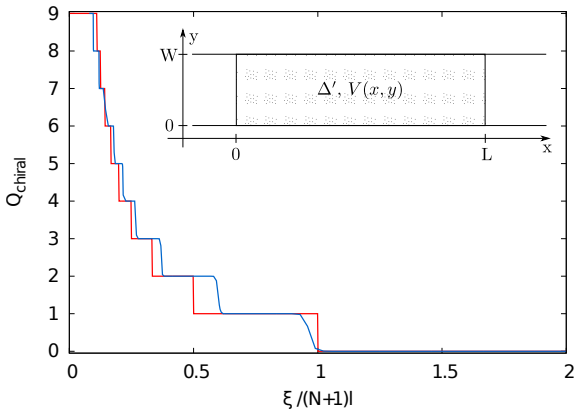

Figure 3.1: Topological number Q_{chiral} for a wire with width $2W/\lambda_F = 9.5$ such that the channel number is $N = 9$, as a function of the ratio ξ/l of disorder strength and induced superconductivity. Data shown are for a single disorder realization with $\lambda_F/l = 0.011$ and wire length $L/l \sim 2100$. The red curve shows the analytical prediction (3.22) and the blue one the numerical data. Inset: Schematic picture of a disordered superconducting wire with two ideal normal-metal leads.

3.7 Conclusions

In conclusion, we investigated the effect of disorder on the topological phase in a multichannel p-wave superconducting wire. From an analytical study in the limit of thin wires $W \ll \xi$, we derived a series of topological phases transitions in which the system alternates between trivial and nontrivial phases. A numerical analysis shows that this holds true also for thicker wire $W \lesssim \xi$

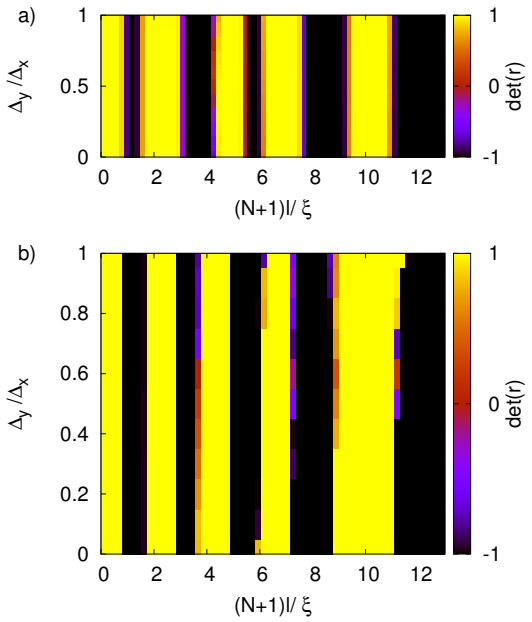

Figure 3.2: Phase diagrams showing the topological number $Q = \det(r)$ of a wire with $2W/\lambda_F = 9.5$ as a function of the ratio l/ξ and the transverse coupling Δ'_y in a spinless superconducting wire witih $N = 9$ channels in the limit of weak and strong disorder (panel **a)** and **b)**, resp.). The disorder strength is $\lambda_F/l = 0.011$ (panel **a)**) and $\lambda_F/l = 0.43$ (panel **b)**). The data were obtained for a wire length $L/l = 150$ (panel **a)**) and $L/l \sim 770$ (panel **b)**).

4 Density of states at disorder-induced phase transitions in a multichannel Majorana wire

An N-channel spinless p-wave superconducting wire is known to go through a series of N topological phase transitions upon increasing the disorder strength. Here, we show that at each of those transitions the density of states shows a Dyson singularity $\nu(\varepsilon) \propto \varepsilon^{-1}|\ln \varepsilon|^{-3}$, whereas $\nu(\varepsilon) \propto \varepsilon^{|\alpha|-1}$ has a power-law singularity for small energies ε away from the critical points. Using the concept of "superuniversality" introduced in Ref. [Gruz 05], we are able to relate the exponent α to the wire's transport properties at zero energy and, hence, to the mean free path l and the superconducting coherence length ξ. The content of this chapter is published in Ref. [Ried 14].

4.1 Introduction

Though stable against moderate amounts of disorder, topological phases are typically susceptible to strong disorder. This is particularly true for topological phases in one and two dimensions, for which strong disorder eventually leads to a localization of all electronic states. However, there are examples in which the effect of disorder may not be simply the transition from the topological into a topologically trivial localized phase, but more diverse physics appears.

The most prominent such example is the quantum Hall effect where disorder is an essential element needed to stabilize the topological phase and, hence, to explain the quantization of the conductance.[Chal 99] In the context of time-reversal invariant topological insulators, an initially topologically trivial, metallic system may be driven into a nontrivial phase by disorder, as it happens for topological Anderson insulators.[Li 09, Grot 09, Guo 10b, Guo 10a] Also, when disorder preserves certain symmetries on the average, the disorder itself may drive a topological insulator into a new type of topological phase.[Nomu 08, Ring 12, Fu 12, Fulg 14] Topological superconductors, finally, can display thermal metal [Fulg 12] or glassy phases [Crep 14] or enter a topologically nontrivial phase upon increasing disorder strength.[Adag 14]

An example where disorder leads to a particularly rich phase diagram is that of a multichannel spinless superconducting wire. In Ref. [Ried 13], the authors, together with Adagideli, showed that upon increasing the disorder strength such a wire goes through a series of topological phase transitions, alternating between states with and without a Majorana bound state at the wire's end.[Ried 13] For a wire with N transverse channels,

there are N such transitions, which take place at mean-free path

$$l_{\mathrm{crit}}^{(n)} = \frac{n\xi}{N+1}, \quad n = 1, 2, \ldots, N, \tag{4.1}$$

where ξ the superconducting coherence length. Note that multichannel disordered wires with chiral symmetry, but without superconducting pairing, are also known to exhibit series of topological phase transitions as a function of the disorder strength, see Refs. [Brou 98, Brou 00].

Whereas Ref. [Ried 13] identified the location of the topological phase transitions, it did not discuss the system's spectral and transport properties in the vicinity of the critical point. A theoretical framework in which this question can be addressed was provided by Gruzberg, Read, and Vishveshwara, [Gruz 05] who argued that there exists a "superuniversality", according to which all disorder-induced critical points in (quasi-)one dimension are of the same type as the critical point in the one-dimensional non-superconducting chiral class. For the chiral class, at the critical point the density of states displays a Dyson singularity [Dyso 53] $\nu(\varepsilon) \propto \varepsilon^{-1} |\ln \varepsilon|^{-3}$, whereas away from the transition, a power law $\nu(\varepsilon) \propto \varepsilon^{|\alpha|-1}$ is expected as $\varepsilon \to 0$, where α is a dimensionless parameter that measures the distance to the critical point. The statistics of wavefunctions and transmission probabilities (in the case of a system coupled to source and drain leads) is parameterized by the same parameter α. The density-of-states singularity and the associated wavefunction or transmission statistics occur in a wide range of physical systems, including lattice models with random hopping, [Theo 76, Egga 78] quantum XY chains, [Fish 94, Fish 95] narrow-gap semiconductors,[Ovch 77] dimerized polymer chains, [Su 79, Jack 83, Rice 82] and single-channel spinless superconductors. [Motr 01, Brou 11a, Gruz 05] Following the reasoning of Ref. [Gruz 05] the same critical behavior is expected to apply to the multichannel Majorana wire. It remains to express the non-universal dimensionless parameter α in terms of the model parameters, the mean free path l and the coherence length ξ.

4.2 Multichannel Majorana wire

We consider a disordered spinless p-wave superconducting wire in two dimensions, in a wire geometry with width W and length $L \to \infty$. The Hamiltonian for such a system has the form

$$H = \left[\frac{p^2}{2m} + V(x,y) - \mu\right]\sigma_z + \Delta'_x p_x \sigma_x + \Delta'_y p_y \sigma_y, \tag{4.2}$$

where $0 < x < L$ and $0 < y < W$ are longitudinal and transverse coordinates, respectively, the matrices $\sigma_{x,y,z}$ are Pauli matrices in electron/hole space, μ is the chemical potential, m the electron mass, $\Delta'_{x,y}$ are the p-wave superconducting pairing terms in the longitudinal and transversal directions, and $V(x,y)$ is the disorder potential, which is characterized through the elastic mean free path l. The number of channels N is defined as the number of propagating modes at the Fermi level in the absence of superconductivity, in particular $N = \mathrm{int}\,(2W/\lambda_{\mathrm{F}})$, where λ_{F} is the Fermi wavelength. The model (4.2) is an effective low-energy description of a system in which the superconducting correlations come from

proximity coupling to a nearby s-wave spinfull superconductor, [Fu 08, Lutc 10, Oreg 10, Cook 11, Duck 11, Ried 12] so that no self-consistency condition for Δ'_x and Δ'_y needs to be accounted for. The Hamiltonian H of Eq. (4.2) has no other symmetries than particle-hole symmetry, implying that the system is in symmetry class "D" according the Cartan classification. [Altl 97, Ryu 10, Ever 08]

For thin wires $W \ll \xi$, with the superconducting coherence length $\xi = \hbar/m\Delta'_x$, the term $\Delta'_y p_y \sigma_y$ only has a small effect on the wavefunctions and the spectrum and can be treated in perturbation theory. Without it, H obeys the chiral symmetry $\sigma_y H \sigma_y = -H$. [Tewa 12a, Kell 12a] In the Cartan classification this corresponds to symmetry class "BDI". Since the presence of the chiral symmetry significantly simplifies the calculation of the Majorana end states, Ref. [Ried 13] first analyzes the model (4.2) without the term $\Delta'_y p_y \sigma_y$. Here we take the same approach.

In the absence of disorder, and without the term $\Delta'_y p_y \sigma_y$, there are N Majorana bound states at each end of the wire, with a wavefunction that decays exponentially with decay length ξ upon moving away from the wire's end. With disorder, but still in symmetry class "BDI", a suitable basis of transverse channels can be chosen, such that the wavefunction envelope of the nth Majorana state at the wire's left end decays as [Ried 13]

$$\psi^{(n)}_{L/R}(x) \propto e^{-x/\xi + xn/(N+1)l}, \quad n = 1, 2, \ldots, N, \tag{4.3}$$

where l is the mean free path for scattering from the disorder potential V. At the critical disorder strengths $l^{(n)}_{\text{crit}}$ the wavefunction of the nth Majorana end state becomes delocalized, indicating a (topological) phase transition. At the phase transition, the nth Majorana end states at the two ends of the wire hybridize and annihilate. Increasing the disorder strength therefore leads to a series of N topological phase transitions in which the N Majorana bound states at the wire's end disappear one by one until the system reaches the topologically trivial state without Majorana end states.

The effect of including the term $\Delta'_y p_y \sigma_y$ is that Majorana end states at the same end of the wire can annihilate pairwise. Hence, one Majorana end state remains if the number of Majorana end states before including $\Delta'_y p_y \sigma_y$ was odd, and no Majorana end state remains if the number of Majorana end states was even. Thus, for the full Hamiltonian (4.2), the number of Majorana end states alternates between zero and one upon increasing the disorder strength, with the transitions approximately (with corrections that vanish in the limit $W/\xi \to 0$) taking place at the critical disorder strengths specified in Eq. (4.1).

In Ref. [Ried 13] this conclusion was reached by attaching source and drain leads to the Majorana wire with Hamiltonian (4.2) and formally mapping the scattering matrix of this problem to that of the disordered wire in the normal state (at a slightly renormalized chemical potential). In this mapping, the total quasiparticle conductance T of the Majorana wire in the limit $L \gg \xi$, Nl can be easily expressed in terms of the transmission eigenvalues τ_n of the disordered wire in the normal state

$$T = \sum_{n=1}^{N} \frac{(\tau_n/2)e^{2L/\xi}}{[1 + (\tau_n/4)e^{2L/\xi}]^2}. \tag{4.4}$$

The probability distribution of the transmission eigenvalues τ_n for large L and weak dis-

order is known in the literature, [Been 97]

$$\langle \log \tau_n \rangle = -\frac{2nL}{(N+1)l}, \quad \text{var} \log \tau_n = \frac{4L}{(N+1)l}. \tag{4.5}$$

For a mean free path l near the critical value $l_{\text{crit}}^{(n)} = n\xi/(N+1)$, the quasiparticle transmission is dominated by the nth transmission eigenvalue τ_n. Using the parameterization

$$T = 1/\cosh^2 z, \tag{4.6}$$

one finds

$$\langle z \rangle = \left(\frac{l_{\text{crit}}^{(n)}}{\xi} - \frac{l}{\xi} \right) \frac{L}{l}, \quad \text{var}\, z = \frac{L}{(N+1)l}. \tag{4.7}$$

Indeed, at the critical disorder strength (and at the critical disorder strength only) quasiparticle wavefunctions are delocalized throughout the sample. [Akhm 11]

The mapping between the scattering matrices of the disordered wire with and without superconductivity that was used in Ref. [Ried 13] exists for zero energy only. For that reason, Ref. [Ried 13] could not access the density of states $\nu(\varepsilon)$ of the multichannel Majorana wire in the vicinity of the critical points. We now show how the density of states can be obtained from the transmission statistics of Eq. (4.6) and (4.7) using the "superuniversality" argument of Ref. [Gruz 05].

4.3 Mapping to one-dimensional model with chiral symmetry

According to the "superuniversality" argument of Gruzberg, Read, and Vishveshwara, [Gruz 05] the quasiparticle transmission distribution T and the density of states $\nu(\varepsilon)$ in the vicinity of the critical point should be the same as that of a one-dimensional disordered wire in the chiral symmetry class. (In this respect, the three chiral classes BDI, AIII, and CII are interchangeable.) Such systems have been analyzed abundantly in the literature, see, *e.g.*, Refs. [Comt 95, Brou 98, Brou 01, Theo 76, Egga 78, Ston 81, Tito 01], and we here summarize the main results of relevance to the present problem.

A prototype of the disordered wire with chiral symmetry in one dimension is described by the Hamiltonian [Comt 95]

$$H_{\text{chiral}} = -v_{\text{F}} p \sigma_z + w(x)\sigma_x, \tag{4.8}$$

where v_{F} is the Fermi velocity and w is a random potential with mean $\langle w(x) \rangle = (\hbar v_{\text{F}} \alpha)/(2\bar{l})$ and variance $\langle w(x)w(x') \rangle = (\hbar^2 v_{\text{F}}^2/\bar{l})\delta(x-x')$. The parameter α measures the distance to the critical point; $\bar{l}$ is the mean free path in this system. In the vicinity of the critical point, the transmission $T = 1/\cosh^2 z$ of such a disordered one-dimensional wire of length L, coupled to ideal source and drain leads has a distribution given by

$$\langle z \rangle = \alpha \frac{L}{2\bar{l}}, \quad \text{var}\, z = \frac{L}{\bar{l}}. \tag{4.9}$$

The density of states $\nu(\varepsilon)$ has a singularity at zero energy, which is best described through the integrated density of states

$$N(\varepsilon) = \int_0^\varepsilon \nu(\varepsilon)\,. \tag{4.10}$$

An expression for the density of states can be derived by adapting existing calculations of the density of states in a wire with chiral symmetry at the critical point $\alpha = 0$. Here we take Ref. [Tito 01] as our starting point, where the density of states was calculated from the stationary distribution $P(x)$ of the reflection eigenvalue $R = \tanh^2(x)$ of a wire with Hamiltonian (4.8), evaluated at the *imaginary* energy $\varepsilon = -i\omega$, $\omega > 0$, and in the limit of a large wire length L. In Ref. [Tito 01] this distribution is found as the stationary solution of the Fokker-Planck equation

$$\frac{\partial P(x)}{\partial L} = \frac{\partial}{\partial x}\left[\frac{\omega}{v_\mathrm{F}}\sinh 2x + \frac{1}{2\bar{l}}J\frac{\partial}{\partial x}J^{-1}\right]P(x), \tag{4.11}$$

where J is a Jacobian which, for the case of a one-dimensional wire with chiral symmetry takes the value $J = 1$ at the critical point $\alpha = 0$. Solving Eq. (4.11) gives the stationary solution

$$P(x) = \frac{1}{Z(a)}|J|e^{-a\cosh 2x}, \tag{4.12}$$

with $a = \omega l/\hbar v_\mathrm{F}$ and $Z(a)$ a normalization factor. The key result of Ref. [Tito 01] is a general relation between the integrated density of states $N(\varepsilon)$ and this normalization factor,

$$N(\varepsilon) = \frac{L}{\pi\bar{l}}\,\mathrm{Im}\left[a\frac{\partial}{\partial a}\ln Z(a)\right]_{a\to -i\bar{l}\varepsilon/\hbar v_\mathrm{F}}. \tag{4.13}$$

The calculation of Ref. [Tito 01] is easily generalized to the case $\alpha \neq 0$: Nonzero α gives rise to a constant drift term in the Fokker-Planck equation (4.11) [Brou 98] or, equivalently, an exponential factor in the Jacobian J,

$$J = e^{-\alpha x}. \tag{4.14}$$

The stationary solution and the integrated density of states are then obtained in the same way as described above. One finds

$$Z(a) = K_{\alpha/2}(a), \tag{4.15}$$

where $K_\nu(x)$ is the Bessel function of the second kind. from which follows

$$N(\varepsilon) = \frac{L}{2\bar{l}|K_{\alpha/2}(2i\varepsilon v_\mathrm{F}/\hbar\bar{l})|^2}\,. \tag{4.16}$$

For $\alpha = 0$ Eq. (4.16) reproduces the Dyson singularity $\nu(\varepsilon) \propto 1/[\varepsilon \ln^3(\varepsilon v_\mathrm{F}/\hbar\bar{l})]$, whereas for nonzero α one has the asymptotic dependence $\nu(\varepsilon) \propto |\varepsilon|^{|\alpha|-1}$. Near the critical point

$\alpha = 0$ Eq. (4.16) is to be preferred over the asymptotic power-law dependence, because it applies to a much wider range of energies than the simple asymptotic power law $\nu(\varepsilon) \propto |\varepsilon|^{|\alpha|-1}$.

Comparing Eqs. (4.7) and (4.9), one immediately identifies

$$\alpha_n = \frac{2(N+1)}{\xi}\left(l_{\text{crit}}^{(n)} - l\right), \quad \bar{l} = (N+1)l, \tag{4.17}$$

as the dimensionless distance to the nth critical point for the disordered multichannel Majorana wire, and the equivalent mean free path in the model (4.8), respectively. The density of states and transmission statistics are governed by the distance to the closest critical point,

$$|\alpha| = \min_{n=1}^{N} |\alpha_n|. \tag{4.18}$$

4.4 Numerics

We now compare our predictions to numerical simulations of a disordered multichannel Majorana wire. For technical reasons, we first present numerical calculations for a slight variation of the model (4.2), in which the Majorana wire is represented by N coupled one-dimensional channels with Hamiltonian

$$H_{mn} = \delta_{mn}\left[\left(-\frac{\hbar^2}{2m}\partial_x^2 - \mu\right)\sigma_z - i\Delta_x'\partial_x\sigma_x\right] + u_{mn}(x)\sigma_z, \tag{4.19}$$

with a disorder term $u_{mn}(x)$ that has zero mean and variance

$$\langle u_{ij}(x)u_{kl}(x')\rangle = \frac{(\hbar v_{\text{F}})^2}{l(N+1)}\delta(x-x')\left(\delta_{ik}\delta_{jl} + \delta_{il}\delta_{jk}\right), \tag{4.20}$$

l being the mean free path. The technical advantage of Eq. (4.19) is that the normal-state distribution (4.5) of the transmission eigenvalues also holds up to moderately strong disorder strengths, so that numerical calculations can be performed for (comparatively) smaller system sizes. The Hamiltonian (4.19) anticommutes with σ_y, *i.e.*, it is in symmetry class BDI.

In order to determine the density of states, we couple one end of the N-channel wire to an ideal lead, keeping the other end closed. Following the method of Ref. [Brou 11a] we calculate the wire's scattering matrix $S(\varepsilon, L)$ as a function of the length L of the disordered wire. The integrated density of states $N(\varepsilon)$ can be obtained by numerically integrating the relation

$$\frac{\partial N(\varepsilon)}{\partial L} = \frac{1}{2\pi}\text{Im}\,\frac{\partial \log\det S(\varepsilon)}{\partial L}. \tag{4.21}$$

The integrated density of states obtained this way can be fitted to the functional form (4.16), which allows us to obtain the dimensionless parameter α as a function of the disorder strength. Results for Majorana wires with $N = 1$ and $N = 3$ are shown in

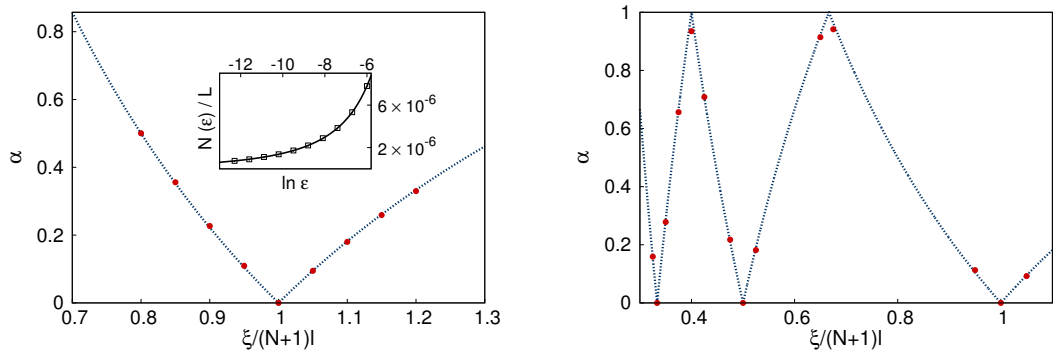

Figure 4.1: Dimensionless distance to the critical point as a function of the ratio ξ/l of superconducting coherence length and mean free path. The red dots show the exponent α obtained by fitting the numerically computed integrated density of states to the functional form in Equation (4.16) for a single-channel wire (top) and a three-channel wire (bottom). The dashed curve is the exponent expected from the mapping onto a single channel hopping model, see Eq. (4.18). Inset: Example of a fit of the integrated density of states normalized by the wire length as a function of energy. The squares show the numerically obtained data and the continuous curve is the analytical result, Eq. (4.16), using the value $\alpha = 0.0906$ obtained from the fitting procedure. The value of $\bar{l}$ can be obtained directly from the model parameters and need not be fitted, see Eqs. (4.17) and (4.20).

Fig. 4.1. The agreement is excellent and holds throughout the entire range of disorder strengths, including points far away from the critical disorder strengths.

We have also performed numerical calculations for the two-dimensional Hamiltonian (4.2) in a strip geometry. We choose the two pairing terms Δ'_x and Δ'_y to be equal. Since such a system is no longer in class BDI, we expect slight deviations in the quantitative estimates of the critical disorder strength and the dimensionless distance to the critical point. The numerical results for a wire with $N = 2$ indeed show a slight deviation of the critical disorder strength at the second phase transition, although, within the accuracy of our numerical calculations, no deviation for the dimensionless distance α can be discerned, see Fig 4.2.

4.5 Conclusions

We have investigated the density of states of a multichannel spinless superconducting wire, as it goes through a series of disorder-driven topological phase transitions. Using the concept of "superuniversality" of Gruzberg, Read, and Vishveshwara [Gruz 05], we could establish a relation between the known quasiparticle transmission statistics at zero energy and the singular contribution to the density of states at finite energies. A comparison with a numerical solution of the problem is in excellent agreement with these analytical results. Our results are a powerful demonstration of the concept of superuniversality, showing that

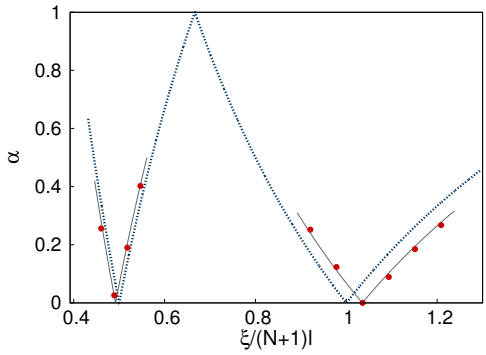

Figure 4.2: Dimensionless distance α to the critical point for the model (4.2) with $\Delta'_x = \Delta'_y$ and $N = 2$ transverse channels. The dashed line is the analytical prediction (4.18). The continuous line is the analytical prediction Eq. (4.17) corrected for the slight shift of the critical disorder strength at the second phase transition by inserting the value of $l^{(n)}_{\text{crit}}$ observed in the numerics.

in one dimension, as well as in quasi one dimension, the scaling relations for the density of states remain valid across boundaries between symmetry classes.

5 Conclusion

Topological phases of matter have attracted great interest in the last years. Particularly, topologically superconducting wires, which harbor special excitations—the Majorana states —at their ends are studied extensively in theoretical and experimental works. Experimental realizations are based on hybrid structures of semiconductor or ferromagnetic wires proximity-coupled to a conventional superconductor. The general idea behind these approaches is that if one succeeds to induce superconductivity into a spin-polarized system, the pairing potential must be odd in momentum. In the simplest case this results in a one-dimensional p-wave superconductor, the prototype of topologically superconducting wires, which is realized in these hybrid systems as an effective low-energy theory. The superconductivity is then topological in nature, which is signified by the existence of a Majorana bound state at the wire's ends—the edges of a one-dimensional system.

In real systems, one is generally not concerned with strictly one-dimensional but rather multi-mode systems, which can lead to an effective multichannel p-wave superconductor. The latter can be modeled with the (topologically nontrivial) two-dimensional $p + ip$ superconductor, characterized by the superconducting pairing potential $\Delta(p) = \Delta'(p_x + ip_y)$, which is restricted to a narrow-strip geometry. Then, the transverse momentum p_y is quantized and the number of occupied channels N is determined by the chemical potential. Each of the channels by itself constitutes a one-dimensional p-wave superconductor, which is coupled to the others by the transverse superconducting coupling $\Delta' p_y$. The Majorana states associated with the individual channels gap out pairwise and therefore the parity of the number of channels decides whether the system is in a topologically non-trivial phase or not. The gapped Majoranas form fermionic states which cluster around zero energy. They remain well below the superconducting gap Δ, with a typical energy scale $\varepsilon_{\text{typ}} \propto \Delta(W/\xi)^2$, with the wire width W and the superconducting coherence length ξ [Kell 12a]. The energy of the lowest-lying states is even smaller by a factor $1/N$. This accumulation of states around the gap center is an indication of a small parameter in the problem, the transverse coupling $\Delta' p_y$. It can be interpreted with an additional symmetry effectively obeyed by the system: To zero-th order perturbation theory in the transverse coupling the wire displays an effective time-reversal symmetry, which, in the language of symmetry classifications, places it in class BDI, where several Majorana bound states can exist at each end; in this case one per channel. Beyond zero-th order, this symmetry is broken. The system is now to be placed in symmetry class D and at most a single Majorana can remain at the wire's end. This transition happens just by the pairwise gapping of Majorana states mentioned before. The fact that the gapped states remain close to zero energy indicates that the perturbation theory is well justified and the wire is effectively in symmetry class BDI. This observation can be used generally when discussing the low-energy spectrum or topological phases of a multichannel p-wave superconductor, allowing for an analytical treatment.

In this Thesis we discussed several aspects of such quasi-one dimensional p-wave superconducting wires. In particular we considered the effect of disorder and various wire geometries on the low-energy spectrum, and the topological phases and spectral properties of a p-wave superconducting wire at arbitrary disorder strength.

In Chapter 2, based on Ref. [Ried 12], we discussed the low-energy spectrum of a multi-channel p-wave superconductor formed by the gapped Majorana states. It has been pointed out that the clustering of subgap states with the small scaling mentioned above is an artifact of the particular rectangular strip geometry considered [Pott 12]. The all too perfect shape of the wire leads to destructive interference between the wave functions of Majoranas stemming from different channels, which cancels the leading contribution to $\varepsilon_{\mathrm{typ}}$. The first part of Chapter 2 discusses the influence of various forms of wire-endings on the scaling of the subgap states' typical energy scale. The general procedure we pursued for this analysis is in terms of a scattering matrix that describes electrons entering the metal stub and getting reflected back into the wire. Already for a short rectangular metal stub of length $k_F^{-1} \ll L \ll W$ the destructive interference of the leading order term is canceled and leads to a parametrically larger typical energy scale $\varepsilon_{\mathrm{typ}} \propto \Delta L/\xi$, which is much smaller than the gap. For smaller lengths the cancellation from interference steps in to recover the result from Ref. [Kell 12a]. The largest scaling of the typical energies is observed for quadratic stubs, where $\varepsilon_{\mathrm{typ}} \propto \varepsilon_{\mathrm{m}} \Delta W/\xi$. At very large lengths $L \gg \xi$ the energies of the subgap states decrease again as $1/L$, which is just the decrease of level spacing with system size. Considering a chaotic cavity for the metallic stub two different limits, distinguished by the dwell time $\bar{\tau}$ of the cavity, can be considered: For small cavities, $\hbar\bar{\tau}^{-1} \gg \Delta$, the scaling is again bigger and dominated by the wire width $\varepsilon_{\mathrm{typ}} \sim \varepsilon_{\mathrm{m}}$. The subgap states 'live' mainly in the wire. In contrast, in the large cavity limit $\bar{\tau}^{-1} \lesssim \Delta$ most weight of the states lies in the cavity, decreasing the typical energy scaling $\varepsilon_{\mathrm{typ}} \sim \hbar W/\bar{\tau}\xi$. The smallest energy level in these case is generally $\varepsilon_{\mathrm{min}} \sim \varepsilon_{\mathrm{typ}}/N \ln N$.

An important point to consider here is that the pairing potential, which, in this analysis, was modeled as a step function that marks a clear boundary between the superconducting wire and the normal metal stub. However, the wire is assumed to inherit the pairing by proximity-coupling from a bulk superconductor surrounding it and the stub can then be seen as a piece of this wire sticking out of the superconductor. The proximity effect in the wires is due to many Andreev reflections of the wire's electrons at the interface with the superconductor. If the wire has a non-negligible width $W \geq k_F^{-1}$, the electrons can be pictured as moving mainly along the longitudinal direction while bouncing off the wires transverse boundaries. Thus, the induced pairing should decay on a scale of this width into the stub rather than just dropping to zero. At first sight this seems to have the implication that the destructive interference is annihilated already without the rectangular stub, whose addition would then have no significant further effect as long as it is not too long. However, it is also known that variations in terminating potentials that are smooth on a scale of the coherence length ξ can have the effect of decoupling two gapped Majorana states, see Refs. [Ried 12, Kell 12b]. An interesting task for future research would be to study the actual behavior of the subgap states for a smooth decay of the pairing potential.

In Chapter 2, we also discussed the influence of potential disorder on the low-energy spectrum. With respect to our previous discussion of geometries and interference of wavefunctions, one would expect that disorder would, similarly to a chaotic cavity, scramble

the wavefunctions. This would annihilate the destructive interference, causing the leading order of the subgap energies to reappear. For a few disorder configurations this is indeed that case but we found that on average, disorder pushes down the subgap states down towards $\varepsilon = 0$. This can be seen as the first steps in the direction of a disorder-induced topological phase transition, which is accompanied by a closing of the excitation gap and will be discussed below.

As a concluding remark to Chapter 2 we note that different imperfections, such as various geometrical terminations or disorder, of a multichannel p-wave superconducting wire can have different effects on the subgap states. In experiments probing the density of states of such a wire one needs to take special care of what is actually measured. A zero-bias peak in a tunneling conductance measurement could also originate from fermionic subgap states that are present whether or not the wire is in a topologically non-trivial phase. A good resolution of the measured peak due to low temperatures and low transmission of the tunneling parameter could rule out this scenario.

In Chapter. 2 it was noted that weak disorder not only pushes down the subgap states but also decreases the total gap, which turns out to be the onset of a disorder-induced topological phase transition, which is discussed in Chapter 3. There, we consider a multichannel p-wave superconductor with Gaussian white noise disorder on top of the chemical potential. In contrast to a spin-singlet superconductor, disorder can be effective in a p-wave superconductor: localized states appear in the gap and accumulate around its center as the disorder strength is increased. The disorder is parametrized by the mean free path l in the normal state. There are two relevant length (or respectively energy) scales in the system: the mean free path l and the superconducting coherence length ξ, which parametrizes the pairing strength with respect to a clean system. We find a series of N disorder-induced topological phase transitions, at $\xi = (N+1)l/n$ where $n = 1, ..., N$ and N is the number of channels. In each of those transitions the bulk gap closes and the topological phase changes between trivial and non-trivial, thus, a Majorana state appears or vanishes. At each phase transition point the system delocalizes at zero energy and displays a perfect transmission, which otherwise is exponentially suppressed in the wire length.

The analysis of the topological phase of a $p + ip$ superconducting wire is carried out by means of a scattering matrix describing the electronic transport in metallic leads attached to each wire end. Then, for long enough wires, the reflection matrix encodes the information on the topological phase: for the full system (in symmetry-class D), the determinant of the reflection matrix is $+1$ or -1 in the trivial and non-trivial phase respectively. In the effective class-BDI wire the non-zero eigenvalues of the Andreev reflection matrix count the number of Majorana bound states at each end. We showed in Chapter 3 that at zero energy the p-wave superconductor can be mapped onto a disordered normal metal. Such systems and their scattering matrices are well studied. What is relevant to this case is that in a quasi-one dimensional system each channel has a different localization length $l_n = nl/(N+1)$ associated with it. We find that this scale individually competes for each mode with the coherence length and a phase transition in this particular channel occurs when they equal each other, independently from the other channels. The analytical approach is strictly valid only for the zero-th order approximation to the $p + ip$ superconducting wire. In this case, the wire harbors N Majorana states in the clean limit which

disappear one by one. The full system is then expected to show an alternation between trivial and non-trivial phases, which is verified by a numerical analysis.

In a one-dimensional system a single phase transition occurs when the mean free path is of the order of the coherence length. We showed that a multichannel wire can sustain topologically non-trivial phases for much larger disorder strengths: Tuning the disorder, the first phase transition occurs when $l \sim \xi$ while the last transition from a non-trivial to a trivial phase happens only at $l \sim \xi/N$.

The disorder-induced phase transitions happen due to an accumulation of disorder-localized states in the superconducting gap. At the critical points enough states have accumulated at zero energy to hybridize with the two Majorana end states in the critical channel causing them to gap out. This process can be tracked in the density of states of the wire, which is the subject of Chapter 4. There, it is shown that in a multichannel p-wave superconducting wire the density of states is dominated by the channel closest to criticality. At low enough energies the microscopic details of the system become unimportant and the density of states exhibits a power law $\nu(\varepsilon) \propto |\varepsilon|^{|\alpha|-1}$, where α is a dimensionless parameter that measures the distance to the closest critical point, in particular the smallest values of $\alpha_n = 2(N+1)(l_n - l)/\xi$ for $n = 1, .., N$. The critical disorder strength of the n-th channel for the class-BDI system is given by $l_{\text{crit}}^{(n)} = n\xi/(N+1)$. In the full class-$D$ Hamiltonian these values deviate slightly from the analytical values and have to be extracted numerically.

To calculate the density of states during the phase transitions, we used an approach following the evolution of the scattering phase, related to the density of states, under an increase of the wire length. As the critical behavior is governed by only one channel one can restrict to a single-channel system with the appropriate critical point. Further, the superuniversality argument introduced in Ref. [Gruz 05] implies that the scaling of the scattering phases of a wire with a single lead is tightly connected to the scaling of the transmission eigenvalues for a wire with two leads. The latter is known exactly for the class-BDI Hamiltonian from the analysis of the scattering matrix in Chapter 3. Using these observations we can calculate the density of states at arbitrary disorder strengths as given above. For the full p-wave superconducting wire we conjecture a similar scaling accounted for a shift in the critical disorder strength, which is verified in a numerical simulation.

Note that the results imply that the density of states exhibits a peak at zero energy already at a disorder strength $\sim l_N(1 + 1/2N)$, well before the first phase transition. For larger channel numbers the disorder strengths in which this peaks has not appeared is increased. The singularity in the density of states appears only for larger disorder strengths giving rise to a wider parameter space to observe the actual Majorana state in e.g. a tunneling conductance experiment. This can be intuitively understood when thinking of the multichannel wire as a narrow 2-dimensional system. Localization by disorder is much more effective in 1D as the electrons are restricted to a single degree of freedom. Adding more channels to the system allows electrons to avoid localization to some extent. Between the different phase transitions in the multichannel wire the density of states is always peaked around $\varepsilon = 0$ and could therefore obscure the Majorana states that come and go.

The results of this Thesis are particularly interesting in the context of experiments that set out to measure signature of Majorana bound states in topologically superconducting

wires [Mour 12, Das 12, Chur 13, Nadj 14].

The experiments by Mourik et al. [Mour 12], Das et al. [Das 12], and Churchill et al. [Chur 13] aim to realize an effective p-wave superconductor with a semiconductor wire (InSb in Refs. [Mour 12, Chur 13] and InAs in Ref.[Das 12]) that is proximity coupled to a bulk superconductor. In all cases a magnetic field is applied to induce spin-splitting and gates below the wire are used to change the chemical. Only a part of the semiconductor wire is in contact with the superconductor, forming the topological superconductor, the other part stay in the normal state. In this way a normal metal-superconductor (NS) junction is naturally formed, with the tunneling strength controlled by an additional gate voltage. As discussed in the introduction, the tunneling conductance reflects the density of states at the wire end. All experiments report the existence of a zero-bias peak that appears at a critical magnetic field, remains stable for a range of magnetic fields, and splits when the field strength becomes too large. These observations are consistent with the existence of a topologically superconducting phase in the wire. Using the parameters of Ref. [Mour 12], with a spin-orbit energy of $\sim 50/, \mu eV$ and a Zeeman energy $\sim 300\,\mu eV$ at the first appearance of the peak, one can assume the superconducting gap to be dominated by the spin-orbit coupling. With this, the length scale on which a possible Majorana state would be localized is $\sim 100\,nm$. In Ref. [Mour 12] a normal-state mean free path $\sim 300\,nm$, one order of magnitude less than the wire length $\sim 1\,\mu m$, making the transport quasi-ballistic. In Ref. [Das 12] a mean free path longer than the wire length is suggested, implying ballistic transport, while in Ref. [Chur 13] the disorder strength is not specified. Thus, a peak in the density of states at zero-bias could also be caused by disorder.

In Chapter 3 we discussed how the model of a semiconductor wire with strong spin-orbit coupling in proximity to a superconductor is related to a $p + ip$-superconducting wire. A Zeeman field B is used to spin-polarize several channels in which the induced superconductivity will then be of a spin-triplet and thus p-wave pairing type. The gap associated with the topological protection is proportional to the spin-orbit coupling but scales inversely with the magnetic field $\Delta_{\text{top}} \sim \hbar k_F \alpha \Delta / B$. Here, Δ is the induced gap without any magnetic field. Applying stronger magnetic fields thus also reduces the gap, which, at first sight, seems to contradict the feasibility for a realization of a multichannel wire. However, for a wider wire the reduced spacing between the transverse channels results in an effective multichannel p-wave superconductor already for smaller magnetic fields. Even though the experiments using semiconductor wires are believed to realize an effective one-dimensional p-wave superconductor, the multichannel regime could be of relevance for future experiments. In particular, the multichannel regime would be desirable as it allows for higher disorder strengths without a singularity in the density of states due to localized states in the gap (see the discussion above).

In the experiment by Nadj-Perge et al. [Nadj 14], where chains of Fe-atoms are placed on bulk Pb, a superconductor with strong spin-orbit coupling, a spatially resolved measurement of the density of states is performed. Also there, the authors report the observation of a zero-bias peak, strongly localized at the chain's ends. When the Fe-atoms build a ferromagnetic chain, the 10 energy levels in Fe's outer electronic shell hybridize to form bands. The majority spin bands lie well below the Fermi level and do not contribute. The 5 minority-spin bands cut the Fermi level and each by itself forms a p-wave superconductor. This seems to realize a multichannel situation, however, 2 bands have an inverted

dispersion relation such that their Fermi velocities are reversed. The Majorana states that are formed in these bands are of such a nature that they gap out with 2 Majoranas of the remaining 3 bands and only a single channel remains as an effective topological superconductor.

If experiments were to realize topologically superconducting wires with ferromagnetic wires instead of chains it is likely that those would be effective multichannel p-wave superconductors. In this case also the maximum amount of disorder could be much stronger than in the semiconductor wires.

In summary, the multichannel regime in a p-wave superconducting wire on the one hand exhibits fascinating physics, like the multiple topological phase transitions, whose observation in experiment would be highly interesting, on the other hand, it also hinders the detection of Majorana states. If a tunneling-conductance measurement on the proximity-coupled semiconductor wire was to happen in the multichannel regime, it is likely that the arising subgap states would obscure the Majorana state in a measurement. From this point of view it would be more favorable to avoid the multichannel regime. However, if these difficulties were to be controlled in an experiment it would be a great opportunity to observe the reentrant topological transitions. The effective disorder strength could in principle be tuned by the chemical potential but instead it would also be possible to change the induced topological gap. In the setup using a semiconductor wire, for instance, the gap is inversely proportional to the magnetic field providing an experimental knob which is relatively easy to handle.

For future research it would be important to study the effect of a smoothly terminating induced superconducting gap on the subgap states in a multichannel p-wave superconductor as well as in the multichannel semiconductor model with a single channel realizing a topological superconductor. Another important point to bear in mind is that of the model for the disorder used here. In the analysis we considered Gaussian white noise potential disorder, which could result from impurities or lattice imperfections. However, another source of disorder could be a poor contact between the wire and the superconductor, causing electrons to form charge puddles that exert an effective potential on the wire. Also, in the case of magnetic atoms on a superconductor, there will always be some disorder in the hopping amplitudes from variations in the distances between atoms. Then, the effective disorder might be of a more complex form and it would be important to find a proper description and study its effect.

Bibliography

[Adag 14] i. d. I. Adagideli, M. Wimmer, and A. Teker, *"Effects of electron scattering on the topological properties of nanowires: Majorana fermions from disorder and superlattices"*, Phys. Rev. B, **89**, 144506, Apr 2014.

[Akhm 11] A. R. Akhmerov, J. P. Dahlhaus, F. Hassler, M. Wimmer, and C. W. J. Beenakker, *"Quantized Conductance at the Majorana Phase Transition in a Disordered Superconducting Wire"*, Phys. Rev. Lett., **106**, 057001, Jan 2011.

[Alic 10] J. Alicea, *"Majorana fermions in a tunable semiconductor device"*, Phys. Rev. B, **81**, 125318, Mar 2010.

[Alic 11] J. Alicea, Y. Oreg, G. Refael, F. von Oppen, and M. P. A. Fisher, *"Non-Abelian statistics and topological quantum information processing in 1D wire networks"*, Nature Physics, **7**, 412–417, (2011).

[Alic 12] J. Alicea, *"New directions in the pursuit of Majorana fermions in solid state systems"*, Reports on Progress in Physics, **75**, 076501, (2012).

[Altl 09] A. Altland and B. Simons. *Condensed Matter Field Theory.* Cambridge University Press, (2009).

[Altl 97] A. Altland and M. R. Zirnbauer, *"Nonstandard symmetry classes in mesoscopic normal-superconducting hybrid structures"*, Phys. Rev. B, **55**, 1142–1161, Jan 1997.

[Ande 59] P. Anderson, *"Theory of dirty superconductors"*, Journal of Physics and Chemistry of Solids, **11**, 26 – 30, (1959).

[Ando 74] T. Ando, *"Theory of Quantum Transport in a Two-Dimensional Electron System under Magnetic Fields. III. Many-Site Approximation"*, Journal of the Physical Society of Japan, **37**, 622–630, (1974).

[Andr 64] A. F. Andreev, *"Thermal conductivity of the intermediate state of superconductors"*, Sov. Phys. JETP, **19**, 1228, (1964).

[Badi 11] D. M. Badiane, M. Houzet, and J. S. Meyer, *"Nonequilibrium Josephson Effect through Helical Edge States"*, Phys. Rev. Lett., **107**, 177002, Oct 2011.

[Been 13a] C. Beenakker, *"Search for Majorana Fermions in Superconductors"*, Annual Review of Condensed Matter Physics, **4**, 113–136, (2013).

[Been 13b] C. Beenakker, *"Search for Majorana Fermions in Superconductors"*, Annual Review of Condensed Matter Physics, **4**, 113–136, (2013).

[Been 91] C. Beenakker and H. van Houten. "Quantum Transport in Semiconductor Nanostructures". In: H. Ehrenreich and D. Turnbull, Eds., *Semiconductor Heterostructures and Nanostructures*, 1 – 228, Academic Press, (1991).

[Been 97] C. W. J. Beenakker, *"Random-matrix theory of quantum transport"*, Rev. Mod. Phys., **69**, 731–808, Jul 1997.

[Bern 06] B. A. Bernevig, T. L. Hughes, and S.-C. Zhang, *"Quantum Spin Hall Effect and Topological Phase Transition in HgTe Quantum Wells"*, Science, **314**, 1757–1761, (2006).

[Bloc 58] C. Bloch, *"Sur la théorie des perturbations des états liés"*, Nuclear Physics, **6**, 329 – 347, (1958).

[Blon 82] G. E. Blonder, M. Tinkham, and T. M. Klapwijk, *"Transition from metallic to tunneling regimes in superconducting microconstrictions: Excess current, charge imbalance, and supercurrent conversion"*, Phys. Rev. B, **25**, 4515–4532, Apr 1982.

[Brou 00] P. W. Brouwer, C. Mudry, and A. Furusaki, *"Density of States in Coupled Chains with Off-Diagonal Disorder"*, Phys. Rev. Lett., **84**, 2913–2916, Mar 2000.

[Brou 01] P. Brouwer, C. Mudry, and A. Furusaki, *"Transport properties and density of states of quantum wires with off-diagonal disorder"*, Physica E: Low-dimensional Systems and Nanostructures, **9**, 333 – 339, (2001). Proceedings of an International Workshop and Seminar on the Dynamics of Complex Systems.

[Brou 03] P. W. Brouwer, A. Furusaki, and C. Mudry, *"Universality of delocalization in unconventional dirty superconducting wires with broken spin-rotation symmetry"*, Phys. Rev. B, **67**, 014530, Jan 2003.

[Brou 11a] P. W. Brouwer, M. Duckheim, A. Romito, and F. von Oppen, *"Probability Distribution of Majorana End-State Energies in Disordered Wires"*, Phys. Rev. Lett., **107**, 196804, Nov 2011.

[Brou 11b] P. W. Brouwer, M. Duckheim, A. Romito, and F. von Oppen, *"Topological superconducting phases in disordered quantum wires with strong spin-orbit coupling"*, Phys. Rev. B, **84**, 144526, Oct 2011.

[Brou 97] P. W. Brouwer, K. M. Frahm, and C. W. J. Beenakker, *"Quantum Mechanical Time-Delay Matrix in Chaotic Scattering"*, Phys. Rev. Lett., **78**, 4737–4740, Jun 1997.

[Brou 98] P. W. Brouwer, C. Mudry, B. D. Simons, and A. Altland, *"Delocalization in Coupled One-Dimensional Chains"*, Phys. Rev. Lett., **81**, 862–865, Jul 1998.

[Butt 86] M. Büttiker, *"Four-Terminal Phase-Coherent Conductance"*, Phys. Rev. Lett., **57**, 1761–1764, Oct 1986.

[Butt 88] M. Büttiker, *"Symmetry of electrical conduction"*, IBM J. Res. Dev., **32**, 317, (1988).

[Caro 64] C. Caroli, P. D. Gennes, and J. Matricon, *"Bound Fermion states on a vortex line in a type II superconductor"*, Physics Letters, **9**, 307 – 309, (1964).

[Chal 99] J. Chalker. "The integer quantum Hall effect and Anderson localisation". In: A. Comtet, T. Jolicoeur, S. Ouvry, and F. David, Eds., *Ecole des Houches: Topological Aspects of low dimensional systems*, Springer, (1999).

[Choy 11] T.-P. Choy, J. M. Edge, A. R. Akhmerov, and C. W. J. Beenakker, *"Majorana fermions emerging from magnetic nanoparticles on a superconductor without spin-orbit coupling"*, Phys. Rev. B, **84**, 195442, Nov 2011.

[Chun 11] S. B. Chung, H.-J. Zhang, X.-L. Qi, and S.-C. Zhang, *"Topological superconducting phase and Majorana fermions in half-metal/superconductor heterostructures"*, Phys. Rev. B, **84**, 060510, Aug 2011.

[Chur 13] H. O. H. Churchill, V. Fatemi, K. Grove-Rasmussen, M. T. Deng, P. Caroff, H. Q. Xu, and C. M. Marcus, *"Superconductor-nanowire devices from tunneling to the multichannel regime: Zero-bias oscillations and magnetoconductance crossover"*, Phys. Rev. B, **87**, 241401, Jun 2013.

[Comt 95] A. Comtet, J. Desbois, and C. Monthus, *"Localization Properties in One-Dimensional Disordered Supersymmetric Quantum Mechanics"*, Annals of Physics, **239**, 312 – 350, (1995).

[Cook 11] A. Cook and M. Franz, *"Majorana fermions in a topological-insulator nanowire proximity-coupled to an s-wave superconductor"*, Phys. Rev. B, **84**, 201105, Nov 2011.

[Crem 02] J. N. H. J. Cremers and P. W. Brouwer, *"Dephasing in a quantum pump"*, Phys. Rev. B, **65**, 115333, Mar 2002.

[Crep 14] F. m. c. Crépin, G. Zaránd, and P. Simon, *"Nonperturbative phase diagram of interacting disordered Majorana nanowires"*, Phys. Rev. B, **90**, 121407, Sep 2014.

[Das 12] A. Das, Y. Ronen, Y. Most, Y. Oreg, M. Heiblum, and H. Shtrikman, *"Zero-bias peaks and splitting in an Al-InAs nanowire topological superconductor as a signature of Majorana fermions"*, Nature Physics, **8**, 887, (2012).

[Deng 12] M. T. Deng, C. L. Yu, G. Y. Huang, M. Larsson, P. Caroff, and H. Q. Xu, *"Anomalous Zero-Bias Conductance Peak in a Nb-InSb Nanowire-Nb Hybrid Device"*, Nano Letters, **12**, 6414–6419, (2012). PMID: 23181691.

[Deng 14] M. T. Deng, C. L. Yu, G. Y. Huang, M. Larsson, P. Caroff, and H. Q. Xu, *"Parity independence of the zero-bias conductance peak in a nanowire based topological superconductor-quantum dot hybrid device"*, Sci. Rep., **4**, 12 2014.

[Domi 12] F. Domínguez, F. Hassler, and G. Platero, *"Dynamical detection of Majorana fermions in current-biased nanowires"*, Phys. Rev. B, **86**, 140503, Oct 2012.

[Duck 11] M. Duckheim and P. W. Brouwer, *"Andreev reflection from noncentrosymmetric superconductors and Majorana bound-state generation in half-metallic ferromagnets"*, Phys. Rev. B, **83**, 054513, Feb 2011.

[Dyso 53] F. J. Dyson, *"The Dynamics of a Disordered Linear Chain"*, Phys. Rev., **92**, 1331–1338, Dec 1953.

[Egga 78] T. P. Eggarter and R. Riedinger, *"Singular behavior of tight-binding chains with off-diagonal disorder"*, Phys. Rev. B, **18**, 569–575, Jul 1978.

[Engl 78] T. Englert and K. V. Klitzing, *"Analysis of ρ_{xx} minima in surface quantum oscillations on (100) n-type silicon inversion layers"*, Surface Science, **73**, 70 – 80, (1978).

[Ever 08] F. Evers and A. D. Mirlin, *"Anderson transitions"*, Rev. Mod. Phys., **80**, 1355–1417, Oct 2008.

[Finc 13] A. D. K. Finck, D. J. Van Harlingen, P. K. Mohseni, K. Jung, and X. Li, *"Anomalous Modulation of a Zero-Bias Peak in a Hybrid Nanowire-Superconductor Device"*, Phys. Rev. Lett., **110**, 126406, Mar 2013.

[Fish 94] D. S. Fisher, *"Random antiferromagnetic quantum spin chains"*, Phys. Rev. B, **50**, 3799–3821, Aug 1994.

[Fish 95] D. S. Fisher, *"Critical behavior of random transverse-field Ising spin chains"*, Phys. Rev. B, **51**, 6411–6461, Mar 1995.

[Free 02] M. Freedman, M. Larsen, and Z. Wang, *"A Modular Functor Which Is Universal for Quantum Computation"*, Commun. Math. Phys., **227**, 605–622, (2002).

[Free 98] M. H. Freedman, *"P/NP, and the quantum field computer"*, Proceedings of the National Academy of Sciences, **95**, 98–101, (1998).

[Fu 07a] L. Fu and C. L. Kane, *"Topological insulators with inversion symmetry"*, Phys. Rev. B, **76**, 045302, Jul 2007.

[Fu 07b] L. Fu, C. L. Kane, and E. J. Mele, *"Topological Insulators in Three Dimensions"*, Phys. Rev. Lett., **98**, 106803, Mar 2007.

[Fu 08] L. Fu and C. L. Kane, *"Superconducting Proximity Effect and Majorana Fermions at the Surface of a Topological Insulator"*, Phys. Rev. Lett., **100**, 096407, Mar 2008.

[Fu 10] L. Fu, *"Electron Teleportation via Majorana Bound States in a Mesoscopic Superconductor"*, Phys. Rev. Lett., **104**, 056402, Feb 2010.

[Fu 12] L. Fu and C. L. Kane, *"Topology, Delocalization via Average Symmetry and the Symplectic Anderson Transition"*, Phys. Rev. Lett., **109**, 246605, Dec 2012.

[Fulg 11] I. C. Fulga, F. Hassler, A. R. Akhmerov, and C. W. J. Beenakker, *"Scattering formula for the topological quantum number of a disordered multimode wire"*, Phys. Rev. B, **83**, 155429, Apr 2011.

[Fulg 12] I. C. Fulga, A. R. Akhmerov, J. Tworzydło, B. Béri, and C. W. J. Beenakker, *"Thermal metal-insulator transition in a helical topological superconductor"*, Phys. Rev. B, **86**, 054505, Aug 2012.

[Fulg 14] I. C. Fulga, B. van Heck, J. M. Edge, and A. R. Akhmerov, *"Statistical topological insulators"*, Phys. Rev. B, **89**, 155424, Apr 2014.

[Gibe 12] M. Gibertini, F. Taddei, M. Polini, and R. Fazio, *"Local density of states in metal-topological superconductor hybrid systems"*, Phys. Rev. B, **85**, 144525, Apr 2012.

[Grot 09] C. W. Groth, M. Wimmer, A. R. Akhmerov, J. Tworzydło, and C. W. J. Beenakker, *"Theory of the Topological Anderson Insulator"*, Phys. Rev. Lett., **103**, 196805, Nov 2009.

[Gruz 05] I. A. Gruzberg, N. Read, and S. Vishveshwara, *"Localization in disordered superconducting wires with broken spin-rotation symmetry"*, Phys. Rev. B, **71**, 245124, Jun 2005.

[Guo 10a] H.-M. Guo, *"Topological invariant in three-dimensional band insulators with disorder"*, Phys. Rev. B, **82**, 115122, Sep 2010.

[Guo 10b] H.-M. Guo, G. Rosenberg, G. Refael, and M. Franz, *"Topological Anderson Insulator in Three Dimensions"*, Phys. Rev. Lett., **105**, 216601, Nov 2010.

[Hald 88] F. D. M. Haldane, *"Model for a Quantum Hall Effect without Landau Levels: Condensed-Matter Realization of the "Parity Anomaly""*, Phys. Rev. Lett., **61**, 2015–2018, Oct 1988.

[Hasa 10] M. Z. Hasan and C. L. Kane, *"Colloquium : Topological insulators"*, Rev. Mod. Phys., **82**, 3045–3067, Nov 2010.

[Hasa 11] M. Z. Hasan and J. E. Moore, *"Three-Dimensional Topological Insulators"*, Annual Review of Condensed Matter Physics, **2**, 55–78, (2011).

[Hata 96] N. Hatano and D. R. Nelson, *"Localization Transitions in Non-Hermitian Quantum Mechanics"*, Phys. Rev. Lett., **77**, 570–573, Jul 1996.

[Hews 93] A. C. Hewson. *The Kondo Problem to Heavy Fermions.* Cambridge University Press, (1993). Cambridge Books Online.

[Hsie 08] D. Hsieh, D. Qian, L. Wray, Y. Xia, Y. S. Hor, R. J. Cava, and M. Z. Hasan, *"A topological Dirac insulator in a quantum spin Hall phase"*, Nature, **452**, 970–974, 04 2008.

[Ivan 01] D. A. Ivanov, *"Non-Abelian Statistics of Half-Quantum Vortices in p-Wave Superconductors"*, Phys. Rev. Lett., **86**, 268–271, Jan 2001.

[Jack 83] R. Jackiw and G. Semenoff, *"Continuum Quantum Field Theory for a Linearly Conjugated Diatomic Polymer with Fermion Fractionization"*, Phys. Rev. Lett., **50**, 439–442, Feb 1983.

[Jian 11] L. Jiang, D. Pekker, J. Alicea, G. Refael, Y. Oreg, and F. von Oppen, *"Unconventional Josephson Signatures of Majorana Bound States"*, Phys. Rev. Lett., **107**, 236401, Nov 2011.

[Jord 08] S. P. Jordan and E. Farhi, *"Perturbative gadgets at arbitrary orders"*, Phys. Rev. A, **77**, 062329, Jun 2008.

[Kane 05a] C. L. Kane and E. J. Mele, *"Quantum Spin Hall Effect in Graphene"*, Phys. Rev. Lett., **95**, 226801, Nov 2005.

[Kane 05b] C. L. Kane and E. J. Mele, *"Z_2 Topological Order and the Quantum Spin Hall Effect"*, Phys. Rev. Lett., **95**, 146802, Sep 2005.

[Kato 49] T. Kato, *"On the Convergence of the Perturbation Method. I"*, Progress of Theoretical Physics, **4**, 514–523, (1949).

[Kawa 78] S. Kawaji, *"Quantum galvanomagnetic experiments in silicon inversion layers under strong magnetic fields"*, Surface Science, **73**, 46 – 69, (1978).

[Kell 12a] G. Kells, D. Meidan, and P. W. Brouwer, *"Low-energy subgap states in multichannel p-wave superconducting wires"*, Phys. Rev. B, **85**, 060507, Feb 2012.

[Kell 12b] G. Kells, D. Meidan, and P. W. Brouwer, *"Near-zero-energy end states in topologically trivial spin-orbit coupled superconducting nanowires with a smooth confinement"*, Phys. Rev. B, **86**, 100503, Sep 2012.

[Kita 01] A. Y. Kitaev, *"Unpaired Majorana fermions in quantum wires"*, Physics-Uspekhi, **44**, 131, (2001).

[Kita 03] A. Kitaev, *"Fault-tolerant quantum computation by anyons"*, Annals of Physics, **303**, 2 – 30, (2003).

[Kita 06] A. Kitaev, *"Anyons in an exactly solved model and beyond"*, Annals of Physics, **321**, 2 – 111, (2006). January Special Issue.

[Kita 09] A. Kitaev, *"Periodic table for topological insulators and superconductors"*, AIP Conference Proceedings, **1134**, 22–30, (2009).

[Kjae 12] M. Kjaergaard, K. Wölms, and K. Flensberg, *"Majorana fermions in superconducting nanowires without spin-orbit coupling"*, Phys. Rev. B, **85**, 020503, Jan 2012.

[Klit 80] K. v. Klitzing, G. Dorda, and M. Pepper, *"New Method for High-Accuracy Determination of the Fine-Structure Constant Based on Quantized Hall Resistance"*, Phys. Rev. Lett., **45**, 494–497, Aug 1980.

[Koni 07] M. König, S. Wiedmann, C. Brüne, A. Roth, H. Buhmann, L. W. Molenkamp, X.-L. Qi, and S.-C. Zhang, *"Quantum Spin Hall Insulator State in HgTe Quantum Wells"*, Science, **318**, 766–770, (2007).

[Land 57] R. Landauer, *"Spatial Variation of Currents and Fields Due to Localized Scatterers in Metallic Conduction"*, IBM J. Res. Dev., **1**, 223, (1957).

[Land 87] R. Landauer, *"Electrical transport in open and closed systems"*, Zeitschrift für Physik B Condensed Matter, **68**, 217–228, (1987).

[Laug 81] R. B. Laughlin, *"Quantized Hall conductivity in two dimensions"*, Phys. Rev. B, **23**, 5632–5633, May 1981.

[Law 09] K. T. Law, P. A. Lee, and T. K. Ng, *"Majorana Fermion Induced Resonant Andreev Reflection"*, Phys. Rev. Lett., **103**, 237001, Dec 2009.

[Lee 12] E. J. H. Lee, X. Jiang, R. Aguado, G. Katsaros, C. M. Lieber, and S. De Franceschi, *"Zero-Bias Anomaly in a Nanowire Quantum Dot Coupled to Superconductors"*, Phys. Rev. Lett., **109**, 186802, Oct 2012.

[Li 09] J. Li, R.-L. Chu, J. K. Jain, and S.-Q. Shen, *"Topological Anderson Insulator"*, Phys. Rev. Lett., **102**, 136806, Apr 2009.

[Lim 12] J. S. Lim, L. m. c. Serra, R. López, and R. Aguado, *"Magnetic-field instability of Majorana modes in multiband semiconductor wires"*, Phys. Rev. B, **86**, 121103, Sep 2012.

[Liu 12] J. Liu, A. C. Potter, K. T. Law, and P. A. Lee, *"Zero-Bias Peaks in the Tunneling Conductance of Spin-Orbit-Coupled Superconducting Wires with and without Majorana End-States"*, Phys. Rev. Lett., **109**, 267002, Dec 2012.

[Lutc 10] R. M. Lutchyn, J. D. Sau, and S. Das Sarma, *"Majorana Fermions and a Topological Phase Transition in Semiconductor-Superconductor Heterostructures"*, Phys. Rev. Lett., **105**, 077001, Aug 2010.

[Lutc 11] R. M. Lutchyn, T. D. Stanescu, and S. Das Sarma, *"Search for Majorana Fermions in Multiband Semiconducting Nanowires"*, Phys. Rev. Lett., **106**, 127001, Mar 2011.

[Mart 12] I. Martin and A. F. Morpurgo, *"Majorana fermions in superconducting helical magnets"*, Phys. Rev. B, **85**, 144505, Apr 2012.

[Medv 10] M. V. Medvedyeva, J. Tworzydło, and C. W. J. Beenakker, *"Effective mass and tricritical point for lattice fermions localized by a random mass"*, Phys. Rev. B, **81**, 214203, Jun 2010.

[Mels 96] J. A. Melsen, P. W. Brouwer, K. M. Frahm, and C. W. J. Beenakker, *"Induced superconductivity distinguishes chaotic from integrable billiards"*, EPL (Europhysics Letters), **35**, 7, (1996).

[Mess 81] A. Messiah. *Quantum Mechanics. Quantum Mechanics*, North-Holland, (1981).

[Moor 07] J. E. Moore and L. Balents, *"Topological invariants of time-reversal-invariant band structures"*, Phys. Rev. B, **75**, 121306, Mar 2007.

[Motr 01] O. Motrunich, K. Damle, and D. A. Huse, *"Griffiths effects and quantum critical points in dirty superconductors without spin-rotation invariance: One-dimensional examples"*, Phys. Rev. B, **63**, 224204, May 2001.

[Mour 12] V. Mourik, K. Zuo, S. M. Frolov, S. R. Plissard, E. P. A. M. Bakkers, and L. P. Kouwenhoven, *"Signatures of Majorana Fermions in Hybrid Superconductor-Semiconductor Nanowire Devices"*, Science, **336**, 1003–1007, (2012).

[Nadj 14] S. Nadj-Perge, I. K. Drozdov, J. Li, H. Chen, S. Jeon, J. Seo, A. H. MacDonald, B. A. Bernevig, and A. Yazdani, *"Observation of Majorana fermions in ferromagnetic atomic chains on a superconductor"*, Science, **346**, 602–607, (2014).

[Naya 08] C. Nayak, S. H. Simon, A. Stern, M. Freedman, and S. Das Sarma, *"Non-Abelian anyons and topological quantum computation"*, Rev. Mod. Phys., **80**, 1083–1159, Sep 2008.

[Nils 08] J. Nilsson, A. R. Akhmerov, and C. W. J. Beenakker, *"Splitting of a Cooper Pair by a Pair of Majorana Bound States"*, Phys. Rev. Lett., **101**, 120403, Sep 2008.

[Nomu 08] K. Nomura, S. Ryu, M. Koshino, C. Mudry, and A. Furusaki, *"Quantum Hall Effect of Massless Dirac Fermions in a Vanishing Magnetic Field"*, Phys. Rev. Lett., **100**, 246806, Jun 2008.

[Oreg 10] Y. Oreg, G. Refael, and F. von Oppen, *"Helical Liquids and Majorana Bound States in Quantum Wires"*, Phys. Rev. Lett., **105**, 177002, Oct 2010.

[Ovch 77] A. A. Ovchinnikov and N. S. Erikhman, *"Temperature and frequency dependence of the electron conductivity in a two-band model with impurities"*, JETP Letters, **46**, 340, (1977). Zh. Eksp. Teor. Fiz. **73**, 650 (1977).

[Piku 12] D. I. Pikulin and Y. V. Nazarov, *"Phenomenology and dynamics of a Majorana Josephson junction"*, Phys. Rev. B, **86**, 140504, Oct 2012.

[Pott 10] A. C. Potter and P. A. Lee, *"Multichannel Generalization of Kitaev's Majorana End States and a Practical Route to Realize Them in Thin Films"*, Phys. Rev. Lett., **105**, 227003, Nov 2010.

[Pott 11a] A. C. Potter and P. A. Lee, *"Engineering a p+ip superconductor: Comparison of topological insulator and Rashba spin-orbit-coupled materials"*, Phys. Rev. B, **83**, 184520, May 2011.

[Pott 11b] A. C. Potter and P. A. Lee, *"Erratum: Engineering a p + ip superconductor: Comparison of topological insulator and Rashba spin-orbit-coupled materials [Phys. Rev. B **83** , 184520 (2011)]"*, Phys. Rev. B, **84**, 059906, Aug 2011.

[Pott 12] A. C. Potter and P. A. Lee, *"Topological superconductivity and Majorana fermions in metallic surface states"*, Phys. Rev. B, **85**, 094516, Mar 2012.

[Pran 12] R. Prange, K. Klitzing, and S. Girvin. *The Quantum Hall Effect. Graduate Texts in Contemporary Physics*, Springer New York, (2012).

[Qi 11] X.-L. Qi and S.-C. Zhang, *"Topological insulators and superconductors"*, Rev. Mod. Phys., **83**, 1057–1110, Oct 2011.

[Read 00] N. Read and D. Green, *"Paired states of fermions in two dimensions with breaking of parity and time-reversal symmetries and the fractional quantum Hall effect"*, Phys. Rev. B, **61**, 10267–10297, Apr 2000.

[Rice 82] M. J. Rice and E. J. Mele, *"Elementary Excitations of a Linearly Conjugated Diatomic Polymer"*, Phys. Rev. Lett., **49**, 1455–1459, Nov 1982.

[Ried 12] M.-T. Rieder, G. Kells, M. Duckheim, D. Meidan, and P. W. Brouwer, *"End-states in multichannel spinless p-wave superconducting wires"*, Phys. Rev. B, **86**, 125423, Sep 2012.

[Ried 13] M.-T. Rieder, P. W. Brouwer, and i. d. I. m. c. Adagideli, *"Reentrant topological phase transitions in a disordered spinless superconducting wire"*, Phys. Rev. B, **88**, 060509, Aug 2013.

[Ried 14] M.-T. Rieder and P. W. Brouwer, *"Density of states at disorder-induced phase transitions in a multichannel Majorana wire"*, Phys. Rev. B, **90**, 205404, Nov 2014.

[Ring 12] Z. Ringel, Y. E. Kraus, and A. Stern, *"Strong side of weak topological insulators"*, Phys. Rev. B, **86**, 045102, Jul 2012.

[Rokh 12] L. P. Rokhinson, X. Liu, and J. K. Furdyna, *"The fractional a.c. Josephson effect in a semiconductor-superconductor nanowire as a signature of Majorana particles"*, Nat Phys, **8**, 795–799, (2012).

[Roy 09] R. Roy, *"Topological phases and the quantum spin Hall effect in three dimensions"*, Phys. Rev. B, **79**, 195322, May 2009.

[Ryu 10] S. Ryu, A. P. Schnyder, A. Furusaki, and A. W. W. Ludwig, *"Topological insulators and superconductors: tenfold way and dimensional hierarchy"*, New Journal of Physics, **12**, 065010, (2010).

[San 12] P. San-Jose, E. Prada, and R. Aguado, *"ac Josephson Effect in Finite-Length Nanowire Junctions with Majorana Modes"*, Phys. Rev. Lett., **108**, 257001, Jun 2012.

[Sau 10] J. D. Sau, R. M. Lutchyn, S. Tewari, and S. Das Sarma, *"Generic New Platform for Topological Quantum Computation Using Semiconductor Heterostructures"*, Phys. Rev. Lett., **104**, 040502, Jan 2010.

[Schn 08] A. P. Schnyder, S. Ryu, A. Furusaki, and A. W. W. Ludwig, *"Classification of topological insulators and superconductors in three spatial dimensions"*, Phys. Rev. B, **78**, 195125, Nov 2008.

[Schn 09] A. P. Schnyder, S. Ryu, A. Furusaki, and A. W. W. Ludwig, *"Classification of Topological Insulators and Superconductors"*, AIP Conference Proceedings, **1134**, 10–21, (2009).

[Smit 60] F. T. Smith, *"Lifetime Matrix in Collision Theory"*, Phys. Rev., **118**, 349–356, Apr 1960.

[Stan 11] T. D. Stanescu, R. M. Lutchyn, and S. Das Sarma, *"Majorana fermions in semiconductor nanowires"*, Phys. Rev. B, **84**, 144522, Oct 2011.

[Ston 81] A. D. Stone and J. D. Joannopoulos, *"Probability distribution and new scaling law for the resistance of a one-dimensional Anderson model"*, Phys. Rev. B, **24**, 3592–3595, Sep 1981.

[Su 79] W. P. Su, J. R. Schrieffer, and A. J. Heeger, *"Solitons in Polyacetylene"*, Phys. Rev. Lett., **42**, 1698–1701, Jun 1979.

[Tewa 12a] S. Tewari and J. D. Sau, *"Topological Invariants for Spin-Orbit Coupled Superconductor Nanowires"*, Phys. Rev. Lett., **109**, 150408, Oct 2012.

[Tewa 12b] S. Tewari, T. D. Stanescu, J. D. Sau, and S. Das Sarma, *"Topological minigap in quasi-one-dimensional spin-orbit-coupled semiconductor Majorana wires"*, Phys. Rev. B, **86**, 024504, Jul 2012.

[Theo 76] G. Theodorou and M. H. Cohen, *"Extended states in a one-demensional system with off-diagonal disorder"*, Phys. Rev. B, **13**, 4597–4601, May 1976.

[Thou 82] D. J. Thouless, M. Kohmoto, M. P. Nightingale, and M. den Nijs, *"Quantized Hall Conductance in a Two-Dimensional Periodic Potential"*, Phys. Rev. Lett., **49**, 405–408, Aug 1982.

[Tito 01] M. Titov, P. W. Brouwer, A. Furusaki, and C. Mudry, *"Fokker-Planck equations and density of states in disordered quantum wires"*, Phys. Rev. B, **63**, 235318, May 2001.

[Volo 76] G. Volovik and V. Mineev, *"Line and point singularities in superfluid He3"*, JETP Letters, **24**, 561, (1976). Zh. Eksp. Teor. Fiz. **24**, 605 (1976).

[Volo 99a] G. Volovik, *"Fermion zero modes on vortices in chiral superconductors"*, JETP Letters, **70**, 609–614, (1999).

[Volo 99b] G. Volovik, *"Monopole, half-quantum vortex, and nexus in chiral superfluids and superconductors"*, JETP Letters, **70**, 792–796, (1999).

[Wied 15] J. Wiedenmann, E. Bocquillon, S. Deacon, R. S. Hartinger, T. M. Klapwijk, L. Maier, C. Ames, C. Brüne, K. Ishibashi, S. Tarucha, H. Buhmann, and L. W. Molenkamp. "*Zero-energy Andreev bound states in a HgTe-based topological Josephson junction". (2015). arXiv:1503.05591.*

*[Wign 55] E. P. Wigner, "Lower Limit for the Energy Derivative of the Scattering Phase Shift", Phys. Rev., **98**, 145–147, Apr 1955.*

*[Wilc 09] F. Wilczek, "Majorana returns", Nat Phys, **5**, 614–618, 09 2009.*

*[Wilc 82] F. Wilczek, "Quantum Mechanics of Fractional-Spin Particles", Phys. Rev. Lett., **49**, 957–959, Oct 1982.*

*[Will 12] J. R. Williams, A. J. Bestwick, P. Gallagher, S. S. Hong, Y. Cui, A. S. Bleich, J. G. Analytis, I. R. Fisher, and D. Goldhaber-Gordon, "Unconventional Josephson Effect in Hybrid Superconductor-Topological Insulator Devices", Phys. Rev. Lett., **109**, 056803, Jul 2012.*

*[Wimm 10] M. Wimmer, A. R. Akhmerov, M. V. Medvedyeva, J. Tworzydło, and C. W. J. Beenakker, "Majorana Bound States without Vortices in Topological Superconductors with Electrostatic Defects", Phys. Rev. Lett., **105**, 046803, Jul 2010.*

*[Wimm 11] M. Wimmer, A. R. Akhmerov, J. P. Dahlhaus, and C. W. J. Beenakker, "Quantum point contact as a probe of a topological superconductor", New Journal of Physics, **13**, 053016, (2011).*

*[Xia 09] Y. Xia, D. Qian, D. Hsieh, L. Wray, A. Pal, H. Lin, A. Bansil, D. Grauer, Y. S. Hor, R. J. Cava, and M. Z. Hasan, "Observation of a large-gap topological-insulator class with a single Dirac cone on the surface", Nat Phys, **5**, 398–402, 06 2009.*

*[Zhan 09] H. Zhang, C.-X. Liu, X.-L. Qi, X. Dai, Z. Fang, and S.-C. Zhang, "Topological insulators in Bi2Se3, Bi2Te3 and Sb2Te3 with a single Dirac cone on the surface", Nat Phys, **5**, 438–442, 06 2009.*

*[Zhou 11] B. Zhou and S.-Q. Shen, "Crossover from Majorana edge- to end-states in quasi-one-dimensional p-wave superconductors", Phys. Rev. B, **84**, 054532, Aug 2011.*

6 Acknowledgements

I wish to take the opportunity here to thank the people that played a role in the completion of this thesis and accompanied me on the way there.

First and foremost I want thank my advisor Piet W. Brouwer who gave me the opportunity to work on this thesis in his group. I could not think of a better supervision than his, combining a door always open for questions with the freedom to work on independent projects. He always took time to listen and discuss when I got stuck with a problem, which is invaluable.

A special thanks to all my coauthors for many great discussions, Graham Kells, Mathias Duckheim, Dganit Meidan, Arbel Haim, Tobias Micklitz, Alex Levchenko, Kosty Matveev, and Inanc Adagideli, and to Emil J. Bergholtz for co-refereeing this Thesis.

I further acknowledge financial support by the Alexander-von-Humboldt foundation.

During my time in the Dahlem Center I was accompanied by many great colleagues, some of which have become close friends. I am very greatful for lots of fruitful and inspiring discussions about physics, life, the universe and everything, particularly to Dganit Meidan, Silvia Viola Kusminskiy, Martin Schneider, Michele Filippone, Alexandra Junck, Falko Pientka, Elina Locane, Jeroen Danon, Géraldine Haack, Björn Sbierski, Kristin Rammelkamp and Jörg Behrmann. Furthermore, I wish to thank Gabriele Hermann for administrative support.

Finally, I am deeply grateful to my parents, my sister Anne, and Jens for being by my side.

7 Curriculum Vitae

For reasons of data protection,
the *curriculum vitae* is not included in the online version of this thesis.

8 Publications

Publications, that constitute the content of this thesis:

- Maria-Theresa Rieder, Graham Kells, Mathias Duckheim, Dganit Meidan, and Piet W. Brouwer,
  "Endstates in multichannel spinless p-wave superconducting wires",
  Phys. Rev. B **86**, 125423 (2012), http://dx.doi.org/10.1103/PhysRevB.86.125423 [Chapter 2].

- Maria-Theresa Rieder, Piet W. Brouwer, and İnanç Adagideli,
  "Reentrant topological phase transitions in a disordered spinless superconducting wire",
  Phys. Rev. B **88**, 060509(R) (2013), http://dx.doi.org/10.1103/PhysRevB.88.060509 [Chapter 3].

- Maria-Theresa Rieder and Piet W. Brouwer,
  "Density of states at disorder-induced phase transitions in a multichannel Majorana wire",
  Phys. Rev. B **90**, 205404 (2014), http://dx.doi.org/10.1103/PhysRevB.90.205404 [Chapter 4].

Publications, that have been completed in parallel to this thesis:

- Maria-Theresa Rieder, Tobias Micklitz, Alex Levchenko, and K. A. Matveev,
  "Interaction-induced backscattering in short quantum wires",
  Phys. Rev. B **90**, 165405 (2014), http://dx.doi.org/10.1103/PhysRevB.90.165405.

- Maria-Theresa Rieder, Tobias Micklitz, and Alex Levchenko,
  "Brownian scattering of a spinon in a Luttinger liquid",
  Phys. Rev. B **90**, 245434 (2014), http://dx.doi.org/10.1103/PhysRevB.90.245434.